

POLITECNICO DI TORINO

Collegio di Ingegneria Chimica e dei Materiali

**Corso di Laurea Magistrale
in Ingegneria Chimica e dei Processi Sostenibili**

Tesi di Laurea Magistrale

Microwave-assisted synthesis of Cu-based
catalysts for electroreduction of CO₂ in the
production of Syngas



Relatore/i

prof. C. Fabrizio Pirri
dott. Adriano Sacco
dott. Juqin Zeng

Candidato

Gaia Di Martino

Luglio 2019

CONTENTS

List of abbreviation and symbols	III
Riassunto in italiano	V
Abstract	XVII
1. Introduction	1
1.1 Global warming, causes and effects	1
1.2 Greenhouse gases and greenhouse effect	1
1.3 Carbon cycle	5
1.3.1 Land sink	5
1.3.2 Ocean sink	6
1.3.3 Flux from land to ocean	7
1.3.4 Deforestation flux	7
1.3.5 Fossil fuel combustion	8
1.4 Solutions and Technologies	8
1.4.1 Electroreduction	8
1.4.2 Electroreduction of CO ₂	9
1.4.3 Parameters of electroreduction of CO ₂	11
1.5 Syngas	12
1.6 Introduction to methods and materials	14
1.6.1 Copper and tin	14
1.6.2 Microwave	14
1.7 Aim of the work	15
2. Materials and methods	16
2.1 Materials	16
2.2 Experimental	16
2.2.1 Synthesis of the catalysts	16
2.2.2 Preparation of the electrodes	20
2.3 Characterization and electrochemical analysis	22
2.3.1 Field-emission scanning electron microscopy (FESEM)	22
2.3.2 X-ray diffraction (XRD)	22
2.3.3 X-ray photoelectron spectroscopy (XPS)	23
2.3.4 Chronoamperometry (CA)	23
2.3.5 Gas chromatography (GC)	25
3. Results and discussion	26
3.1 Characterization of the material	26
3.1.1 FESEM	26
3.1.2 XRD	34

3.1.3 XPS	35
3.2 Electrochemical and products analyses.....	41
3.2.1 CA and GC.....	41
3.3 Comparison of results	70
3.4 About Syngas	74
4. Conclusion and future developments.....	76
References	78
Acknowledgement	82

LIST OF ABBREVIATION AND SYMBOLS

AC	Alternating Current
CA	Chronoamperometry
CB	Carbon Black
CEM	Cation Exchange Membrane
CO ₂ RR	CO ₂ Reduction Reaction
CV	Cyclic Voltammetry
E°	Standard Electrode potential (V)
E _B	Bonding Energy (kJ mol ⁻¹)
EG	Ethylene Glycol
EIS	Electrochemical Impedance Spectroscopy
E _K	Kinetic Energy (kJ mol ⁻¹)
FE	Faradaic Efficiency
FESEM	Field-Emission Scanning Electron Microscope
GC	Gas Chromatography
GDE	Gas Diffusion Electrode
GDL	Gas Diffusion Layer
GHG	GreenHouse Gases
Gt C	Gigatons of carbon
GTP	Global Temperature change Potential
GWP	Global Warming Potential
h	Planck constant (kJ s)
HER	Hydrogen Evolution Reaction
I	Current intensity (mA)
NHE	Normal Hydrogen Electrode
PEM	Polymer Electrolyte Membrane
RHE	Reversible Hydrogen Electrode
SHE	Standard Hydrogen Electrode

t	Time (min or s)
V _m	Molar Volume (mL mmol ⁻¹)
XPS	x-Ray Photoelectron Spectroscopy
XRD	x-Ray Diffraction
ΔG	Free Gibbs Energy (kJ mol ⁻¹)
λ	Wavelength (nm)
ν	Frequency (Hz)

RIASSUNTO IN ITALIANO

I. INTRODUZIONE

Il cambiamento climatico e il riscaldamento globale sono argomenti molto attuali e di grande preoccupazione.

Con “cambiamento climatico” si intende la variazione nel lungo periodo del clima della Terra o di una delle sue regioni; con “riscaldamento globale” si intende l’incremento della temperatura media sulla superficie della terra a causa dei gas serra [1].

È stato stimato che la temperatura media aumenterà di 1.5°C rispetto all’era preindustriale tra il 2030 e il 2052 [2], con importanti conseguenze su tutto il sistema terrestre, tra cui condizioni meteo estreme.

Il fenomeno del riscaldamento globale è causato dall’effetto serra: i gas serra (indicati con l’acronimo GHG) sono trasparenti alle radiazioni a corta lunghezza d’onda, ma sono opachi alle radiazioni a lunga lunghezza d’onda (infrarossi). Le radiazioni infrarosse emesse dai corpi riscaldati dal sole sono quindi “intrappolate” e provocano, così, un aumento delle temperature.

È stato valutato che ridurre le emissioni di gas serra sarà utile a limitare, ma non a fermare il riscaldamento globale; infatti, l’accumulo di GHG dalla Rivoluzione Industriale a oggi è tale da avere effetti nei secoli a venire [5].

L’anidride carbonica è il gas serra più presente (circa il 76%) e la maggior parte è di origine antropogenica (Fig.I.1).

La CO₂ non è il composto che presenta il maggiore *Global Warming Potential*, ma è il composto a maggior concentrazione e quindi quello che presenta il maggior contributo all’effetto serra. Quindi, molti degli sforzi per contrastare il riscaldamento globale sono focalizzati sulla riduzione della concentrazione dell’anidride carbonica. Studi indicano che la concentrazione in atmosfera della CO₂ continuerà a crescere negli anni a venire [8].

L’anidride carbonica è un composto che prende parte al ciclo del carbonio, definito come la circolazione di atomi di carbonio attraverso l’oceano, la terraferma e l’atmosfera come risultato di processi fisici, chimici e biologici [10].

Il ciclo del carbonio è stato alterato dalle attività umane a partire dalla Rivoluzione Industriale a causa dell’uso massivo di carburanti fossili.

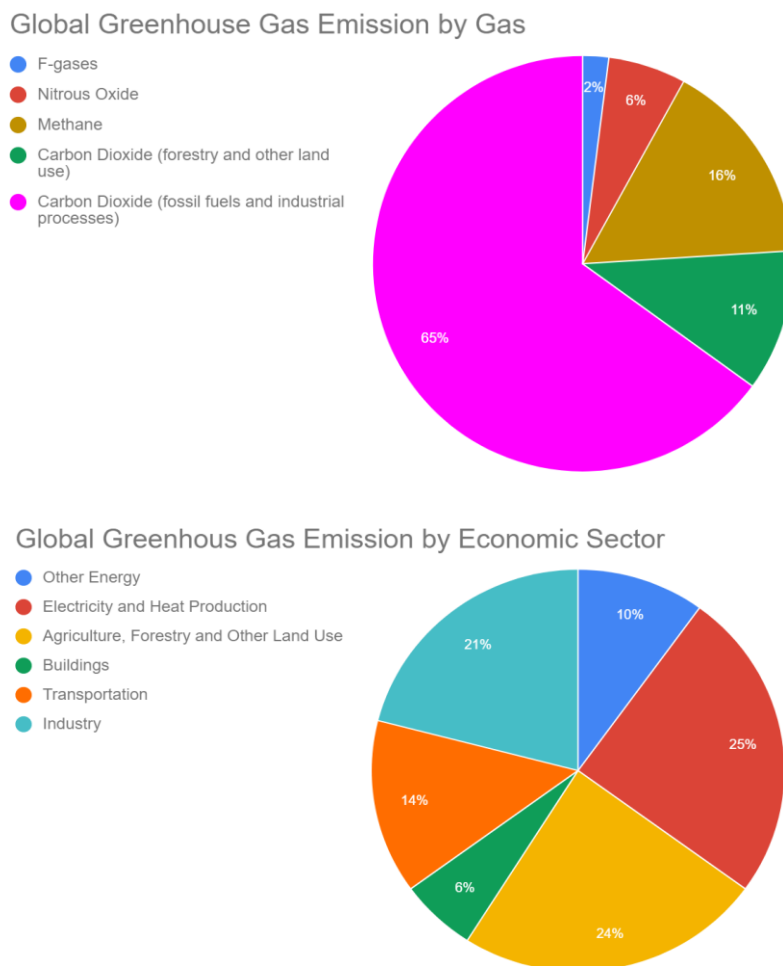


Fig.I.1 Emissioni globali di gas serra nel 2010 [3,4]

Il carbonio è scambiato tra i diversi *sink* (dove è immagazzinato) attraverso i flussi (Fig.I.2); a causa dell'anidride carbonica di origine antropica, il ciclo del carbonio non è più in equilibrio, situazione peggiorata dalla deforestazione. Il risultato è l'accumulo di CO₂.

La risposta al riscaldamento globale deve quindi includere non solo la riduzione delle emissioni, ma anche tecnologie per catturare e trasformare l'anidride carbonica già presente in grandi quantità nell'atmosfera [12].

Sono stati considerate due soluzioni negli ultimi 40 anni: il sequestro geologico e la conversione chimica.

Il sequestro geologico presenta una preoccupazione a lungo termine a causa della possibilità di perdite di anidride carbonica, la quale, oltre certi livelli di concentrazione, è tossica per uomini e animali.

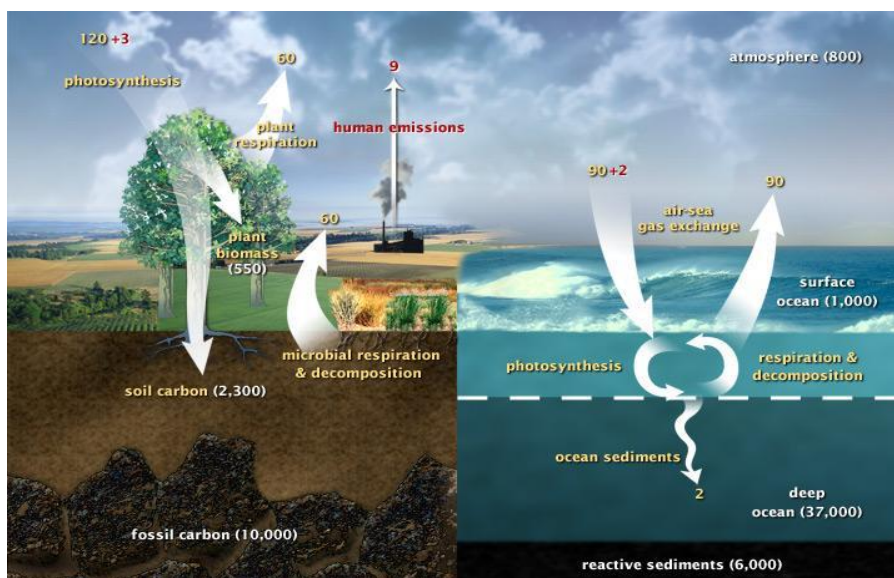


Fig.I.2 Ciclo del carbonio. in giallo sono rappresentati i flussi naturali (gigatonnellate anno⁻¹); in rosso sono rappresentati i flussi di carbonio dovuti alle attività umane (gigatonnellate anno⁻¹); in bianco è rappresentato il carbonio stoccato. Fonte: <https://earthobservatory.nasa.gov/features/CarbonCycle>.

La conversione chimica è quindi ritenuta una soluzione migliore; in particolar modo, la riduzione elettrochimica presenta diversi vantaggi, tra cui il facile controllo della reazione tramite il controllo del potenziale applicato [12,16] e la possibilità di rendere l'intero processo *green* usando elettroliti a basso impatto ambientale e fonti di energia elettrica rinnovabili [35, 14].

L'elettroriduzione è una reazione redox condotta in una cella elettrolitica attraverso l'applicazione di energia elettrica. La riduzione avviene al catodo e l'ossidazione all'anodo di una cella elettrolitica

La CO₂ è una molecola molto stabile ed è richiesta una grande quantità di energia per rompere il legame C=O e convertirla in altri prodotti [13, 17].

Per abbassare questa energia, sono stati studiati sia catalizzatori omogenei che catalizzatori eterogenei. In questo lavoro ci si concentrerà solo sui catalizzatori eterogenei.

Il processo di elettroriduzione della CO₂ con catalizzatore eterogeneo può essere riassunto in tre passaggi: (a) assorbimento della CO₂ sulla superficie del catalizzatore; (b) attivazione con la formazione di un intermedio e riduzione della CO₂; (c) desorbimento dei prodotti [12, 13].

I prodotti che possono formarsi sono vari e ognuno caratterizzato da un particolare potenziale (Tab.I.1).

Tab.I.1 Potenziali e (25°C, pH=7) e energie libere di Gibbs (25°C, pH=0) per la conversione della CO₂ in vari prodotti in condizioni standard [3].

Semireazione	E° (V vs NHE)	ΔG (kJ mol ⁻¹)
CO ₂ + 4H ⁺ + 4e ⁻ → HCHO + H ₂ O	-0.48	27.5
CO ₂ + 2H ⁺ + 2e ⁻ → HCOOH	-0.61	38.4

$\text{CO}_2 + 2\text{H}^+ + 2\text{e}^- \rightarrow \text{CO} + \text{H}_2\text{O}$	-0.53	19.9
$\text{CO}_2 + 6\text{H}^+ + 6\text{e}^- \rightarrow \text{CH}_3\text{OH} + \text{H}_2\text{O}$	-0.24	-17.3
$\text{CO}_2 + 8\text{H}^+ + 8\text{e}^- \rightarrow \text{CH}_4 + 2\text{H}_2\text{O}$	-0.38	-130.8
$\text{CO}_2 + \text{e}^- \rightarrow \text{CO}_2^{\cdot-}$	-1.9	183.32

Siccome la reazione di riduzione della CO₂ è spesso condotta in soluzioni acquose, è molto facile che la reazione di formazione di idrogeno abbia luogo in maniera concorrenziale: questa infatti avviene a potenziali simili ed è spesso favorita [3, 12].

È possibile sfruttare la concorrenza delle due reazioni per la produzione di Syngas, il quale, in base al rapporto H₂/CO, può essere trasformato in combustibile liquido tramite il processo Fischer-Tropsch o in altri composti utili (come ammoniaca e alcoli) [17].

Idealmente, l'anidride carbonica può essere ridotta con i potenziali riportati in Tab.I.1, ma in realtà il potenziale richiesto è più alto. La differenza tra potenziale reale e potenziale ideale è detta sovratensione ed è principalmente causata dalla necessità di energia di attivazione per trasferire l'elettrone alla molecola di CO₂, nonché da perdite ohmiche causate dalla conduttività dell'elettrolita e dell'elettrodo o a limitazioni al trasporto di massa. È quindi possibile dire che il monossido di carbonio (CO) è il prodotto termodinamicamente più facile da ottenere, in quanto solo due elettroni sono coinvolti nella reazione [3].

I parametri usati per valutare le performance dei catalizzatori sono la densità di corrente (definita come la corrente elettrica per unità di superficie) e, nel caso di più prodotti, l'efficienza faradica (definita come il rapporto tra gli elettroni necessari a formare il prodotto e gli elettroni totali coinvolti nel processo).

I parametri che influenzano la distribuzione dei prodotti e le prestazioni del processo di elettroreduzione della CO₂ sono: materiale del catalizzatore, configurazione della cella elettrolitica (poiché influenza i fenomeni di trasporto di cariche e composti), condizioni operative (pressione e temperatura, le quali influenzano soprattutto la solubilità dell'anidride carbonica e la cinetica), morfologia del catodo (in quanto influenza i fenomeni di trasporto), tipo di elettrolita (gli elettroliti agiscono sul pH e di conseguenza sulla sovratensione da applicare), stabilità dell'elettrodo (una maggiore stabilità implica un maggiore utilizzo del catalizzatore e quindi una maggiore produzione) [3, 12, 14, 15].

Nella reazione di riduzione della CO₂, oro e argento presentano alta efficienza e alta selettività verso il CO. A causa, però, del loro costo e non abbondanza, altri materiali sono stati studiati [3]. Tra questi, il rame ha riscosso grande interesse grazie alla buona attività nel ridurre l'anidride carbonica, ma presenta una scarsa selettività verso il CO [3, 12, 17]. È stato, tuttavia, dimostrato che combinando il rame allo stagno (il quale presenta comportamento simile al Cu), la selettività verso il CO [17].

La sintesi assistita da microonde presenta diversi vantaggi se comparati con i classici metodi di sintesi: aumento della efficienza di reazione, miglioramento della conversione dei prodotti, maggiore sicurezza, diminuzione del tempo di reazione e dell'energia richiesta. Inoltre, la sintesi

via microonde presenta un riscaldamento uniforme [18]. Il calore è generato attraverso la frizione delle molecole polari, le quali si muovono per allinearsi al campo elettrico variato (Fig.I.3) [20].

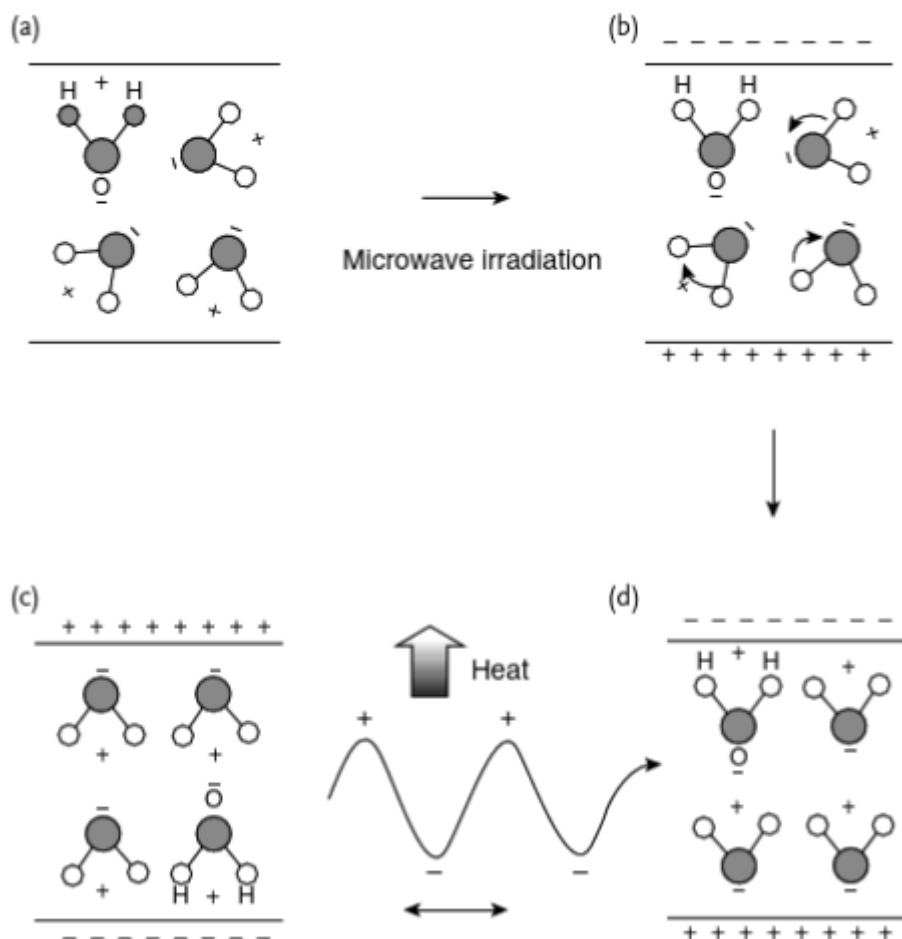


Fig.I.3 Meccanismo di interazione dei dipoli di molecole di acqua. A causa delle radiazioni microonde, le molecole polari si muovono e ruotano per allinearsi con il variato campo elettrico. L'energia cinetica si trasforma in calore a causa della frizione e delle collisioni. Fonte: [21].

Lo scopo di questo lavoro è la sintesi assistita da microonde di catalizzatori a base di Cu; la loro caratterizzazione tramite FESEM, XDR e XPS; lo svolgimento di misure elettrochimiche (CA); la valutazione dei prodotti tramite gas cromatografia. I risultati saranno presentati, comparati e discussi nella prospettiva di futuri sviluppi.

II. MATERIALI E METODI

I materiali usati nella sintesi e nella caratterizzazione dei catalizzatori sono: $\text{SnCl}_2 \cdot 2\text{H}_2\text{O}$, 99.9 %; $\text{SnCl}_4 \cdot 5\text{H}_2\text{O}$, 98 %; $\text{CuSO}_4 \cdot 5\text{H}_2\text{O}$, $\text{Cu}(\text{CH}_3\text{COO})_2 \cdot x\text{H}_2\text{O}$, 98%, 99.0 %; NaOH, 98 %; KHCO_3 , 99.7 %; EG, 99.8 %; Nafion® 117 solution (5 wt. %); isopropanolo. I materiali sono stati acquistati da Sigma-Aldrich.

Inoltre, sono stati usati *acetylene carbon black* (CB, Shawinigan Black AB50) e *carbon paper* equipaggiato di *gas diffusion layer* (GDL; SIGRACET 28BC, SGL Technologies).

I precursori scelti sono due Sali di rame e due sali di stagno:

- CuSO₄; nel lavoro, i campioni fabbricati con questo sale come precursore definiti con “Cu”;
- Cu(CH₃COO)₂; nel lavoro, i campioni fabbricati con questo sale come precursore contengono “Cu(Ace)”;
- SnCl₂; nel lavoro, i campioni fabbricati con questo sale come precursore contengono “Sn(II)”;
- SnCl₄; nel lavoro, i campioni fabbricati con questo sale come precursore contengono “Sn(IV)”.

Le polveri catalitiche sono state sintetizzate combinando un sale di rame e un sale di stagno. I campioni di riferimento a base di Cu sono stati fabbricati attraverso sintesi assistita da microonde con diverse concentrazioni di stagno (Tab.II.1). Campioni a base di sali di rame senza aggiunta di stagno sono stati sintetizzati con lo scopo di confrontare gli effetti dello stagno.

Tab.II.1 Campioni preparati.

		CuSO₄	Cu(CH₃COO)₂
SnCl₂	45 mg (5 wt %)	CuSn(II)5	Cu(Ace)Sn(II)5
SnCl₄	45 mg (5 wt %)	CuSn(IV)5	Cu(Ace)Sn(IV)5
	90 mg (10 wt %)	CuSn(IV)10	Cu(Ace)Sn(IV)10
No sale di Sn	0 mg (0 wt %)	Cu	Cu(Ace)

I passaggi della sintesi e della preparazione dell'elettrodo sono riassunti di seguito:

- Sintesi
 - 900 mg di sale di rame e una quantità proporzionata di sale di stagno sono state sciolte in una soluzione di EG (20 mL) e acqua (10 mL) (soluzione 1);
 - 1600 mg di NaOH sono stati sciolti in una soluzione di EG (30 mL) e acqua (5 mL) (soluzione 2);
 - 25 mL di soluzione 2 sono state aggiunte goccia a goccia alla soluzione 1;
 - quando blu e trasparente (10 minuti di agitazione vigorosa), la miscela è stata trasferita in un recipiente di Teflon (100 mL di volume, riempito per circa 2/3 del volume totale);
 - il recipiente di Teflon è stato posizionato del forno a microonde e connesso a sensori di pressione e temperatura (Milestone STARTSynth, Milestone Inc., Shelton, Connecticut);
 - la miscela è stata irradiata per 10 minuti a 170°C (900 W). Le stabilità della pressione e della temperatura sono state controllate attraverso lo schermo del macchinario;
 - la miscela è stata raffreddata a temperatura e pressione ambiente nel forno;
 - il precipitato sintetizzato è stato separato tramite centrifugazione e lavato due volte con acqua e una volta con EG;
 - il precipitato lavato è stato asciugato durante la notte in un forno sottovuoto a 60°C, ottenendo così una polvere;
- Preparazione dell'elettrodo
 - 15 mg di campione sono state miscelate con 1 mg di CB;
 - 90 µL di Nafion® 117 e 240 µL di isopropanolo sono stati aggiunti alla miscela di campione e CB;

- la miscela è stata sonicata per circa 30 minuti, fino all'ottenimento di un inchiostro uniforme;
- elettrodi di GDL sono stati preparati tagliando sezioni di superficie $2 \times 2.5 \text{ cm}^2$. Nastro adesivo di rame è stato incollato sul bordo superiore e nastro adesivo di Teflon è stato usato per coprire il retro e i bordi del nastro di rame, lasciando una superficie scoperta di $2 \times 1.5 \text{ cm}^2$;
- l'inchiostro è stato usato per ricoprire l'elettrodo su GDL. L'elettrodo ottenuto è stato asciugato a temperatura ambiente durante la notte.

Il carico massico è di 5 mg cm^{-2} di catalizzatore.

I materiali preparati sono stati analizzati attraverso diverse tecniche analitiche, con lo scopo di caratterizzare il materiale per quanto riguarda la morfologia, la composizione e i legami, le proprietà elettrochimiche e i prodotti formati. Le analisi eseguite consistono in: FESEM, XRD, XPS, CA e GC.

- FESEM: i campioni sono stati analizzati tramite FESEM, ZEISS Auriga.
- XRD: i campioni sono stati analizzati tramite la configurazione Bragg-Brentano a geometria simmetrica, usando lo strumento PANalytical X'Pert Pro (radiazione Cu- $K\alpha$, 40 kV and 30 mA) equipaggiato con rivelatore X'Celerator.
- XPS: i campioni sono stati analizzati tramite il sistema PHI 5000 VersaProbe (Physical Electronics). Come sorgente di raggi X è stata usata la radiazione monocromatica Al $K\alpha$ (1486.6 eV). Gli spettri sono stati analizzati usando il software Multipak 9.7.
- CA: i campioni sono stati analizzati utilizzando Bio-Logic electrochemical workstation a temperatura ambiente, con una piastra di platino come contro elettrodo e un elettrodo Ag/AgCl in soluzione NaCl 3M come riferimento. I test sono stati effettuati in una soluzione elettrolitica di KHCO_3 saturata di CO_2 a -0.6, -0.7, -0.8V vs RHE. I potenziali testati sono stati corretti compensando le cadute ohmiche dell'85% tramite lo strumento (iR-compensation).
- GC: i prodotti gassosi sono stati analizzati durante i test di CA tramite gas cromatografo (μGC , Fusion @, INFICON), previa rimozione dell'umidità attraverso un filtro GENIE. Durante la prova è stato mantenuto un flusso costante di CO_2 con una portata volumica di 38 mL min^{-1} per mantenere la soluzione elettrolitica satura. Come gas vettore è stato usato argon.

III. RISULTATI E DISCUSSIONE

I risultati delle analisi dei materiali fabbricati sono riportati e discussi in questo capitolo.

I materiali analizzati al FESEM hanno mostrato diverse morfologie a seconda dei precursori utilizzati: come mostrato in Fig.III.1 e in Fig.III.2, l'aggiunta di Sn(II) non ha avuto effetti sui campioni a base di CuSO_4 ed ha, invece, modificato la morfologia di quelli preparati con Cu(Ace); si può ipotizzare che nel primo caso Sn(II) abbia agito da inibitore di agglomeramento; nel caso di Cu(Ace) è possibile che Sn(II) abbia agito sia da inibitore di agglomeramento che da agente di riduzione della dimensione delle particelle.

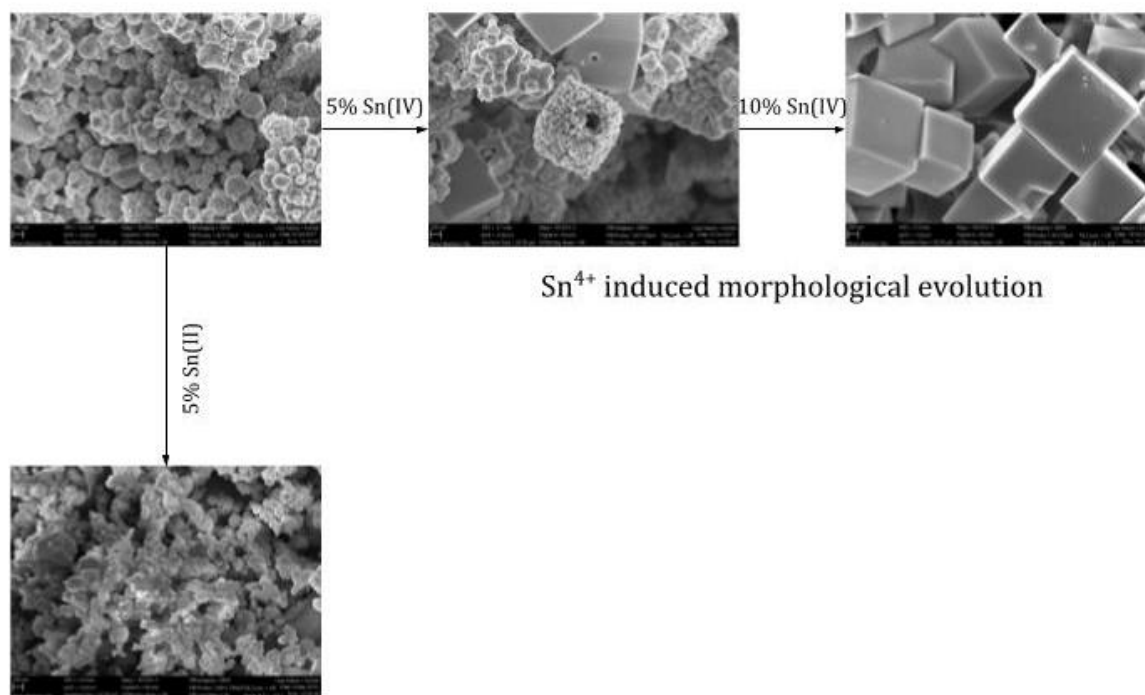


Fig.III.1 Effetti dei Sali di stagno sulla morfologia dei campioni fabbricati con CuSO₄.

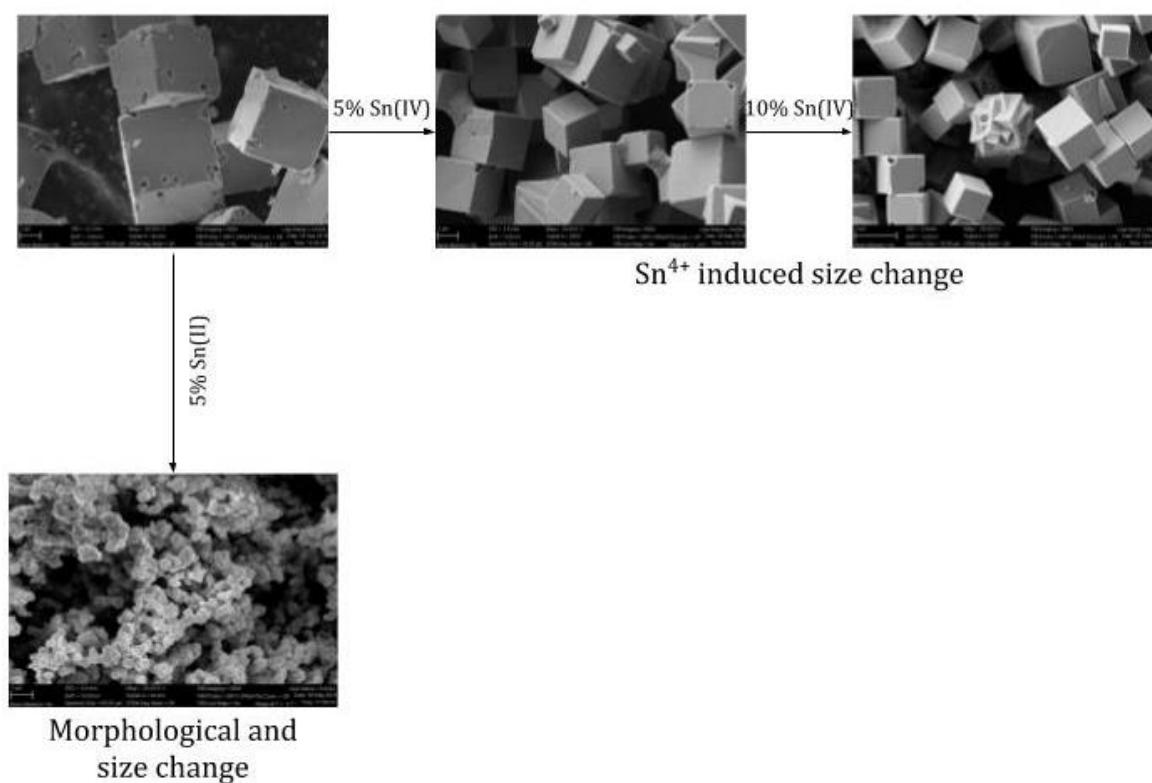


Fig.III.2 Effetto dei Sali di stagno sulla morfologia dei campioni fabbricati con Cu(Ace).

Dalle figure riportate è possibile notare che l'effetto di Sn(IV) sui campioni fabbricati con CuSO₄ è stato quello di cambiamento morfologico a cubetti, tramite l'agglomeramento delle

particelle; considerando il campione fabbricato utilizzando Cu(Ace), l'effetto di Sn(IV) è stato la riduzione delle dimensioni delle particelle cubiche.

Le analisi XRD e XPS hanno evidenziato la composizione dei campioni. Gli elementi maggiormente presenti sono C, O e Cu, con tracce trascurabili di stagno.

In Tab.III.1 e Tab.III.2 sono riportati i parametri di Auger calcolati e i corrispondenti stati di ossidazione.

Tab.III.1 Parametri di Auger e stati di ossidazione del rame per i campioni preparati con solfato rameico.

Campione	Parametro di Auger	Stato di ossidazione di Cu
Cu	1848.9	(I)=(0)+(II)
CuSn(II)5	1851.1	(II)
CuSn(IV)5	1849.0	(I)=(0)+(II)
CuSn(IV)10	1848.8	(I)=(0)+(II)

L'effetto di Sn(II) sul campione fabbricato con CuSO₄ come precursore è stato di modificare la composizione superficiale. Infatti, il campione Cu è composto perlopiù da rame metallico con ossidi di rame misti sulla superficie. L'aggiunta di Sn(II) può comportare una riduzione nella dimensione delle particelle, che divengono, quindi, più facilmente ossidabili all'aria [41], formando CuO sulla superficie del campione CuSn(II)5 (come confermato dai risultati XPS).

Le analisi XRD e XPS hanno mostrato che Sn(IV) ha avuto effetti non solo sulla morfologia, ma anche sulla composizione dei catalizzatori fabbricati con CuSO₄. I campioni sintetizzati con questo sale di stagno hanno una significativa quantità di Cu₂O e ossidi superficiali misti.

Tab.III.2 Parametri di Auger e stati di ossidazione del rame per i campioni preparati con acetato di rame.

Campione	Parametro di Auger	Stato di ossidazione di Cu
Cu(Ace)	1848.9	(I)=(0)+(II)
Cu(Ace)Sn(II)5	1451.3	(II)
Cu(Ace)Sn(IV)5	1848.7	(I)=(0)+(II)
Cu(Ace)Sn(IV)10	1849.3	(I)=(0)+(II)

Il campione Cu(Ace) presenta una composizione formata perlopiù da Cu₂O e da ossidi misti superficiali. I campioni fabbricati con Sn(IV) presentano una composizione analoga

Le analisi XRD e XPS hanno mostrato che il campione CuSn(II)5 è composto da CuO. Infatti, il campione presenta particelle più piccole e, quindi, più facilmente ossidabili.

La cronoamperometria e la gascromatografia hanno permesso il calcolo delle efficienze faradiche per la formazione di CO e H₂ a diversi valori di sovratensioni (Fig.III.3, Fig.III.4 e Fig.III.5). Dai valori di concentrazione delle due specie a 40 minuti forniti dal gascromatografo, sono stati calcolati i rapporti H₂/CO (Tab.III.3)

Le efficienze faradiche sono state calcolate utilizzando la formula riportata:

$$FE_x = \frac{e_x^-}{Q}$$

dove FE_x rappresenta l'efficienza faradica per la specie x, e_x⁻ rappresenta gli elettroni coinvolti nella formazione della specie x e Q rappresenta la quantità totale degli elettroni coinvolti nelle reazioni.

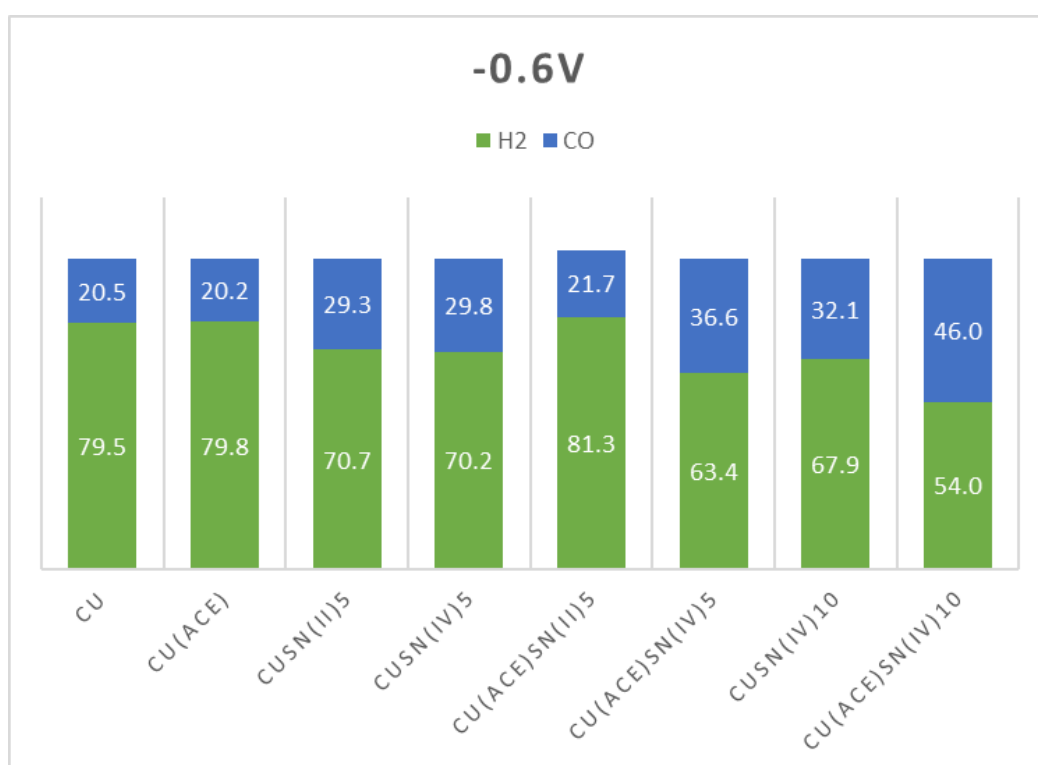


Fig.III.3 Efficienze faradiche per CO e H₂ dei campioni a -0.6V vs RHE.

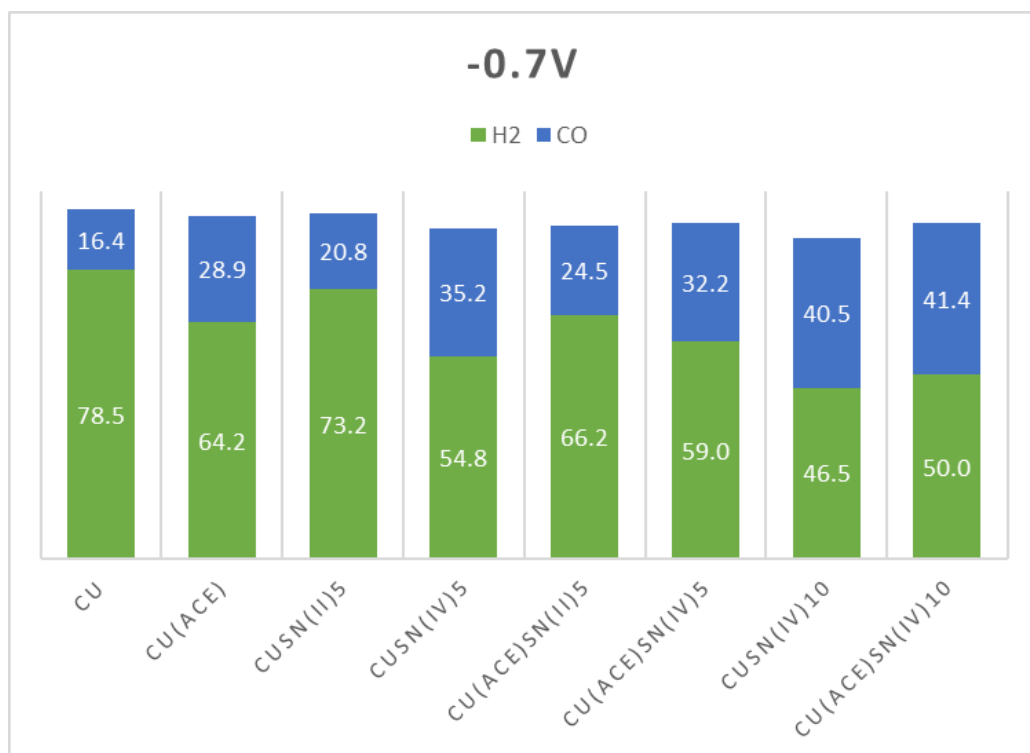


Fig.III.4 Efficienze faradiche per CO e H₂ dei campioni a -0.7V vs RHE.

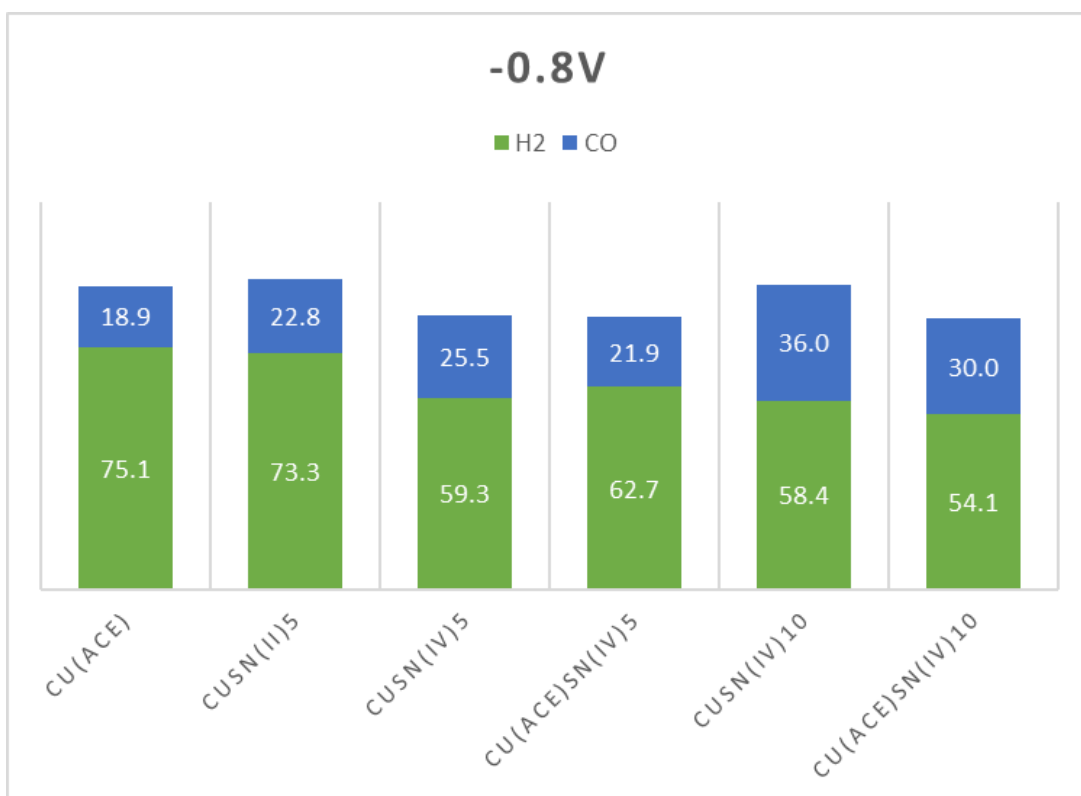


Fig.III.5 Efficienze faradiche per CO e H₂ dei campioni a -0.8V vs RHE.

Tab.III.3 Valori dei rapporti H₂/CO dei campioni ai diversi potenziali.

	Cu	Cu(Ace)	CuSn(II)5	CuSn(IV)5	Cu(Ace)Sn(II)5	Cu(Ace)Sn(IV)5	CuSn(IV)10	Cu(Ace)Sn(IV)10
-0.6V	3.9	3.9	2.4	2.4	3.8	1.7	2.1	1.2
-0.7V	4.8	2.2	3.5	1.6	2.7	1.8	1.1	1.2
-0.8V	-	4.0	3.2	2.3	-	2.9	1.6	1.8

I campioni che presentano morfologia cubica, mostrano migliori FE verso il CO a tutti i potenziali. Gli stessi campioni presentano, inoltre, valori di H₂/CO appropriati per la produzione di Syngas adatto a successive trasformazioni. In particolare, Cu(Ace)Sn(IV)5 produce una miscela che può essere usata nella sintesi di Fischer-Tropsch o nella produzione di metanolo (con valori di rapporto H₂/CO pari a circa 2); CuSn(IV)10 e Cu(Ace)Sn(IV)10 producono una miscela che presenta un rapporto H₂/CO vicino all'unità e pertanto idonea alla produzione di etanolo.

IV. CONCLUSIONI E FUTURI SVILUPPI

Lo scopo del lavoro è stato di sintetizzare e analizzare catalizzatori a base di Cu per la riduzione elettrochimica della CO₂.

I risultati hanno mostrato gli effetti positivi sulla attività catalitica dei campioni dell'aggiunta (in fase di sintesi) di sali di stagno. È, infatti, interessante notare come i sali di Sn non influenzino l'attività catalitica del materiale di per sé (in quanto lo stagno risulta in quantità trascurabili), ma indirettamente, in funzione dei cambiamenti morfologici.

I campioni sintetizzati utilizzando Sn(IV) mostrano un miglior comportamento per quanto riguarda sia le FE verso il CO che i valori del rapporto H₂/CO. Una possibile spiegazione può essere trovata nelle analogie in morfologia e composizione che i materiali presentano.

I materiali dovranno essere sottoposti a ciclo voltammetria (CV) e a spettroscopia elettrochimica di impedenza (EIS), per avere una caratterizzazione completa del materiale. Un altro aspetto da indagare in maniera più approfondita è la stabilità dei catalizzatori, tramite l'esecuzione di test dalla durata maggiore.

In conclusione, questo studio ha mostrato che la sintesi assistita da microonde permette di ottenere materiali paragonabili a quelli prodotti con classici processi di sintesi solvotermica, ma presentando un uso minore di energia e tempo e un migliore controllo dei parametri di processo.

I materiali sintetizzati presentano caratteristiche diverse a seconda dei precursori utilizzati e la loro concentrazione. Molti dei catalizzatori fabbricati sono risultati adatti all'impiego nella produzione di Syngas.

I risultati del lavoro sono promettenti e in linea sia con la necessità di trovare una soluzione al riscaldamento globale che con la necessità di usare carburanti alternativi a quelli fossili.

ABSTRACT

Global warming is a big issue in present days. The main reason for global warming is the high level of CO₂ concentration in the atmosphere, primarily due to the massive use of fossil fuels in human activities.

Different solutions have been evaluated, but the most promising one is the electroreduction of CO₂ approach.

In order to efficiently implement this solution, efforts have to be focused on the design and production of catalysts that are inexpensive, present good catalytic activity, are selective towards CO and other valuable products.

In this work, Cu-based catalysts were synthesised via microwave-assisted process by using a combination of a copper salt, chosen between CuSO₄ and Cu(CH₃COO)₂, and a tin salt (SnCl₂ or SnCl₄). Reference samples were synthesized without adding tin salts. All the samples are listed in Tab.1.

Tab.1 Samples produced

		CuSO₄	Cu(CH₃COO)₂
SnCl₂	45 mg (5 wt %)	CuSn(II)5	Cu(Ace)Sn(II)5
	45 mg (5 wt %)	CuSn(IV)5	Cu(Ace)Sn(IV)5
SnCl₄	90 mg (10 wt %)	CuSn(IV)10	Cu(Ace)Sn(IV)10
	0 mg (0 wt %)	Cu	Cu(Ace)

The materials fabricated were analysed regarding the morphology (FESEM), the composition (XRD and XPS) and the products of the CO₂RR (CA and GC). During the CO₂RR, CA and GC were performed concomitantly, placing the synthesised catalytic powder on GDL electrodes.

The analysis' results of each sample were interpreted and compared, in order to evaluate the effects of the precursors on the final catalyst.

The results show positive effects of Sn(IV) chloride when used as precursor, both regarding Faradaic efficiencies toward CO and the H₂/CO ratio, suitable for the production of Syngas. It is, in fact, showed in Fig.2 and Fig.3 that Sn(IV) had effects on the morphology of the produced catalysts. Further XPS and XRD analyses show that those fabricated with Sn(IV) chloride present similar morphology and composition.

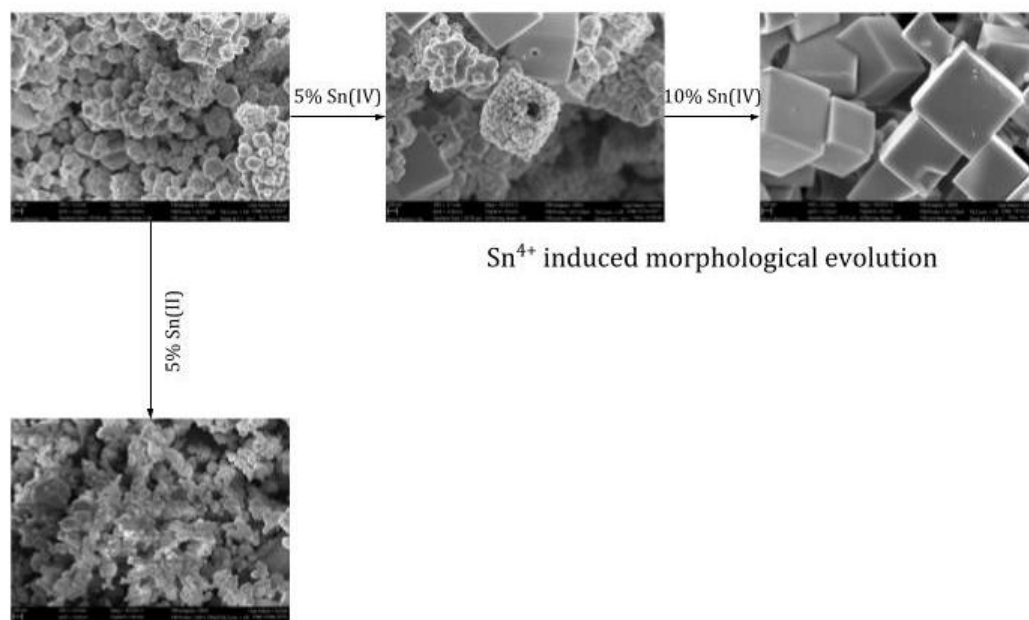


Fig.2 Effects of tin salts on morphology of catalysts fabricated with CuSO₄.

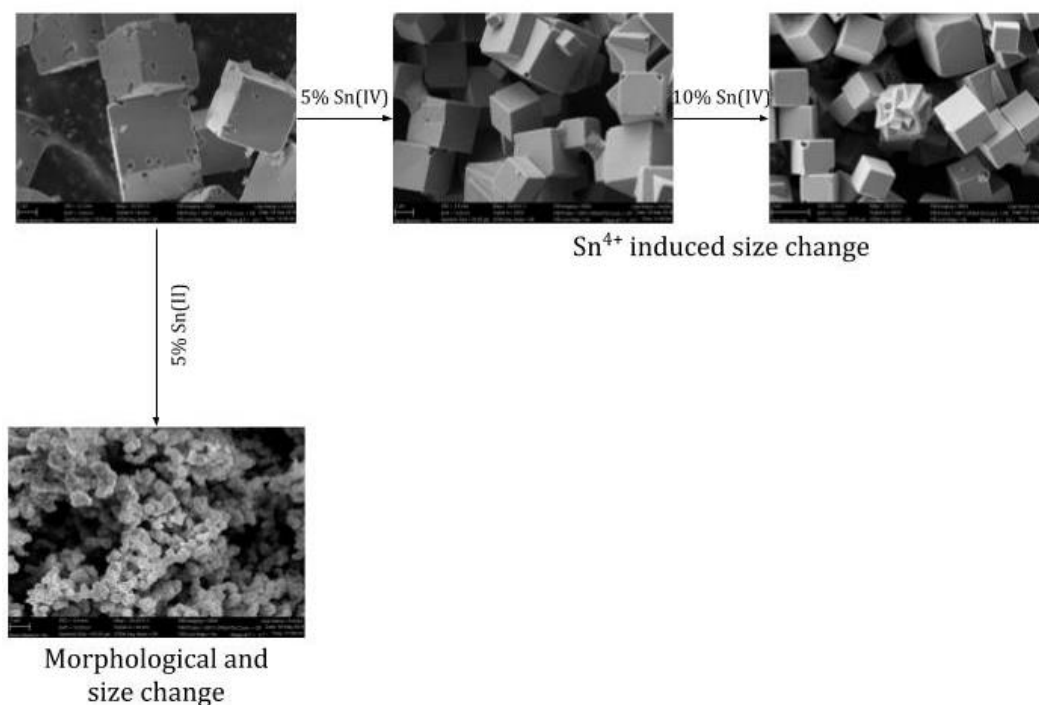


Fig.3 Effects of tin salts on morphology of catalysts fabricated with Cu(CH₃COO)₂.

Promising results were achieved with CA tests and product analysis by GC, but further investigations are needed to understand the electrochemical properties of various samples and to elaborate a kinetic model for the mechanism of electroreduction of CO₂.

1. INTRODUCTION

1.1 GLOBAL WARMING, CAUSES AND EFFECTS

Climate change and global warming are very actual topics, so that different movements have been created to sensitize people and strongly ask for measures against its causes and effects.

Climate change is a variation in the long period of the climate of the Earth of one of its regions.

Global warming is the increment of mean temperature on Earth's surface because of greenhouse gases (GHGs) [1].

Often the two definitions are used as synonymous, but it is clear that the second one concerns variation due to human action.

It has been estimated that average temperature¹ will rise more than 1.5°C between 2030 and 2052 compared to pre-industrial period [2], leading to very important consequences concerning all the earth system: melting glaciers and consequent rise in the level of the oceans and submersion of emerged lands; extreme weather conditions, such as tornadoes, floods, heat waves and cold waves; extinction of some plant and animal species; other events caused directly from the previous ones, difficult to predict with accuracy due to the multivariable nature of the climate.

In order to mitigate the global warming, several measures have been attempted: Kyoto Protocol failed in its goal of controlling emission of CO₂ from those countries that agreed and signed. Researcher and scientists joined in the Intergovernmental Panel on Climate Change (IPCC) to monitor and find solution to the problem of global warming. Alongside the official institutions, media and prominent personalities work to make people aware of the subject (one recent example is the teenager Greta Thunberg, who is currently nominated for the Nobel Prize for peace).

It has also been evaluated that reducing anthropogenic GHG emissions will be useful to limit heating, but not enough to stop it. This is because the accumulation of greenhouse gases (in particular, carbon dioxide) during the industrial era has had and is likely to have effects for centuries to come [5].

1.2 GREENHOUSE GASES AND GREENHOUSE EFFECT

Naturally the Earth is surrounded by greenhouse gases at a certain concentration. They act as a "blanket" on earth surface, making the environment warmer than what it would be.

When the concentration of greenhouse gases increases, the temperature consequently reaches values that are not desirable and dangerous for mankind as much as for all living beings.

¹Geographical and annual average temperature is meant. It has also been estimated that global warming is not homogeneous, but varies according to the area (for example, in the Arctic it is greater than in other regions and on land is greater than on the ocean) and to the time of year.

Main GHG are water vapor ² (H₂O_v), carbon dioxide (CO₂), nitrous oxides (NO_x) and methane (CH₄) [7]. Minor GHGs are represented by fluorinated gases (F-gases).

CO₂ is the most consistent part of GHG (approximately 76%) and the biggest percentage is due to industrial processes and the use of fossil fuels [3]. In Fig.1.1 the values of GHG emissions by gas and by economic sector are reported.

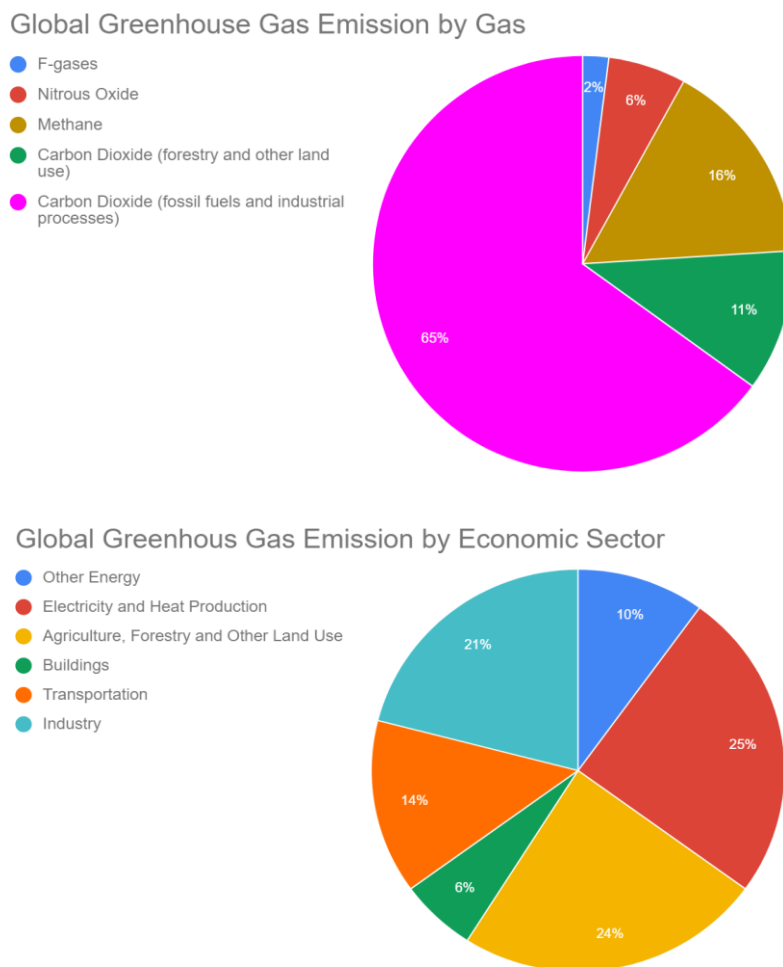


Fig.1.1 GHG global emission in 2010 [3,4].

It has been evaluated that the atmospheric concentration of CO₂ was about 270 ppm in early 1800s and reached 401.3 ppm in July 2015. Predictions say that by the end of this century CO₂ concentration will increase up to 600 ppm [8].

Those forecasts are confirmed by data from the Global Monitoring Division of the Earth System Research Laboratory: measurements are showing the fast increment of CO₂ concentration (Tab.1.1) and the trend in the last eighty years (Fig.1.2).

² Generally, in the description of the "greenhouse effect" phenomenon, the contribution of water vapor is not considered, as it is abundant in the atmosphere in a natural way and therefore "not anthropogenic".

1. Introduction

Tab.1.1 Values of CO₂ concentration in the atmosphere. Source: National Oceanic and Atmospheric Administration/Earth System Research Laboratory (www.esrl.noaa.gov/gmd/ccgg/trends/)

Year	ppm
2019	414.37
2018	410.77
2009	389.79

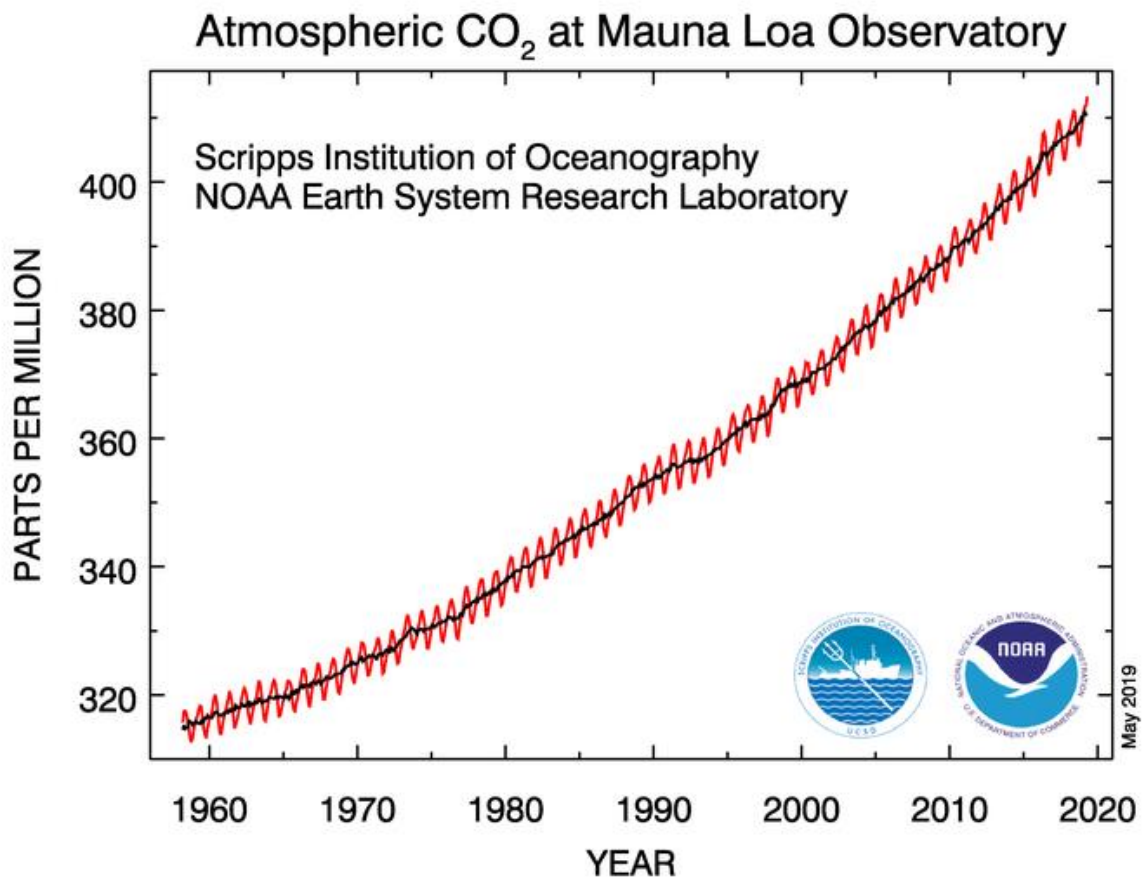


Fig.1.2 Atmospheric concentration of CO₂ from 1958. Red curve represents the measured data, whilst the black curve represents the seasonally corrected data. Source: National Oceanic and Atmospheric Administration/Earth System Research Laboratory (www.esrl.noaa.gov/gmd/ccgg/trends/)

The consequence of the great concentration of CO₂ is the greenhouse effect.

GHG are transparent to the components of short wavelength of solar radiation (UV and visible) but opaque to those of great wavelength (infrared). The infrared radiations emitted by the bodies heated by the sun are then "trapped", leading to an increase in temperature creating the so-called greenhouse effect (Fig.1.3).

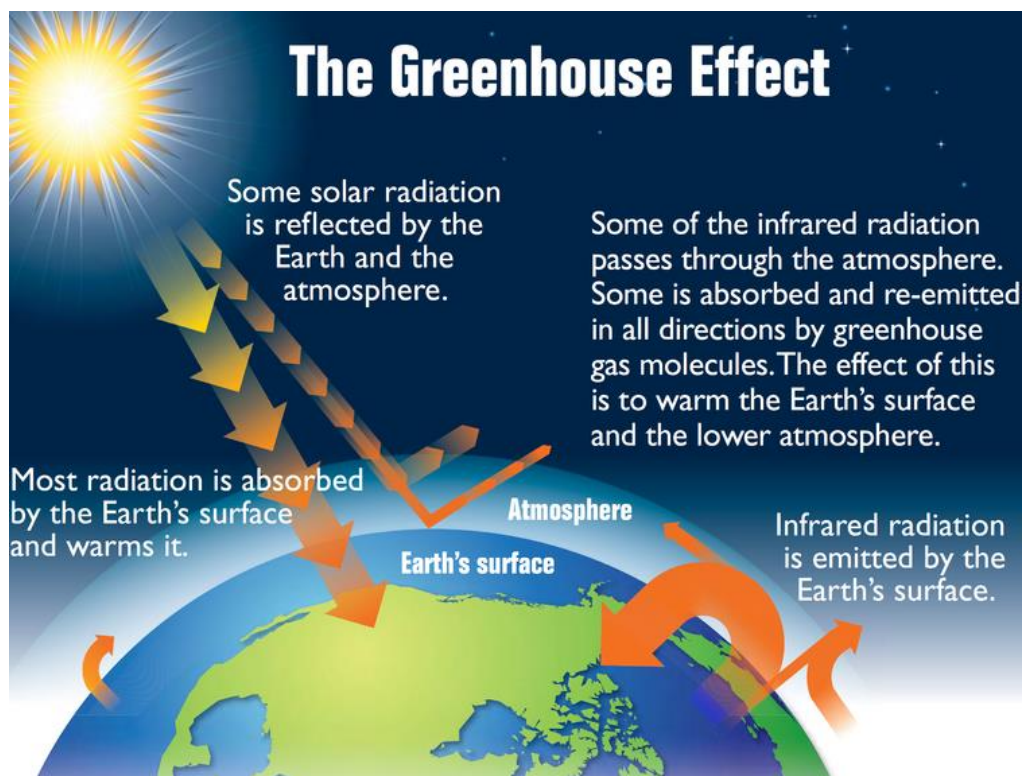


Fig.1.3 Greenhouse effect. Source: "The Greenhouse Effect" in: "Introduction," in: US EPA (December 2012) *Climate Change Indicators in the United States*, 2nd edition, Washington, DC, USA: US EPA, p.3. EPA 430-R-12-004. Author US EPA.

When talking about greenhouse gases and greenhouse effect it is important to introduce two parameters: Global Warming Potential (GWP) and Global Temperature change Potential (GTP). According to the IPCC, GWP is «an index measuring the radiative forcing following an emission of a unit mass of a given substance, accumulated over a chosen time horizon, relative to that of the reference substance, CO₂. The GWP thus represents the combined effect of the differing times these substances remain in the atmosphere and their effectiveness in causing radiative forcing» and GTP is «an index measuring the change in global mean surface temperature at a chosen point in time following an emission of a unit mass of a given substance, relative to that of the reference substance, CO₂. The GTP thus represents the combined effect of the differing times these substances remain in the atmosphere, their effectiveness in causing radiative forcing and the response of the climate system» [4].

As shown in Tab.1.2, CO₂ (which is used as reference) is not the most powerful component in the greenhouse effect, but since its concentration is the largest, it gives the biggest contribution. Hence, many of the efforts to fight the global warming are focused on reducing the carbon dioxide concentration.

Tab.1.2 GWP and GTP values for 20 and 100 years of main greenhouse gases [9].

	Lifetime (yr)	GWP 20	GWP 100	GTP 20	GTP100
CO₂	-	1	1	1	1
CH₄	12.4	84	28	67	4
N₂O	121	264	265	277	234
CF₄	50000	4880	6630	5270	8040
HFC-152a	1.5	506	138	174	19

1.3 CARBON CYCLE

According to J. Grace, «The carbon cycle is the circulation of carbon atoms between the ocean, land, and atmosphere by physical, chemical, and biological processes» [10].

There are two different types of processes involved in the carbon cycle: those carried by living organism (photosynthesis and respiration) and the “non-living” processes (physical and chemical dissolution of gases in water and the weathering of rocks).

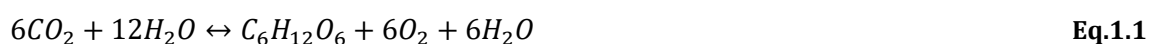
The natural proceeding of the carbon cycle has been altered by human activities since the Industrial Revolution because of the great use of fossil fuels. The effects are amplified by the deforestation.

Due to these factors, the carbon cycle can be defined “out of balance”. In fact, the concentration of carbon in the atmosphere is increasing with a rate of about 4 Gt C annum⁻¹.

Carbon is both stored in sinks and exchanged between different type of sinks (flux) (Fig.1.4).

1.3.1 LAND SINK

In the pre-industrialized age, the amount of CO₂ used in photosynthetic processes was likely in balance with the amount of CO₂ produced by respiration and combustion. This equilibrium can be represented by Eq.1.1:



In this equation, photosynthesis proceeds from left to right, whilst respiration and combustion proceed in the opposite direction.

Observational studies led to the conclusion that forests are the main sinks: in fact, it has been observed that concentration of CO₂ is lower in the air above forested areas.

The belief is that photosynthesis removes about 120 Gt C annum⁻¹, but approximately the half is produced by plants respiration. That given, the photosynthetic process exceeds the sum of autotrophic and heterotrophic respiration of about 2.4 Gt C. It is possible to conclude that the land sink removes globally approximately 29% of carbon released by fossil fuels combustion [10].

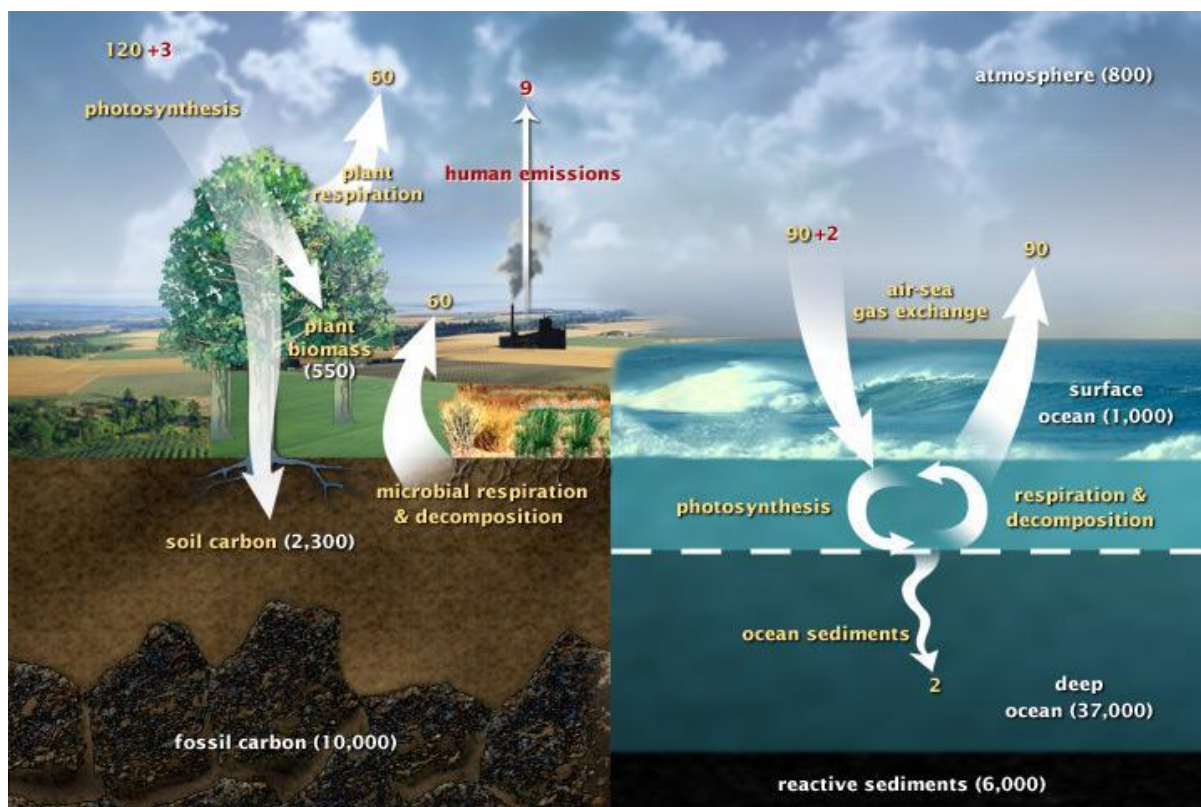
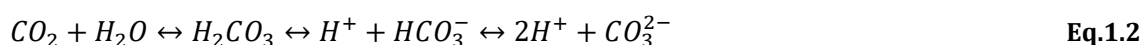


Fig.1.4 Carbon cycle. In yellow, natural fluxes (GigaTonnes/year); in red, anthropogenic carbon fluxes (GigaTonnes/year); in white, stored carbon (GigaTonnes). Source: <https://earthobservatory.nasa.gov/features/CarbonCycle>.

1.3.2 OCEAN SINK

There are two types of ocean sinks: the solubility sink and the biological pump.

The solubility sink is the dissolution of CO₂ in water, described by Eq.1.2



Since the dissolution varies with the temperature³, in warm areas of the ocean the reaction will proceed from right to left. Conversely, in colder areas, the reaction will proceed from left to right, with a rate depending on various factors, including the degree of saturation.

Part of the dissolved CO₂ is used by marine organisms to synthesize CaCO₃ for shells and bones. With the death of the organism, shells and bones reach the sea bed and carbon is removed by surface layers of the ocean. This process creates a concentration gradient that allows further dissolution of CO₂ in water. This mechanism is called biological pump.

Globally, the ocean sink removes approximately 2.3 Gt C, which corresponds to about 27% of carbon released by fossil fuel combustion [10].

³ According to Henry's Law, the lower is the temperature, the higher is the dissolution: at 0°C 3.4g CO₂ are dissolved in 1kg of water; at 10°C 2.5g and at 20°C 1.7g.

1.3.3 FLUX FROM LAND TO OCEAN

Part of the carbon in the land flows to the ocean. It has been estimated that around 1.9 Gt C annum⁻¹ is conveyed from the land to inner waters. 0.2 Gt C annum⁻¹ is trapped as sediment and approximately 0.8 Gt C annum⁻¹ goes back to the atmosphere as CO₂ and CH₄. The rest goes to the ocean and remains for a long time.

1.3.4 DEFORESTATION FLUX

Deforestation is a phenomenon where the number of trees in a certain area is drastically reduced by human action. The causes of deforestation are different and include: space for agriculture, industries and logging.

Deforestation is intimately related to a country development and growth. For example, in Europe, the deforestation rate increased with the increasing of the population before the Industrial Revolution and the activity was spread with colonization in North America and Australia. In the last 50 years, the deforestation targets have been humid tropics, such as Peninsular Malaysia forest.

It is supposed that the emission of CO₂ caused by deforestation is approximately 1.2 Gt C annum⁻¹ (corresponding to 14% of the total anthropogenic emission), although sometimes it has been said that the number is even higher [10].

On the opposite hand, it is estimated that the increment of fossil fuels use since 2000 has slowed down the global deforestation rate and in some countries the positive trend implies reforestation actions (Tab.1.3).

Tab.1.3 Percentage of forest area in 1990, 2010 and 2015 and variation in the period 2010-2015 [11].

	1990	2010	2015	change 2010-2015
AUSTRALIA AND NEW ZEALAND	17.4	16.8	17	0.2
EUROPE AND NORTH AMERICA	40.3	40.9	41	0.1
EASTERN AND SOUTHEAST ASIA	28.5	29.4	29.6	0.2
SUB-SAHARAN AFRICA	30.6	27.7	27.1	-0.6
LATIN AMERICA AND THE CARIBBEAN	51.3	47	46.4	-0.6
CENTRAL AND SOUTH ASIA	9.5	10	10	0
OCEANIA (excluding Australia and New Zealand)	70.1	70.1	70.1	0
NORTH AFRICA AND WESTERN ASIA	3.9	3.8	3.8	0
WORLD	31.6	30.8	30.6	-0.2

1.3.5 FOSSIL FUEL COMBUSTION

The emissions of CO₂ from fossil fuels have been increasing since 2000. The very fast industrial growth of populous countries like India and China is one of the causes of this condition, although the amount of CO₂ pro capita per year in these two countries is less than the emission pro capita in USA, Saudi Arabia, Australia and Canada.

The use of fossil fuels remains one of the biggest issues concerning CO₂ emission problem and searching for alternative sources of energy is a possible solution.

1.4 SOLUTIONS AND TECHNOLOGIES

As said in previous paragraph, global warming has been a concerning and the problem has been topic of discussion since the end of the Seventies. Scientists and researchers have been focusing on how to reduce emission of GHGs [6]. But according to our type of economy, which strongly relies on fossil fuels and on the consequent production of CO₂, and the accumulation of the same in the last two and a half centuries [4], decreasing the emission of carbon dioxide is only partially the answer against the greenhouse effect, answer that must include the trapping and the transformation of the great amount of CO₂ in the atmosphere [12].

Two paths have been considered during the last three decades to lower the concentration of CO₂ in the atmosphere: geological sequestration and molecular conversion.

Regarding geological sequestration, three approaches have been suggested and studied: injection of the gas in appropriate geological reserves (sedimentary rocks filled with oil or natural gas); injection of the gas in deep ocean, expecting it to stay for thousands of years; formation of carbonate rocks.

However, geological sequestration presents a big long-term concern: the possibility of leakage. In fact, CO₂ is very toxic for animals and humans over certain levels.

Molecular conversion is considered a better solution because it permits to synthesize chemicals from CO₂ that can be used. The processes to convert carbon dioxide are multiple and includes: chemical, photochemical, electrochemical, biological and inorganic transformations.

Among them, the electrochemical reduction has several advantages: the conversion is directly related to electrode potential, so that it can be controlled by applying different potentials [12, 16]; compact and up-scalable reactors can be used, as well as green chemicals as electrolytes [35]. In addition, electricity from renewable sources can be used, joining both a smaller production of CO₂ and the conversion of the same [14].

1.4.1 ELECTROREDUCTION

Electroreduction is a reduction reaction conducted in an electrolytic cell whose purpose is to drive non-spontaneous reactions by applying electrical energy (creating an electrons pump).

The electrolytic cell consists of two electrodes, one cathode and one anode, immersed in an electrolytic solution.

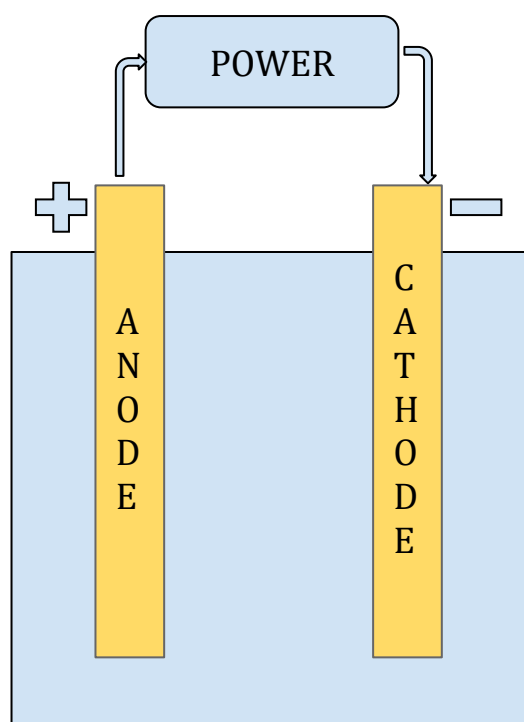


Fig. 1.5 Electrolytic cell. Reduction is at the cathode and oxidation at the anode.

The reduction is conducted on the cathode and the oxidation is conducted on the anode.

To measure how easy is to reduce or oxidize a chemical compound, it is common to refer to standard electrode potentials (E°) of the half reaction; since the potential of a single electrode is impossible to be experimentally determined, the standard hydrogen electrode (SHE) is used. Conventionally it is assumed that the SHE has a potential of 0.00V at standard conditions (25°C and 1 bar, 1N H^+).

Because of the difficulties in building an ideal system, often standard Nernst potential vs normal hydrogen electrode (NHE) is used (25°C and 1 M H^+).

1.4.2 ELECTROREDUCTION OF CO_2

CO_2 is a very stable molecule (free Gibbs formation energy: $\Delta G = -394 \text{ kJ mol}^{-1}$ and bonding energy $E_B = 750 \text{ kJ mol}^{-1}$), hence a great amount of energy is required to break the C=O bond and convert it into other products [13, 17].

In order to lower this energy both homogeneous and heterogeneous catalysts have been studied. The two present very different reaction mechanism and demand different electrochemical cells and experimental protocols [12]. In this work the focus is on heterogeneous type only.

Heterogeneous catalysts consist of solid catalytic particles deposited on a support and they are immersed in an aqueous solution saturated with CO_2 . The electrode containing the catalyst acts as cathode.

Electrochemical CO_2 reduction reaction (CO_2RR) involves multiple electron/proton transfer processes [13, 16] and leads to the formation of various products, such as CO, HCOOH, HCHO, CH_3OH and CH_4 regarding compounds with one carbon atom and HOCCOOH, C_2H_4 , C_2H_6

and CH₃CH₂OH regarding compounds with two carbon atoms [13]. Tab.1.4 reports electrode standard Nernst potentials (E°) and free Gibbs formation energy (ΔG) for reactions involving CO₂.

CO₂RR process promoted by heterogeneous catalysts consists of three steps: (a) adsorption of CO₂ on the catalysts surface; (b) activation with the formation of an intermediate and reduction of CO₂; (c) desorption of products [12, 13].

Tab.1.4 Standard potentials (25°C, pH=7) and free Gibbs energies (25°C, pH=0) for the conversion of CO₂ in various C1 products at standard conditions [3].

Half electrochemical reaction	E° (V vs NHE)	ΔG (kJ mol ⁻¹)
$\text{CO}_2 + 4\text{H}^+ + 4\text{e}^- \rightarrow \text{HCHO} + \text{H}_2\text{O}$	-0.48	27.5
$\text{CO}_2 + 2\text{H}^+ + 2\text{e}^- \rightarrow \text{HCOOH}$	-0.61	38.4
$\text{CO}_2 + 2\text{H}^+ + 2\text{e}^- \rightarrow \text{CO} + \text{H}_2\text{O}$	-0.53	19.9
$\text{CO}_2 + 6\text{H}^+ + 6\text{e}^- \rightarrow \text{CH}_3\text{OH} + \text{H}_2\text{O}$	-0.24	-17.3
$\text{CO}_2 + 8\text{H}^+ + 8\text{e}^- \rightarrow \text{CH}_4 + 2\text{H}_2\text{O}$	-0.38	-130.8
$\text{CO}_2 + \text{e}^- \rightarrow \text{CO}_2^{\bullet-}$	-1.9	183.32

As introduced above, CO₂ is a linear molecule with two equivalent C=O bonds (whose bonding energy is higher than C-C, C-H, C-O), it is very stable and therefore difficult to convert [12,13]. The main aim for catalysts is to break this linearity and to promote the formation of other types of bond. It is clear from Tab.1.4 that the majority of the products of interest do not require very high potential, except for the radical CO₂^{•-}, which is considered the intermediate for any other reaction. Hence, the formation of CO₂^{•-} is considered the first and kinetically limiting step and it is very important that the catalyst is able to reduce the overpotential of the formation and to increase the stability of the molecule once formed [3, 12].

Since CO₂RR is often conducted in aqueous solution, it is very easy for the hydrogen evolution reaction (HER) to take place concurrently or even replaces CO₂RR (due to its being kinetically more favourable) [3, 12]. It is possible to take advantage when the two reactions occur simultaneously to produce Syngas (which will be further discussed in the next paragraph), but this leads to another challenge: the design of catalysts that have a high CO₂ reduction rate and a high CO selectivity in order to reach the technological and commercial success of electroreduction of CO₂ [14].

Ideally, CO₂ can be reduced to form CO or other products at the potentials reported in table 1.4 (the potential of the water oxidation at the anode is $E^\circ=1.23\text{V}$ vs NHE) [3]; but, in reality, it requires a higher potential. The difference between the real potential and the ideal potential is defined as overpotential. The main causes of overpotential can be summarized in: (a) activation energy for the electron transfer to the CO₂ molecule; (b) ohmic losses caused by electrolyte and electrode conductivity; (c) mass transportation restraints. Because of this, it is possible to claim that, despite the values of E° and ΔG , CO is thermodynamically the easiest product to obtain: in fact, only two electrons are involved [3].

1. Introduction

To measure the rate of the reaction and the performance of the catalyst, the parameter used is the current density, which is defined as the electric current per geometric surface unit of the electrode. With the increasing of the current density, the reaction rate increases.

As previously said, different products can form simultaneously. To measure the selectivity regarding one product the Faradaic efficiency is used. Faradaic efficiency can be defined as:

$$FE = \frac{\text{electrons for the desired product}}{\text{total electrons}} \quad \text{Eq.1.3}$$

Ideally, the result of the sum of the FE for all the products should be 100% [3].

1.4.3 PARAMETERS OF ELECTROREDUCTION OF CO₂

The distribution of the products from the CO₂ reduction and its performance are influenced by several parameters: material used for the catalyst, configuration of the electrolytic cell, operational conditions (potential, pressure and temperature), morphology of the cathode, size of the catalytic particles, electrolytes, stability of the material [3,12].

Electrolytic cell configuration, in fact, affects the charge transfer phenomena. Electrolytic cells can consist of two compartment cells separated by a polymeric electrolyte membrane (PEM) not to allow anolyte and catholyte to mix; or one single cell with an electrolytic solution and containing both the anode and the cathode. A very important factor is the material supporting the catalyst particles: it can both be a gas diffusion layer (GDL) which allows the diffusion of the gas in microporosity or a non-porous material. Catalyst particle can also be deposited on the PEM. Often cation exchange membranes (CEM) are used to enhance the diffusion of cations from the anode in the cathode [3].

Temperature and pressure mainly influence the solubility of CO₂ in the electrolytic solution. In some experiments, it was showed that the overpotential decreases as the temperature increases, but the overpotential dropping has not been proven to be only related with temperature. It is possible to claim that the temperature affects the thermodynamic and the kinetic of the reaction, but also the different ohmic resistances (which decrease, leading to a lower overpotential), the conductivity (which increases), and size of the gas bubbles (which decreases, leading to a better contact with the electrolyte). Nevertheless, the CO₂ solubility decreases with the increasing of the temperature, leading to mass transport limitation and favouring HER [3].

CO₂ solubility increases with the pressure, but the main problem is building a reactor able to handle high pressure [3].

The electroreduction of CO₂ is deeply affected by the electronic properties of the cathode material, because it influences the energy for the intermediate species to bind and the activation energy [12]. Different materials have been studied in the last two decades [3, 14], with the aim of finding materials whose catalytic activity is comparable to or better of the one of noble metals. The material should present these characteristics: (a) high FE for CO₂RR (high selectivity); (b) high current density (high reaction rate); (c) good stability; (d) affordability [3, 14].

The topic will be elaborated on in section 1.6.

Solutions with high conductivity are used as electrolytes. Electrolyte affects the distribution of the products by altering the pH at the electrode and therefore the cell overpotential [3].

It has been observed that the morphology and the size of the catalytic particles affect the kinetic and the selectivity in CO₂RR [12]. This can be explained by the influence that geometry of the catalyst has on mass transfer and on the number of active sites. For example, it has been proven that the Faradaic efficiency increases when Cu nano-particles size decreases [15].

Stability and durability of catalysts for CO₂ reduction is one of the biggest problems [12, 14]. In fact, high FE and current density not always reflect large production of compounds from electrochemical reduction of CO₂.

Most of the papers do not report the duration of the experiments and if they do, usually the electrolysis was executed for less than 10 hours [3] as reported in Fig.1.6.

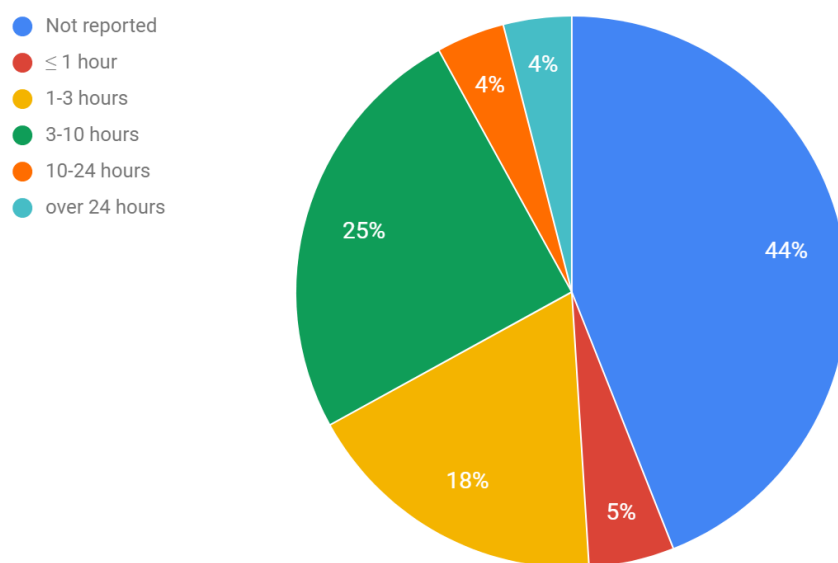


Fig.1.6 Experiment time for CO₂ reduction to CO reported in papers. Source: [3].

1.5 SYNGAS

As previously mentioned, the electroreduction of CO₂ is often accompanied by hydrogen evolution reaction, due to very similar standard potential. In Tab.1.5 are reported values of potentials for CO₂ reduction (V vs RHE⁴) for main compounds.

⁴ Reversible hydrogen electrode is a reference electrode.

1. Introduction

Tab.1.5 Reduction potential V vs RHE [16].

Half electrochemical reaction	V vs RHE
$\text{CO}_2 + 2\text{H}^+ + 2\text{e}^- \rightarrow \text{HCOOH}$	-0.22
$\text{CO}_2 + 2\text{H}^+ + 2\text{e}^- \rightarrow \text{CO} + \text{H}_2\text{O}$	-0.11
$\text{CO}_2 + 6\text{H}^+ + 6\text{e}^- \rightarrow \text{CH}_3\text{OH} + \text{H}_2\text{O}$	+0.03
$\text{CO}_2 + 8\text{H}^+ + 8\text{e}^- \rightarrow \text{CH}_4 + 2\text{H}_2\text{O}$	+0.17
$2\text{H}^+ + 2\text{e}^- \rightarrow \text{H}_2$	0.00

Hence, the reactions happening in the electrolytic cell are most likely two: electrolysis of H_2O (with development of H_2 on the cathode and O_2 on the anode) and reduction of CO_2 .

One way to exploit the competition between these two reactions is the production of syngas [3]. Syngas, in fact, is a mixture of H_2 and CO , whose ratio can be varied according to its subsequent use. Its value in petrochemistry is very high, since it is a precursor for many other interesting products [14].

Syngas can be used as an energy carrier (since it can be transformed in liquid fuels through Fischer-Tropsch process) [17] or converted into other useful products such as ammonia and alcohols (Fig.1.7).

Nowadays, Syngas is mainly produced from natural gas by steam reforming, a process that requires high temperature [17]. For this reason, much effort has been put in developing an electrochemical process that requires less energy and possibly from renewable sources and that allowed an easier control of H_2/CO ratio [3].

In order to achieve this aim, the configuration of the electrochemical reactor, the operation condition and the catalyst are very important parameters [3].

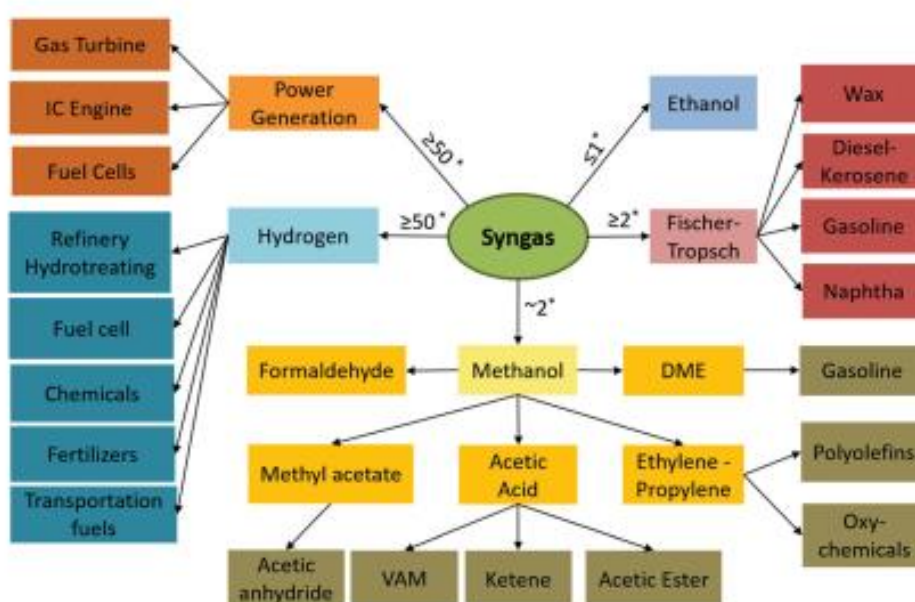


Fig.1.7 Products from syngas (* H_2/CO). Source: [3].

1.6 INTRODUCTION TO METHODS AND MATERIALS

1.6.1 COPPER AND TIN

Gold (Au) and silver (Ag) are very valuable catalyst materials for CO₂ reduction, due to their very high efficiency and selectivity towards CO.

Because of the very high price and deficiency of these noble metals, different studies have been focused on other materials, both precious metals (such as Pd and Rh) and non-precious metals (Cu, In, Bi, Mn, Fe, Mo, Ni, Sn and Zn) [3].

In the last years, the electrode materials have been categorized according to their ability to bind with the radical CO₂^{•-} and to reduce CO. Pb, Hg, In and Cd are part of Group 1, not exhibiting either bonding with the radical and reducing CO ability (producing formate or formic acid). In Group 2 are collected those metals (Au, Ag, Zn and Ga) with the ability of bonding CO^{•-} and producing CO. Cu is in the only metal in Group 3, able to bind CO^{•-} and reduce CO to higher molecular weight products [21].

Copper is a metallic element, historically used for coins: for this reason, Cu has good activity regarding reduction of CO₂ but has a low selectivity for CO [3, 12, 17]. Similar behaviour is shown by tin, which, as Cu, has greater selectivity for methane and formic acid [3, 12].

Nevertheless, it has been shown that by combining copper with tin leads to a higher selectivity towards CO [17], but further steps must be taken in this direction to study deeper the effects of combining these two metals.

1.6.2 MICROWAVE

Due to the growing interest in green chemistry, alternative processes for synthesis have been experienced. Microwave assisted synthesis is one of them and it has been greatly used for several reasons: increased reaction efficiency, improved product yield, more safety, decreased reaction time and required energy. Furthermore, compared to classic methods, the heating is uniform [18]. It has been proved that microwave-assisted synthesis is an environmentally friendly and time and energy saving method [19].

Microwave radiation is electromagnetic radiation with a frequency range between 30 GHz and 300 MHz. It is historically used for communication and heating food, but the need for improved synthesis processes opened the way to “microwave chemistry” [20]. Heating process happens as the radiation makes mobile electric charges in polar solvent move: kinetic energy is therefore transformed into heat by friction. This is referred as dipole interaction [20], as sketched in Fig.1.8.

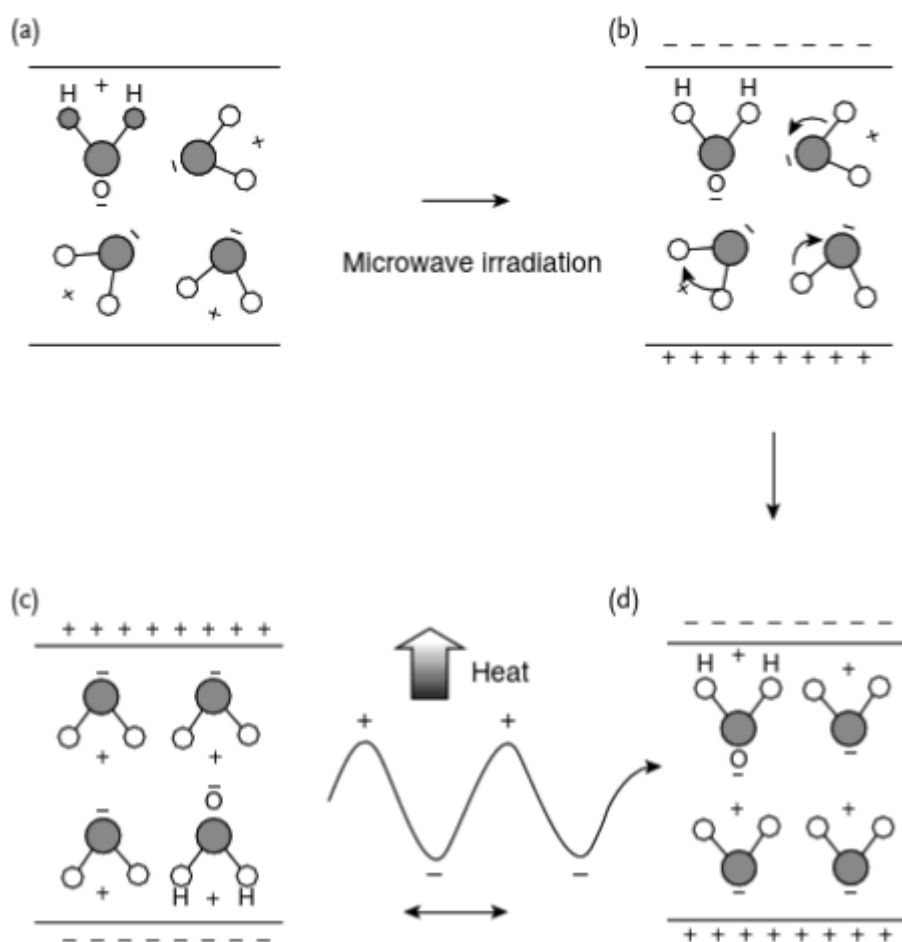


Fig.1.8 Dipole interaction mechanism of water molecules. Due to microwave radiation, polar molecules move and rotate to align to the varied electrical field. The kinetic energy turns into heat because of friction and collision. Source: [21].

1.7 AIM OF THE WORK

Due to the importance of finding a way to reduce CO₂ concentration in the atmosphere and limiting its further production, research is focused on designing and implementing affordable and efficient catalyst, with a high selectivity for CO (that can be used to produce Syngas or as a building block for other products) [3, 12].

The focus of this work is the production of Cu-based catalyst samples via microwave-assisted synthesis, using two salts of Cu and two salts of Sn as precursors; the characterization of the material (FESEM, XRD, XPS); the electrochemical analysis (Cyclic Voltammetry, Electrochemical Impedance Spectroscopy and Chronoamperometry); the evaluation of the products (Gas Chromatography). The results will be compared and discussed, in the perspective of future developments.

2. MATERIALS AND METHODS

2.1 MATERIALS

The materials used in the synthesis and the characterization of the catalysts are: tin(II) chloride dihydrate (SnCl₂·2H₂O, 99.9 %), tin(IV) chloride pentahydrate (SnCl₄·5H₂O, 98 %), copper(II) sulphate pentahydrate (CuSO₄·5H₂O, 99.0 %), copper(II) acetate hydrate (Cu(CH₃COO)₂·xH₂O, 98%), sodium hydroxide (NaOH, 98 %), potassium bicarbonate (KHCO₃, 99.7 %), ethylene glycol (EG, (CH₂OH)₂ 99.8 %), Nafion® 117 solution (5 wt.%) and isopropanol. These materials were purchased from Sigma-Aldrich.

In addition, acetylene carbon black (CB, Shawinigan Black AB50) and carbon paper equipped with gas diffusion layer (GDL; SIGRACET 28BC, SGL Technologies) were used.

Unless otherwise specified, all materials were used as received.

2.2 EXPERIMENTAL

The chosen precursors are two Cu salts and two Sn salts:

Cu:

- | | | |
|--|---------------------|-----------|
| ● CuSO ₄ | Copper(II) sulphate | “Cu” |
| ● Cu(CH ₃ COO) ₂ | Copper(II) acetate | “Cu(Ace)” |

Sn:

- | | | |
|---------------------|------------------|----------|
| ● SnCl ₂ | Tin(II) chloride | “Sn(II)” |
| ● SnCl ₄ | Tin(IV) chloride | “Sn(IV)” |

The powders were synthesized by combining one copper salt and one tin salt.

2.2.1 SYNTHESIS OF THE CATALYSTS

The Cu-based powder samples were fabricated via microwave-assisted solvothermal synthesis. Solvothermal synthesis is performed in an organic medium in a closed vessel at high pressures, and usually at temperatures higher than the boiling point of the solvent [23,24].

Samples were prepared with different concentrations of tin, namely 5 wt % and 10 wt %. According to this, the samples were named as “XYN”, where “X” is equal to “Cu” for samples produced with copper sulphate and to “Cu(ace)” for samples produced with copper acetate, “Y” is equal to “Sn(II)” for samples produced with tin(II) chloride and to “Sn(IV)” for samples produced with tin(IV) chloride, and “N” is equal to “5” for tin concentration equal to 5 wt % and to “10” for tin concentration equal to 10 wt %. Reference copper samples were also fabricated without adding tin salts. All the prepared samples are summarized in Tab.2.1.

The process consisted in several steps.

In the first step, 900 mg of copper salt and a proportionate amount of tin salt were dissolved in a solution of EG (20 mL) and H₂O (5mL) (solution 1).

2. Materials and methods

Afterwards, 1600 mg NaOH was dissolved in a solution of EG (30 mL) and H₂O (5 mL) (solution 2)

25 mL of solution 2 was added dropwise to solution 1.

After 10 minutes of vigorous agitation, the mixture turned blue and transparent (see Fig.2.1) and it was transferred into a Teflon vessel (100 mL volume, filled for about 2/3).

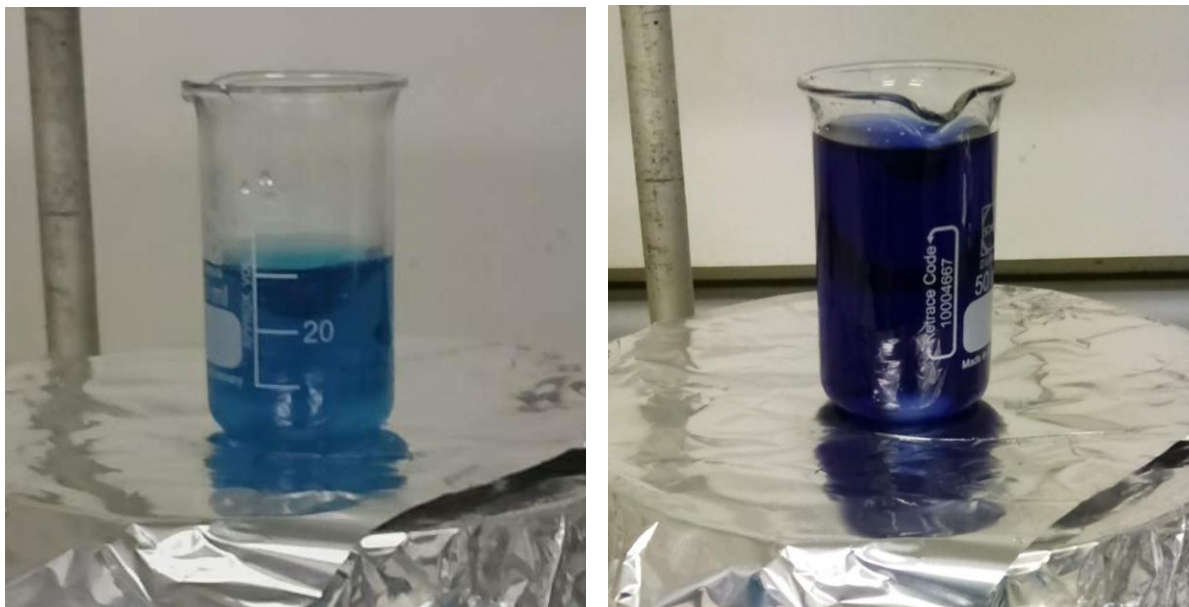


Fig.2.1 From left to right: solution 1; mixture of solution 1 and solution 2 after vigorous agitation.

The Teflon vessel was placed into a microwave oven and connected to pressure and temperature probes (Milestone STARTSynth, Milestone Inc., Shelton, Connecticut), as shown in Fig.2.2 and Fig.2.3

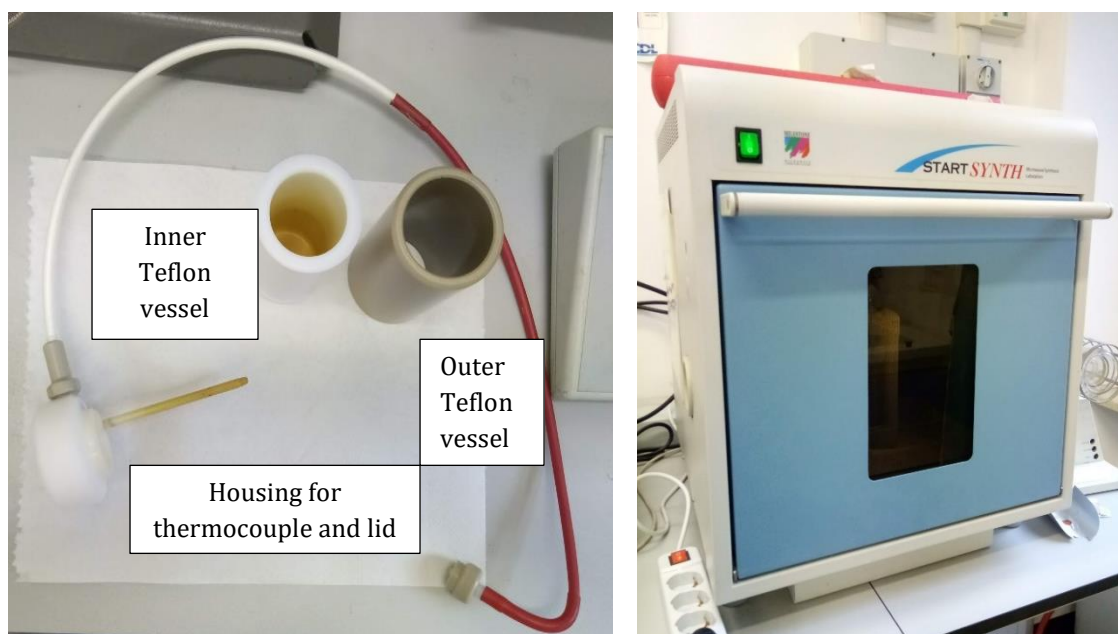


Fig.2.2 Teflon vessel components and microwave.



Fig.2.3 Vessel was assembled and placed in the microwave.

The mixture was irradiated for 10 min at 170°C (max. 900W). Stability of pressure and temperature were checked ($p_{\max} \cong 8$ bar, $T_{\max} \cong 180^{\circ}\text{C}$) through the screen of the machine (Fig.2.4).

The mixture was then cooled to ambient temperature and pressure in the oven.

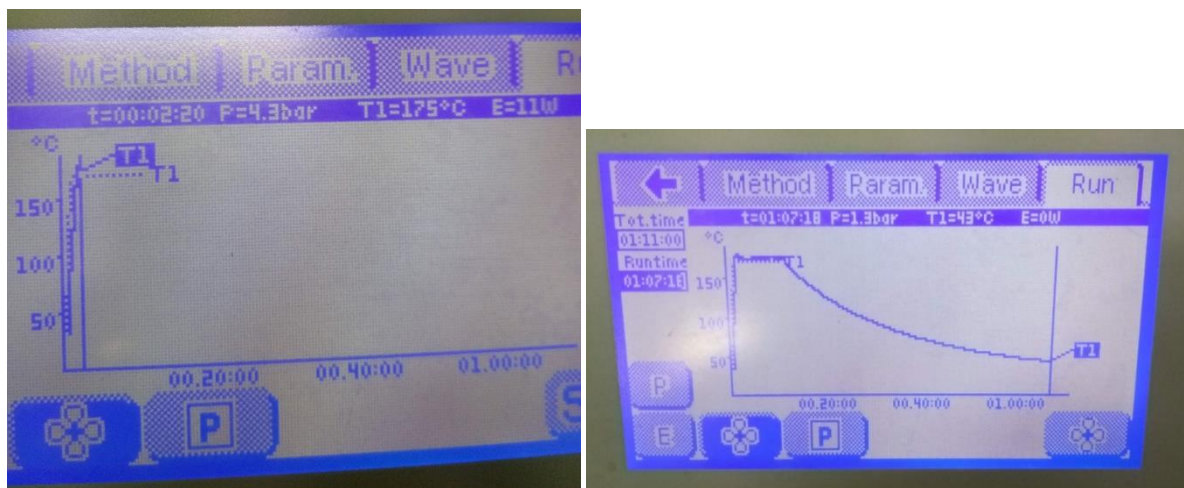


Fig.2.4 Curves showing the temperature trend during the process. Left: temperature at the beginning. Right: temperature while cooling.

The precipitate (Fig.2.5) was separated in a centrifuge and washed twice with H₂O (to remove sodium salts possibly formed or other decomposition products insoluble in EG) and once with ethanol (to remove residues of EG).

The washed precipitate was dried overnight in a vacuum oven at 60°C, obtaining a powder, as shown in Fig.2.6.

2. Materials and methods

Tab.2.1 Prepared samples.

		CuSO₄	Cu(CH₃COO)₂
SnCl₂	45 mg (5 wt %)	CuSn(II)5	Cu(Ace)Sn(II)5
SnCl₄	45 mg (5 wt %)	CuSn(IV)5	Cu(Ace)Sn(IV)5
	90 mg (10 wt %)	CuSn(IV)10	Cu(Ace)Sn(IV)10
No Sn salt	0 mg (0 wt %)	Cu	Cu(Ace)



Fig.2.5 Precipitate before separating and washing.

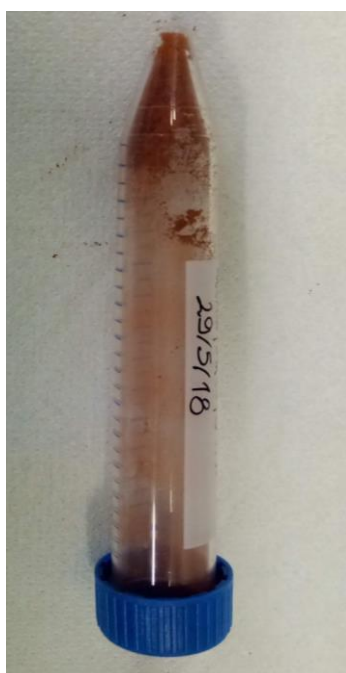


Fig.2.6 Catalyst powder after being dried overnight.

2.2.2 PREPARATION OF THE ELECTRODES

In order to fabricate the electrodes for CO₂RR, the prepared catalysts have to be supported on a current collector. A carbon paper equipped with GDL was chose to this aim. For each sample, an ink was prepared to coat the carbon paper.

15 mg of powder sample were mixed with 1 mg of CB. The function of CB is to make the electrode more conductive and porous.

90 μ L of Nafion® 117 and 240 μ L of isopropanol were added to the solid. Isopropanol was used as a solvent and Nafion® was used because of its ability of exchanging protons and its function as a binder.

The mixture was well mixed and sonicated for approximately 30 minutes, until a uniform ink was obtained (Fig.2.7).



Fig.2.7 Ink containing the catalyst powder, isopropanol and Nafion®.

The electrodes were prepared by cutting pieces of carbon paper with area of 2x2.5 cm². Cu tape was stick in the top and Teflon tape was used to cover the back and the edges of Cu tape, leaving an area of 2x1.5 cm² (Fig.2.8).

2. Materials and methods

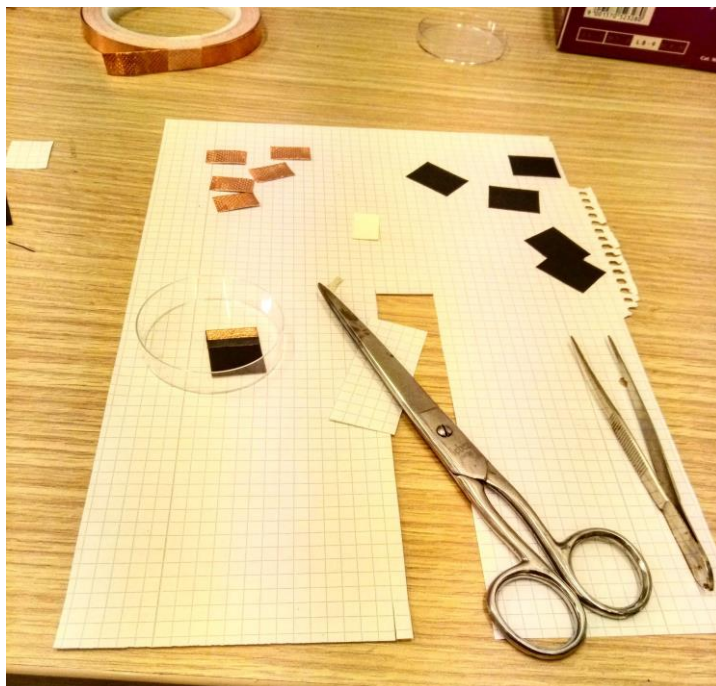


Fig.2.8 Preparation of carbon paper electrodes.

The ink was used to coat the carbon paper electrode. The obtained gas diffusion electrode (GDE) was dried at room temperature overnight. The different stages are shown in Fig.2.9.

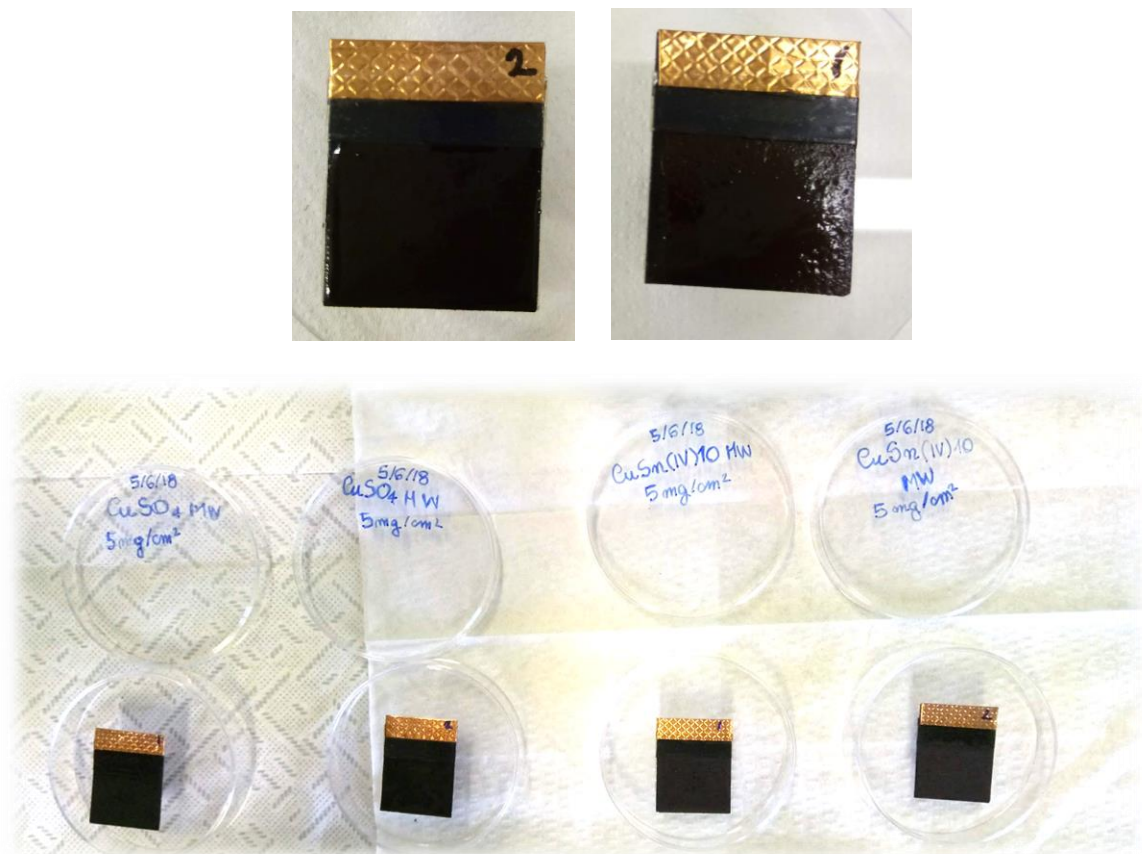


Fig.2.9 Coating of the carbon paper electrodes with the ink. From top left, clockwise: fresh ink; ink after ten minutes; completely dried electrodes.

The mass loading of Cu-based catalyst is 5 mg cm⁻².

2.3 CHARACTERIZATION AND ELECTROCHEMICAL ANALYSIS

The catalytic material was analysed through several analytic techniques, with the aim to characterize the morphology, the composition, the electrochemical properties and the products. Hence, the characterization techniques consisted of: Field-Emission Microscopy (FESEM), X-Ray Diffraction (XRD), X-Ray Photoelectron Spectroscopy (XPS), Chronoamperometry (CA) and Gas Chromatography (GC).

2.3.1 FIELD-EMISSION SCANNING ELECTRON MICROSCOPY (FESEM)

Scanning electron microscopy (SEM) is a morphological technique used since the middle Thirties thanks to its high resolution even in a nanometric scale.

Scanning electron microscopes work by emitting a beam of electrons (primary electrons) to hit the surface of the sample. The electrons on the material surface (secondary electrons) are therefore dislodged by the primary electrons attracted by a griddle positively charged. Secondary electrons are recorded and elaborated in an image of the morphology of the material [25].

FESEM is an analysis where electron emission is induced by an electrostatic field. FESEM, compared to SEM, has a higher resolution due to a narrower energy distribution, but needs larger electric field [26].

A scanning electron microscope consists of three main part: a column, where the electron beam is produced and focused under high-vacuum conditions (less than 10⁻⁸ Torr) [25, 26]; the chamber where samples and detector are located (under vacuum conditions); the monitor, where the images of the sample are shown.

The powder samples were analysed with FESEM, ZEISS Auriga.

2.3.2 X-RAY DIFFRACTION (XRD)

X-ray diffraction is a technique used to identify the crystallographic structure of a material. It is based on the elastic scattering of X-rays when they hit the electron clouds of single atoms of the investigated material [27].

Diffraction is described by Bragg's Law (Eq. 2.1):

$$n\lambda = 2d\sin\theta \quad \text{Eq.2.1}$$

where λ is the wavelength of the incident wave, n is an integer, d is the distance between two crystal planes and θ is the incident angle, as shown in Fig.2.10.

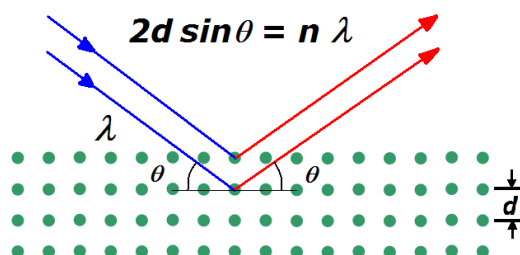


Fig.2.10 Representation of Bragg's Law.

To eliminate the unwanted wavelengths as much as possible, monochromatic x-rays are needed [27, 28].

The main components of hardware for an XRD analysis are an X-ray source and an X-ray detector.

XRD was implemented in Bragg-Brentano symmetric geometry by using a PANalytical X'Pert Pro instrument (Cu-K α radiation, 40 kV and 30 mA) equipped with an X'Celerator detector

2.3.3 X-RAY PHOTOELECTRON SPECTROSCOPY (XPS)

XPS is a technique used to investigate the chemical elements in the surface of material.

The principle is to make the material eject an electron (called X-ray photoelectron) from an electron shell of an atom through an X-ray photon (Fig.2.11). Depending on the binding energy, the ejected electron will present a defined kinetic energy. By measuring the kinetic energy, it is possible to evaluate the binding energy through Eq. 2.2:

$$E_B = h\nu - E_K - \phi \quad \text{Eq.2.2}$$

where E_B is the binding energy, E_K is the kinetic energy, ϕ represent the energy required for an electron to be ejected, h is Planck's constant and ν is the frequency [28].

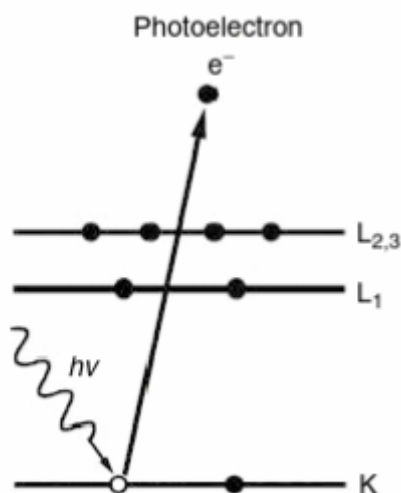


Fig.2.11 Ejecting phenomenon induced by X-ray photon. Source: [28].

XPS was executed with a PHI 5000 VersaProbe (Physical Electronics) system. The X-ray source was a monochromatic Al K α radiation (1486.6 eV). Spectra were analysed using Multipak 9.7 software.

2.3.4 CHRONOAMPEROMETRY (CA)

During chronoamperometry measurements, the potential is shortly brought to the chosen value, and then maintained. The electrolysis current is recorded in time. As long as the potential is applied, the electroreduction takes place, and the formation of reaction products is carried out. Constant current values imply catalyst stability, while decreasing values indicate the consumption of the electroactive species [33].

An electrolytic cell was prepared as shown in Fig.2.12.

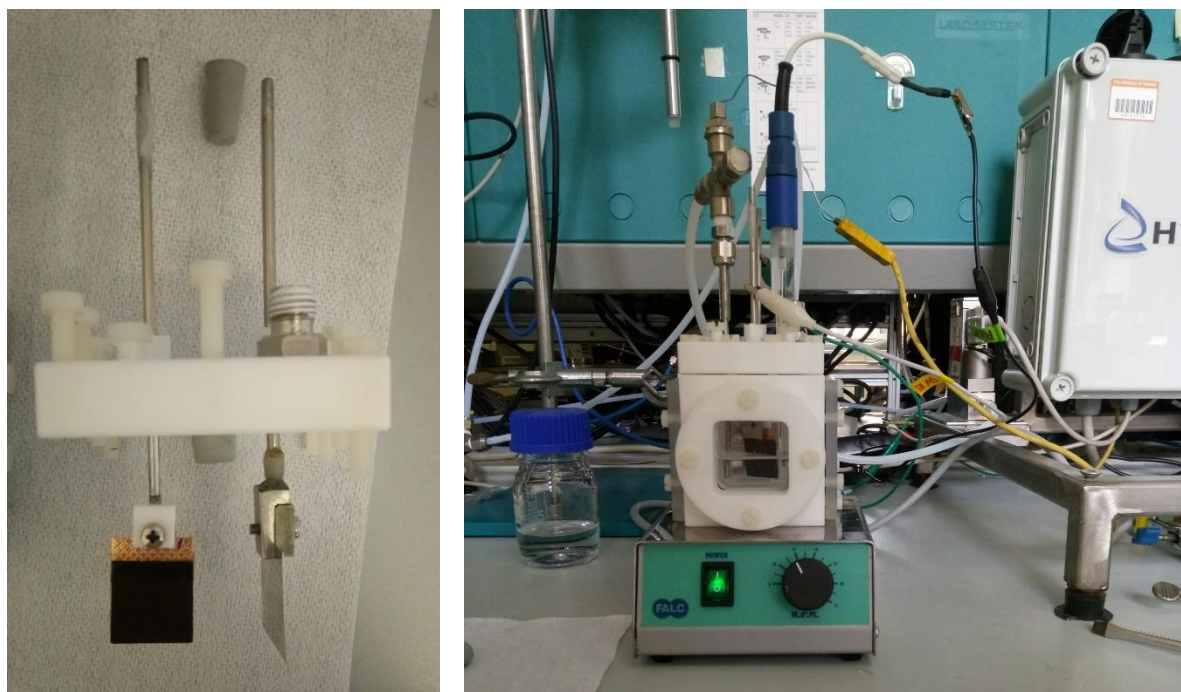


Fig.2.12 Electrolytic cell set up for CA and GC tests.

The tests were performed at room temperature in 60mL of electrolytic solution (KHCO₃ 0.1M) saturated with CO₂. Bio-Logic electrochemical workstation was used. A platinum plate was used as counter electrode. Pt is used because of being conductive and inert. Ag/AgCl (NaCl 3M) was used as reference electrode. The tip of the reference electrode touching the solution is made by porous glass to allow the diffusion of electrons and to avoid the loss of electrolyte. The aim of the reference electrode is to check the potential applied to the cathode.

Working, reference and counter electrodes were connected to the working station, as schematized in Fig.2.13.

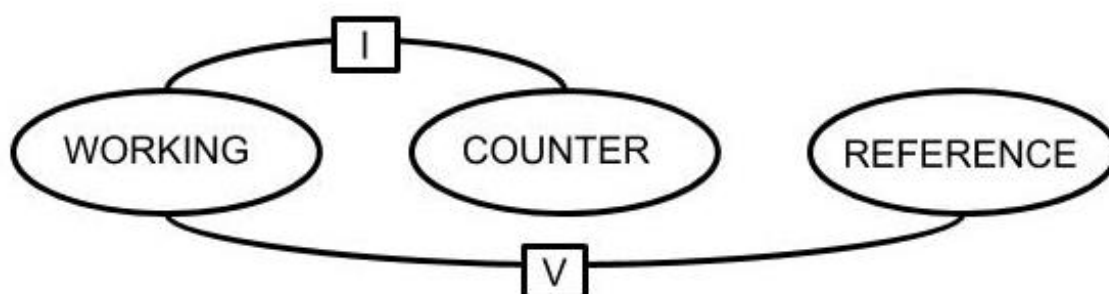


Fig.2.13 Scheme of the connection for electrochemical analysis.

Various potentials vs RHE (-0.8V, -0.7V, -0.6V) were evaluated. Each potential was corrected by compensating the ohmic potential drop, of 85% by the instrument (iR-compensation).

2.3.5 GAS CHROMATOGRAPHY (GC)

Gas chromatography is an analytical technique whose goal is to separate different gases in a mixture. The separation is led in a column containing a fixed (or stationary) phase, showing a large surface. The components in the mixture (that flows through the column) interact differently with fixed phase when reaching equilibrium, resulting in the separation of the different molecules [34].

As shown in Fig.2.14, gas chromatographs consist mainly of a column (where the separation happens), an injector (needed to guarantee that the sample is homogeneous when inserted in the column) contained in a chamber with a controlled temperature and a detector (which provides qualitative and quantitative information).

In the present work, gas chromatography was employed during chronoamperometry tests, in order to on-line monitor the formation of gaseous reaction products. The micro gas chromatograph (μ GC, Fusion®, INFICON) was equipped with two channels with a 10m Rt-Molsieve 5A column and an 8m Rt-Q-Bond column, respectively, and micro thermal conductivity detectors (micro-TCD). The used carrier gas was argon.

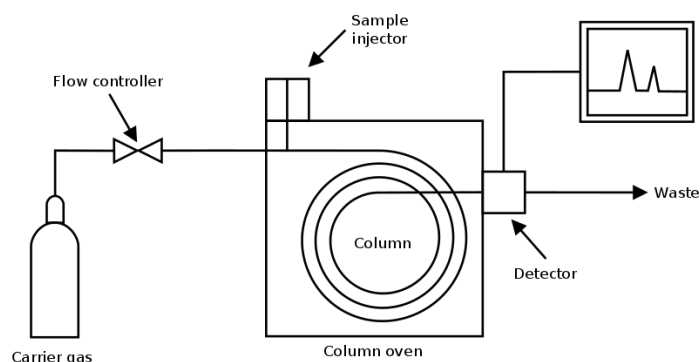


Fig.2.14 Typical configuration of a gas chromatograph. A carrier gas (inert gas) is required to have a controllable and constant flow of the mixture.

Gas products were analysed during the CA with a micro gas chromatograph (μ GC, Fusion®, INFICON). The humidity of the gas products was removed before entering the column by a GENIE filter.

A constant CO_2 flow was maintained with a rate of 38mL min^{-1} , in order to saturate the electrolyte and take out gaseous products.

3. RESULTS AND DISCUSSION

In this section, the obtained results will be presented and discussed. Results for each synthesized catalytic powder will be shown and therefore compared.

3.1 CHARACTERIZATION OF THE MATERIAL

3.1.1 FESEM

3.1.1.1 Cu

This sample was prepared without addition of Tin salt.

From the morphological characterization by FESEM (Fig.3.1), it is possible to see the irregular shape of the particles. Furthermore, the distribution of the size is wide, ranging from a few tens of nanometers to a micrometer.

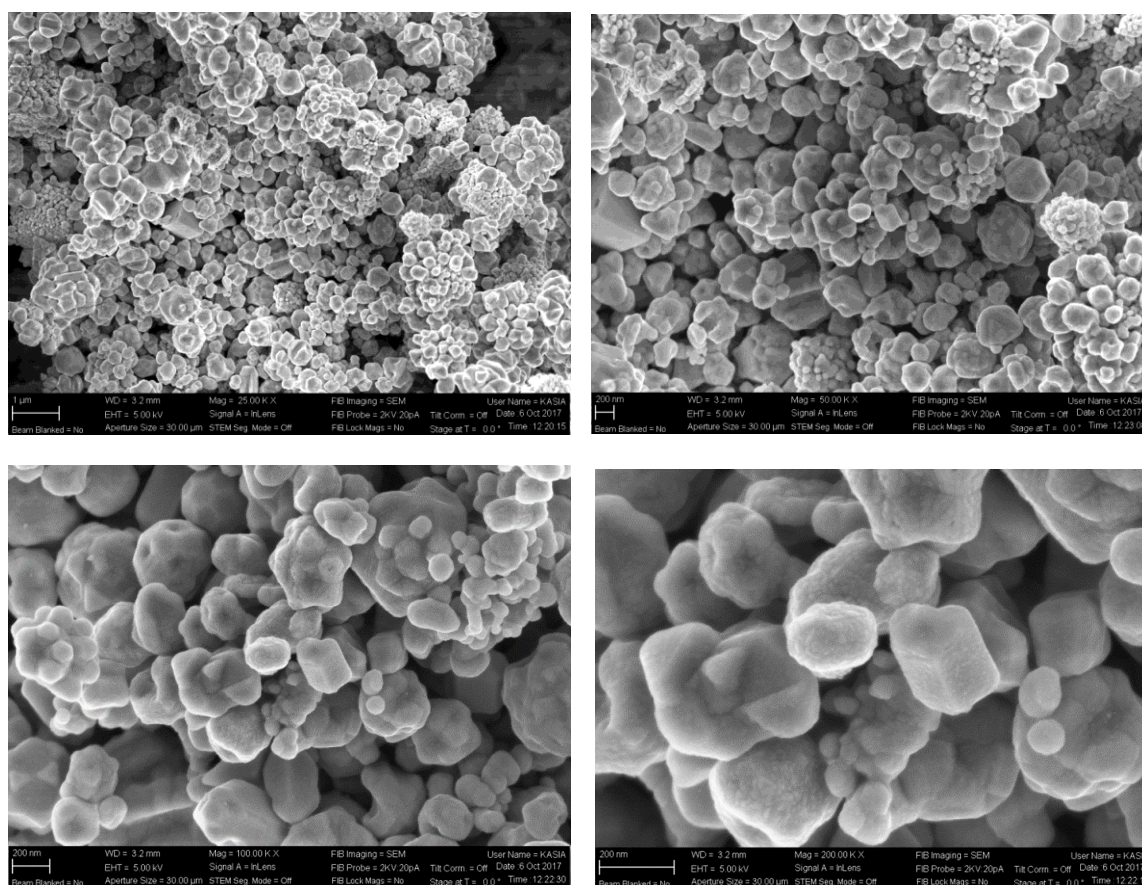


Fig.3.1 FESEM morphological characterization of the sample Cu.

3. Results and discussion

3.1.1.2 Cu(Ace)

In Fig.3.2, it is possible to see particles presenting a cube shape with rough surface and size of approximately 10 μ m. The sample presents a narrower size distribution compared to sample "Cu".

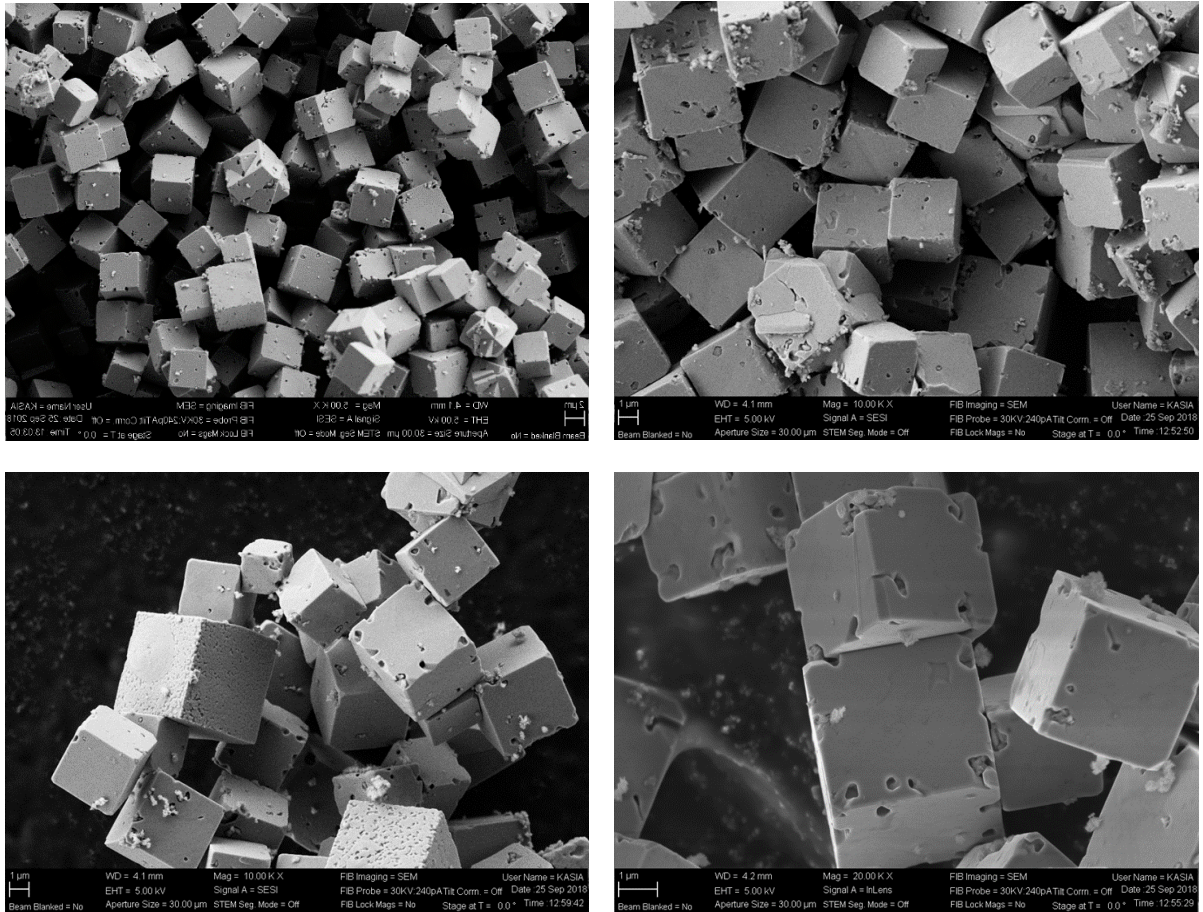


Fig.3.2 FESEM morphological characterization of the sample Cu(Ace).

3.1.1.3 CuSn(II)5

The catalyst shows irregular shaped particles, with a diameter of less than 100 nm (Fig.3.3). Except for few particles, the size distribution is narrow.

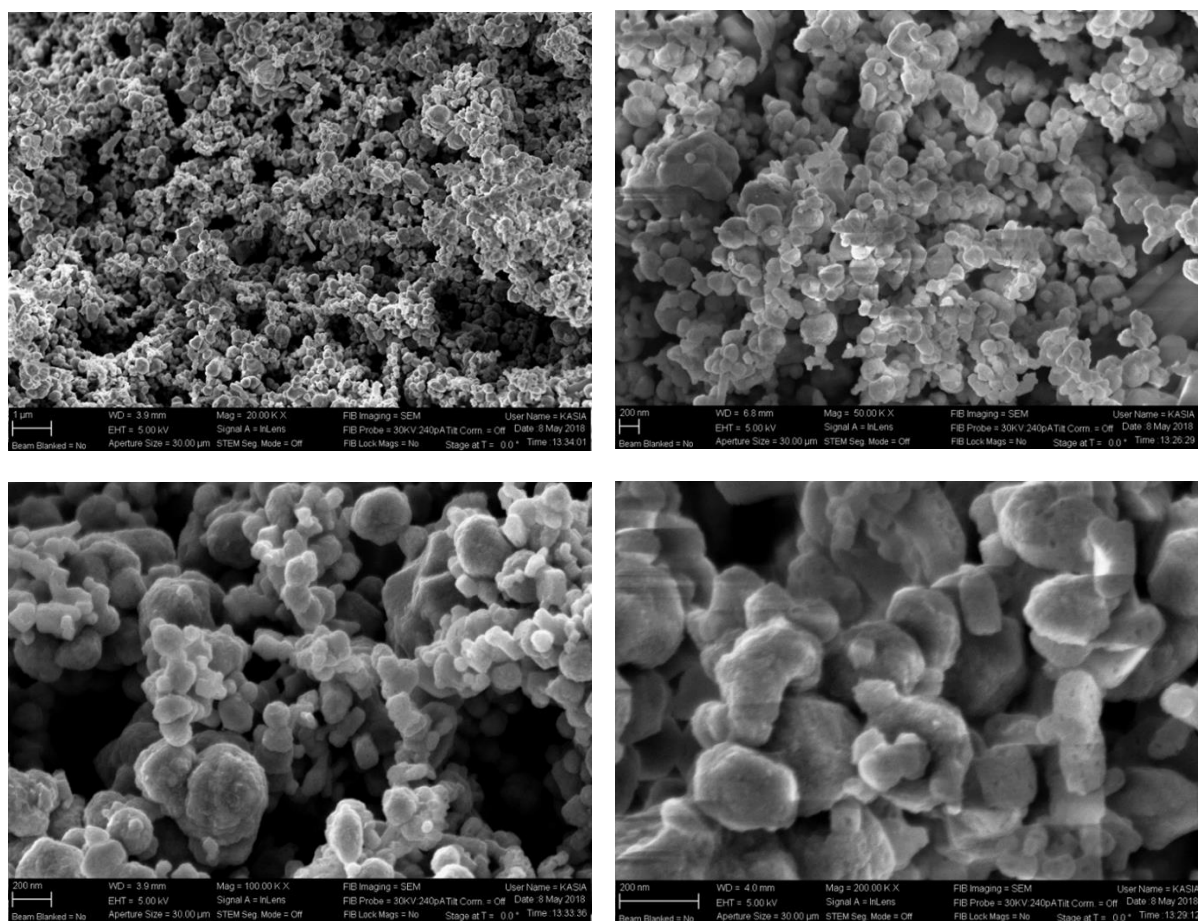


Fig.3.3 FESEM morphological characterization of the sample CuSn(II)5.

3. Results and discussion

3.1.1.4 $Cu(Ace)Sn(II)5$

From the FESEM analysis, in Fig.3.4 particles with irregular shape are displayed, whose edges are sharper when compared with previous samples with irregular particles. The size is of the order of a few hundreds of nanometers. The size distribution is in a limited range.

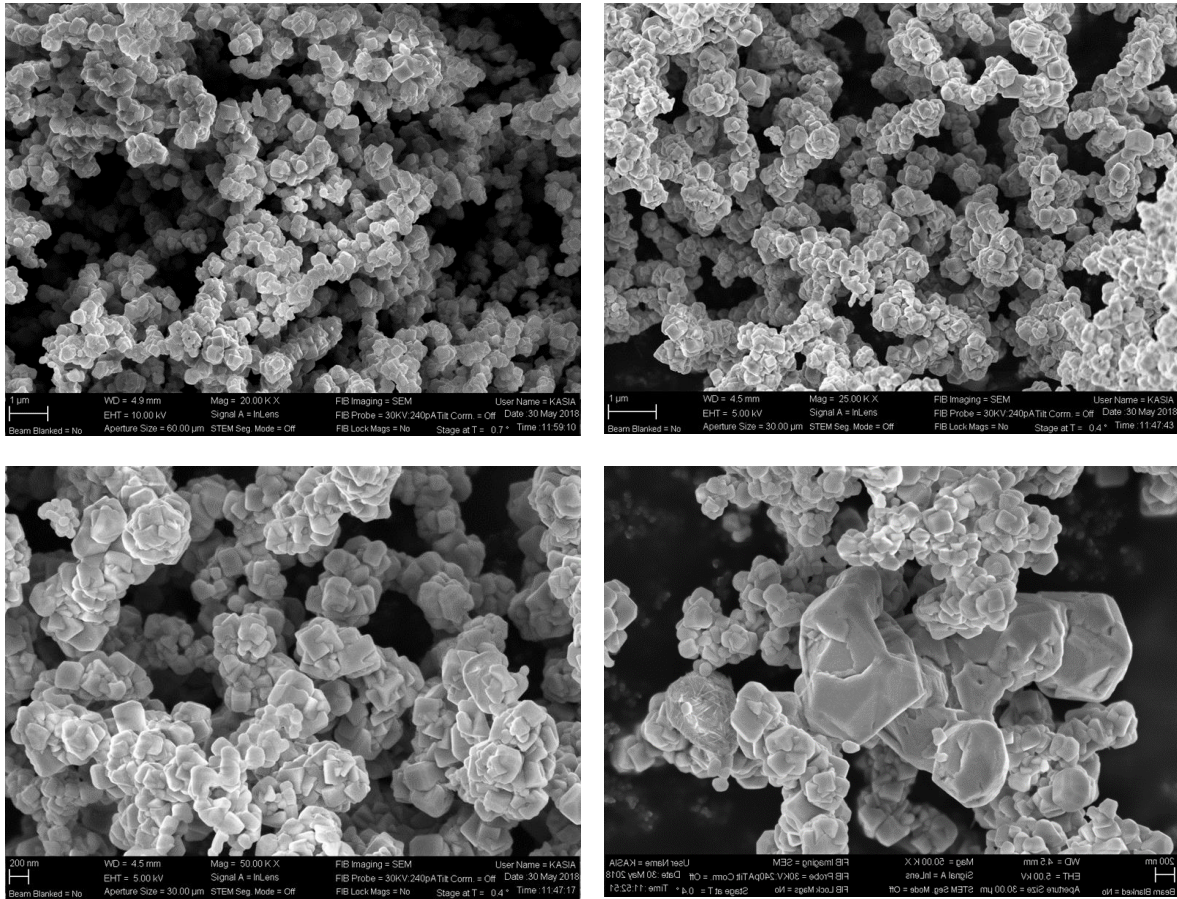


Fig.3.4 FESEM morphological characterization of the sample $Cu(Ace)Sn(II)5$.

3.1.1.5 CuSn(IV)5

The sample exhibits irregularly shaped particle with some cube shaped exceptions (Fig.3.5). The size is variable (between 100nm and few μm). From the FESEM images it is possible to appreciate the formation process of a cubic structure.

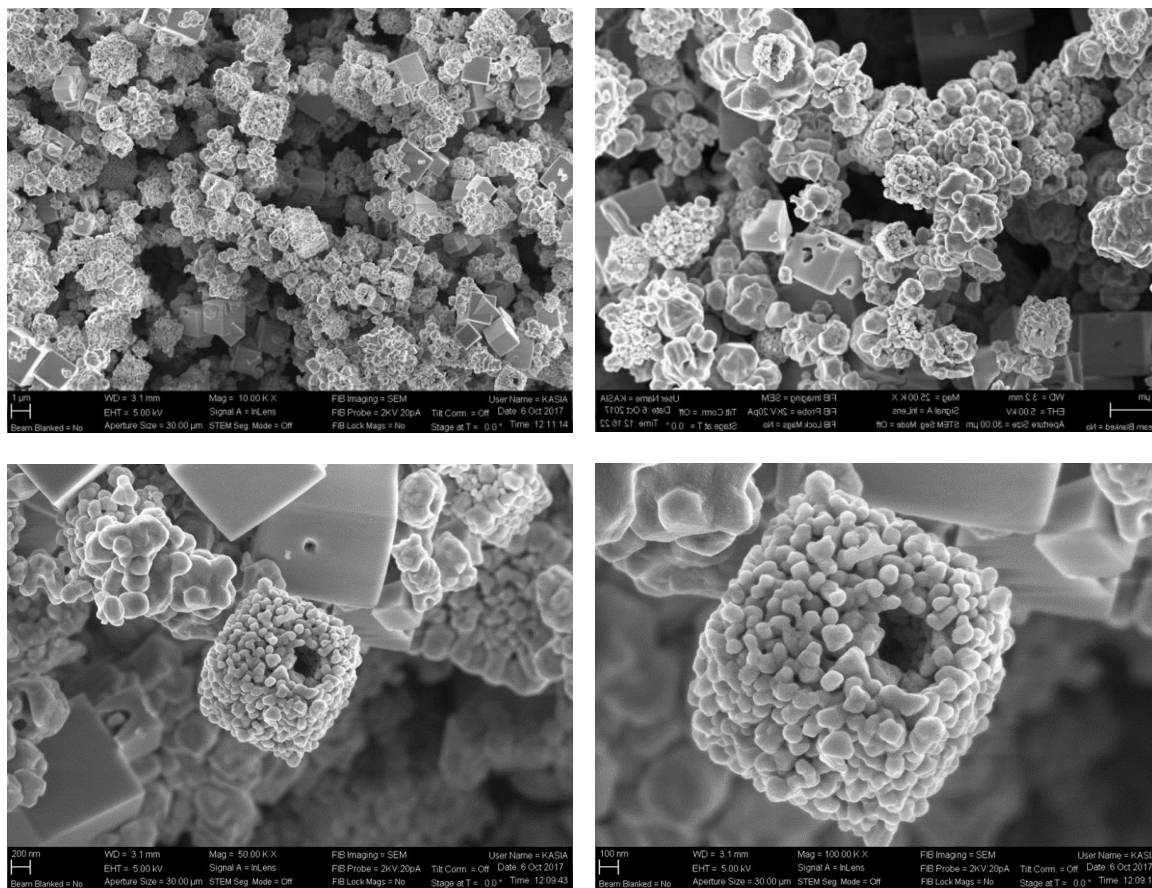


Fig.3.5 FESEM morphological characterization of the sample CuSn(IV)5.

3. Results and discussion

3.1.1.6 $Cu(AcE)Sn(IV)5$

As shown in Fig.3.6, particles are cubic and some exhibit flaws on the surface. The size distribution is mostly narrow and of the order of $2\mu\text{m}$ regarding the side.

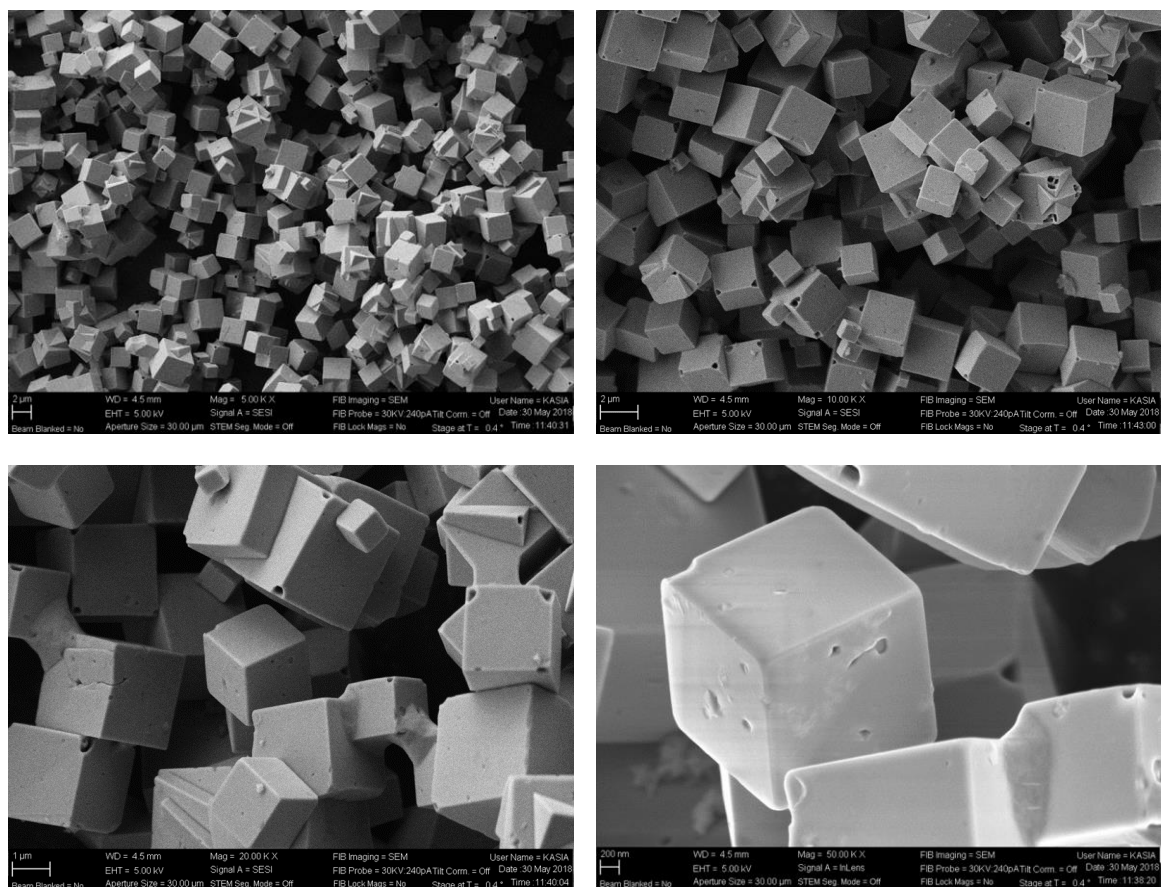


Fig.3.6 FESEM morphological characterization of the sample $Cu(AcE)Sn(IV)5$.

3.1.1.7 CuSn(IV)10

Fig.3.7 shows particles with a cubic shape. Some particles present defect on the surface and incorporations with each other. The size of the particles is of 1-2 μm and the size distribution is in a limited range.

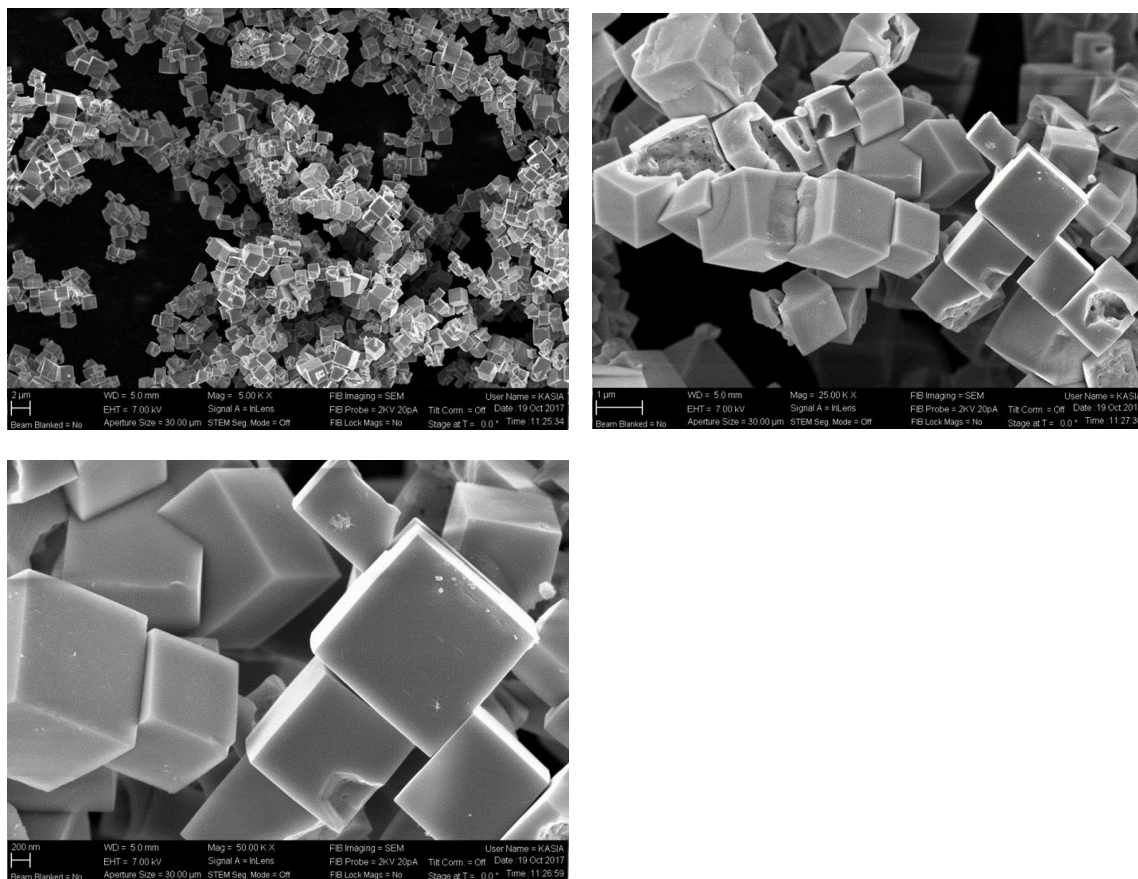


Fig.3.7 FESEM morphological characterization of the sample CuSn(IV)10.

3. Results and discussion

3.1.1.8 $Cu(AcE)Sn(IV)10$

In Fig.3.8 are presented cubic particles, with similar size and size distribution as the $CuSn(IV)10$ sample. Some particles show a polyhedral shape.

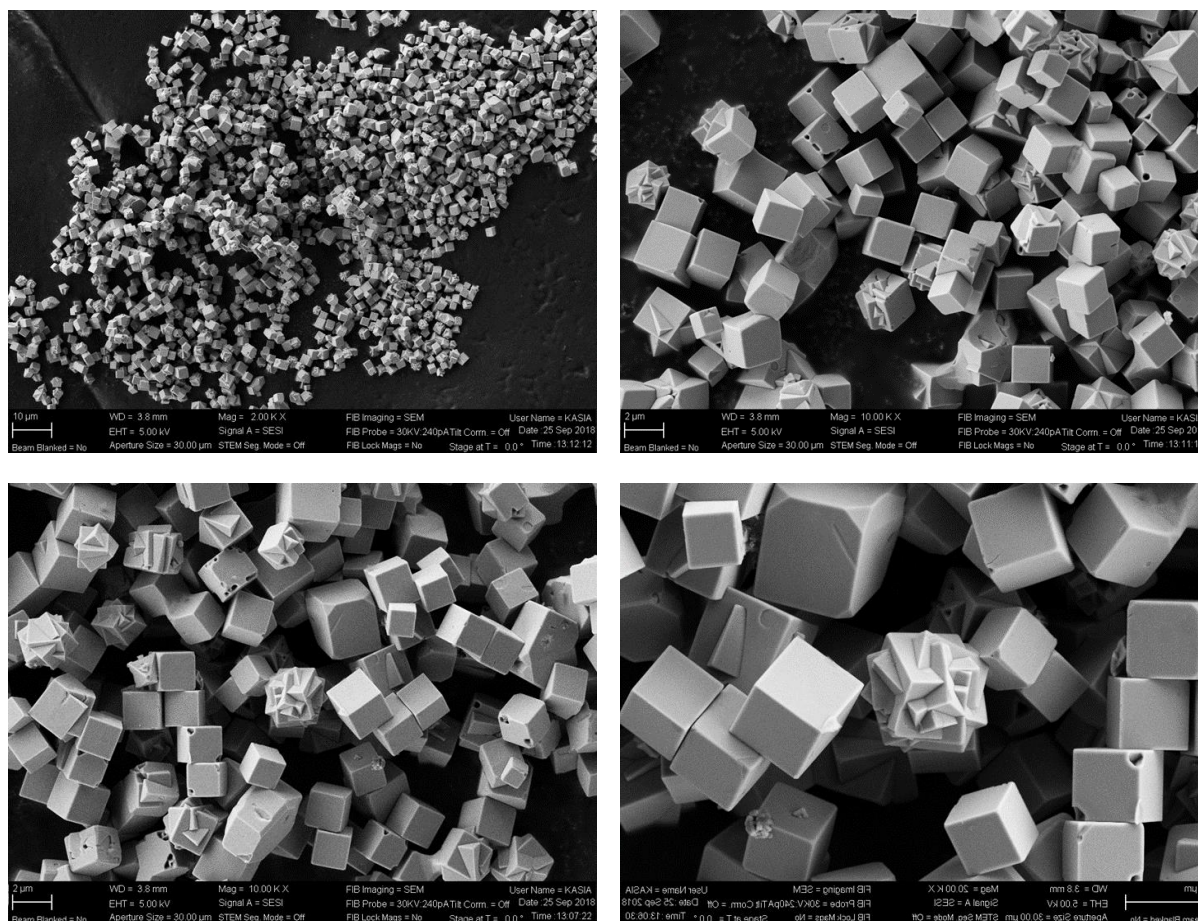


Fig.3.8 FESEM morphological characterization of the sample $Cu(AcE)Sn(IV)10$.

3.1.2 XRD

In this paragraph XRD results are presented.

3.1.2.1 CuSO₄-BASED SAMPLES

In Fig. 3.9, the XRD results for samples synthesised by using CuSO₄ as precursor are reported.

The plot shows that the sample “Cu” contains metallic copper: main peaks corresponding to the reflection from (111), (200), and (220) planes of Cu crystalline phase; two small peaks for (111) and (200) planes of copper(I) oxide (Cu₂O, Cuprite) can also be seen, proving that a small amount of Cuprite is present.

Similar crystalline phases are shown for the sample “CuSn(IV)5”, presenting analogous peaks’ position, height and width.

The XRD results for the sample “CuSn(IV)10” show that metallic Cu is not present, but only Cuprite can be found.

As showed in the FESEM paragraph, “CuSn(II)5” presents nanoparticles, which are easier to be oxidized in air; therefore, peaks related to crystalline CuO can be well seen in addition to those for metallic Cu and Cu₂O.

Crystalline phases typical of tin species were not found in any sample.

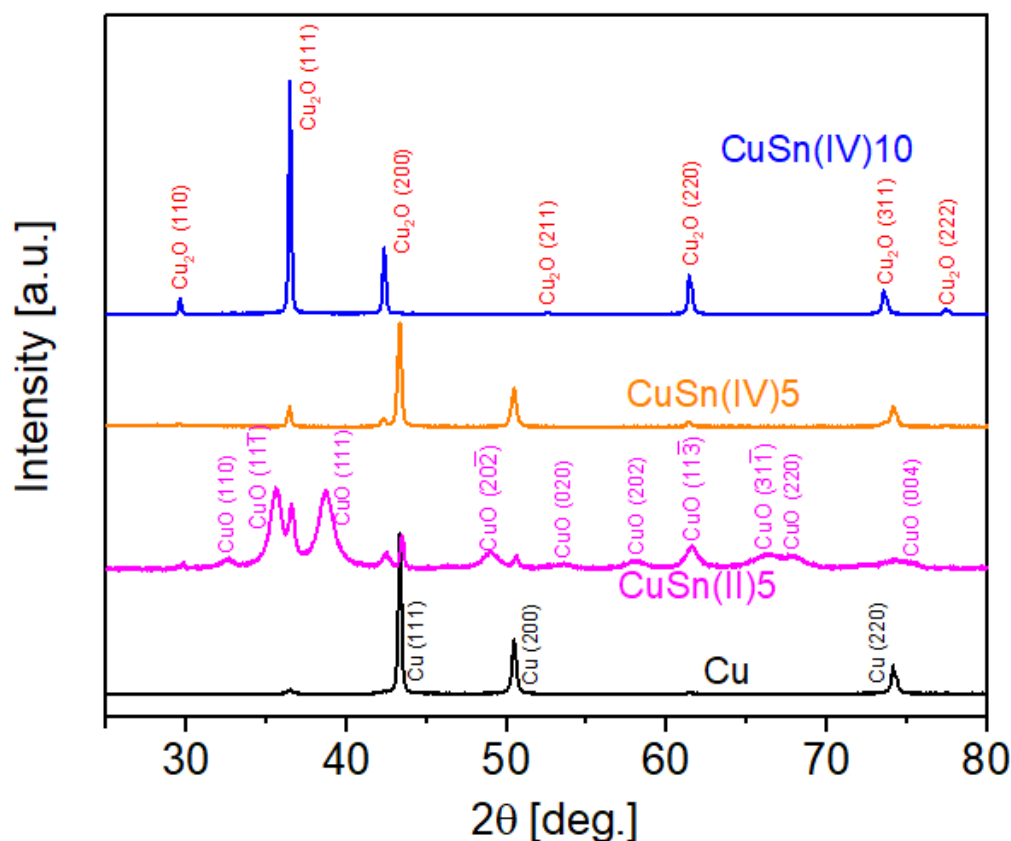


Fig.3.9 XRD results for the samples fabricated with copper sulphate as precursor.

3.1.2.2 Cu(ACE)-BASED SAMPLES

In Fig.3.10 are reported XRD results for the samples fabricated with $\text{Cu}(\text{CH}_3\text{COO})_2$ precursor.

The sample “Cu(Ace)” contains Cu_2O since each peak corresponds to crystalline Cu_2O in the XRD pattern.

Both of the samples containing Sn(IV) present only Cu_2O .

From the pattern for sample “Cu(Ace)Sn(II)5”, peaks related to crystalline CuO can be well seen besides those for metallic Cu and Cu_2O . This sample is made of nanoparticles, which are easier to be oxidized in air, which can explain the high quantity of CuO from XRD analysis.

Peaks of crystalline phases of tin or tin oxides were not found in any sample.

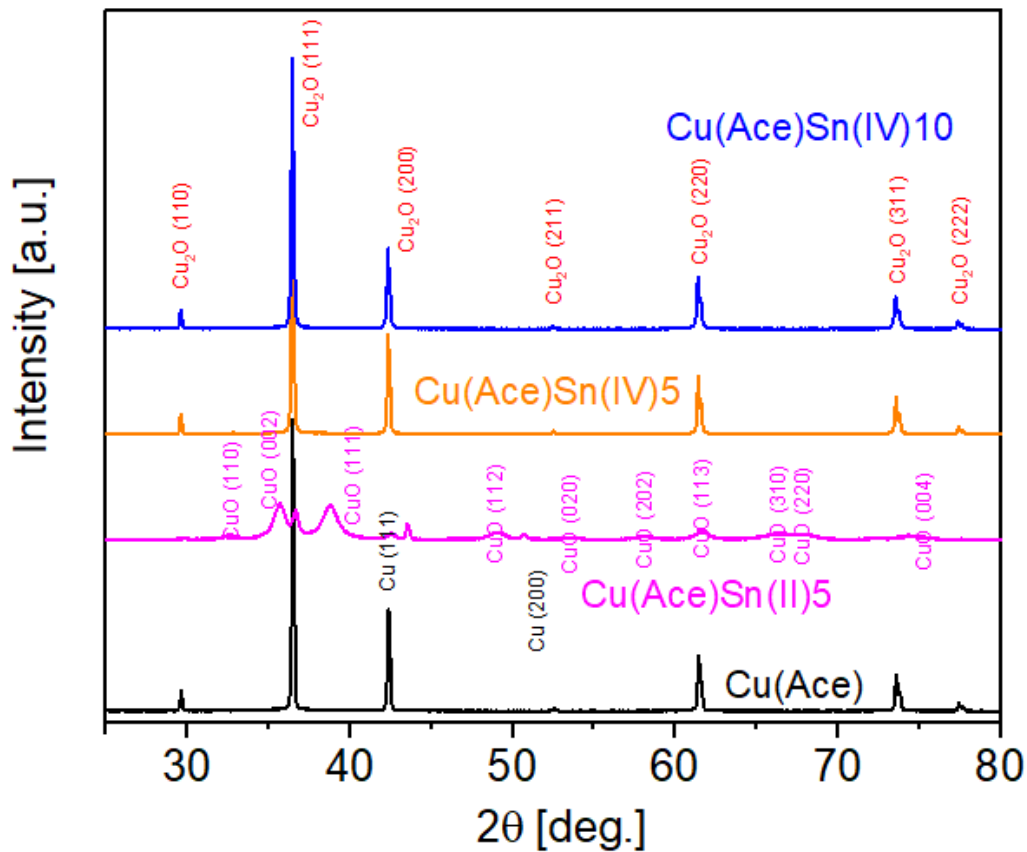


Fig.3.10 XRD results for the samples fabricated with copper acetate as precursor.

3.1.3 XPS

In this paragraph, XPS results are presented.

The Auger Parameter was calculated according to Eq.

$$\text{Auger Parameter} = hv - \text{CuLMM} + \text{Cu}2p_{3/2} \quad \text{Eq.3.1}$$

where CuLMM is the binding energy for Auger LMM region and $\text{Cu}2p_{3/2}$ is the binding energy for $\text{Cu}2p$ doublets.

3.1.3.1 CuSO₄-BASED SAMPLES

Results of XPS analysis for the samples fabricated with copper sulphate are presented.

Cu, O and C are the mainly present elements (Tab.3.1). The presence of C can be attributed to the preparation of the samples or due to adventitious carbon. Only traces of tin are present, which is in the margins of contamination.

Tab.3.1 Relative atomic concentration and relative concentration of Cu and Sn.

Sample	Relative atomic concentration (atomic %) from HR				
	C	O	Cu	Sn	Cu/Sn
Cu	29.4	39.7	30.8	0.2	99.5/0.5
CuSn(II)5	25.8	40.5	33.7	0.1	99.8/0.2
CuSn(IV)5	72.4	-.*	27.2	0.3	98.8/1.2
CuSn(IV)10	40.8	34.1	24.9	0.2	99.4/0.6

* O1s signal has not been acquired in the HR mode

In Fig.3.11 and Fig.3.12 are reported the acquired spectra for both Cu_{2p} and CuLMM regions. The analysis of CuLMM is because the Cu_{2p} peaks are difficult to be deconvoluted due to the presence and overlapping of satellites for each oxidation state.

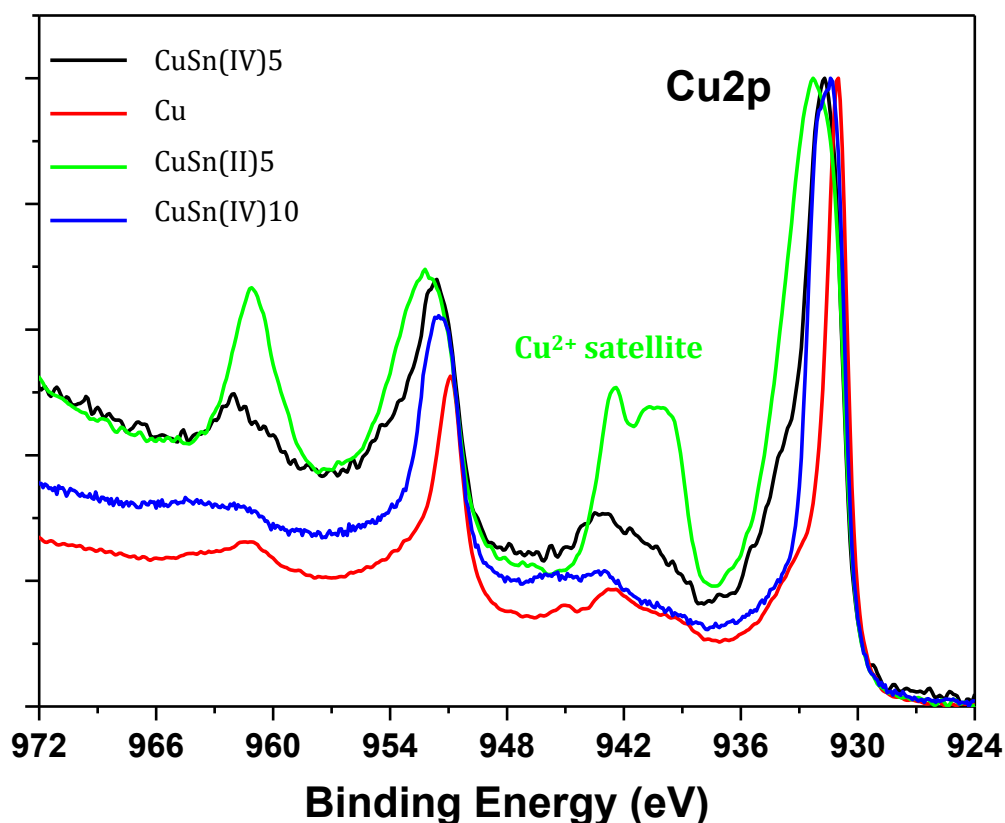


Fig.3.11 XPS results for Cu_{2p_{3/2}} of samples fabricated with copper sulphate as precursor.

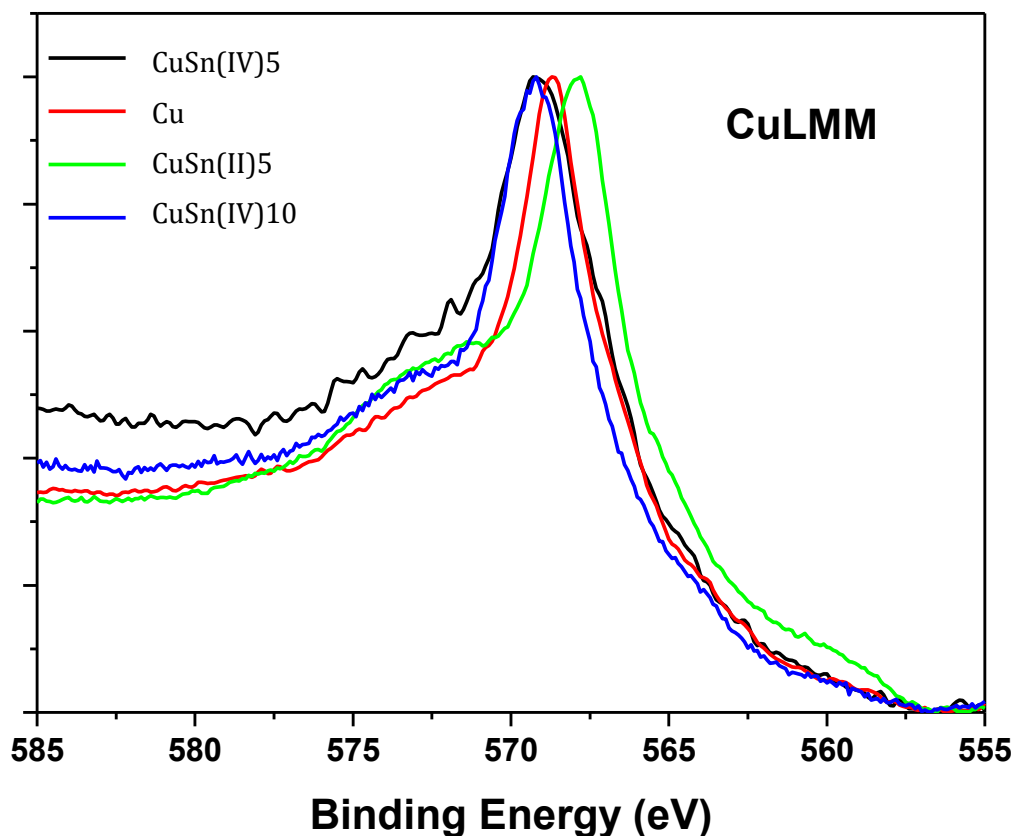


Fig.3.12 XPS results for CuLMM of samples fabricated with copper sulphate as precursor.

As shown in Fig.3.11, “Cu”, “CuSn(IV)5” and “CuSn(IV)10” show a structure related to the mixed oxidation states of Cu: Cu(0), Cu(I) and Cu(II). The sample “CuSn(II)5” presents the typical spectrum related to Cu(II) only [36].

In tab.3.2 are also reported the calculated Auger parameters. For “Cu”, “CuSn(IV)5” and “CuSn(IV)10” samples, this is approximately 1849 eV, which corresponds to an average surface oxidation state of Cu(I) [36]. In XRD patterns of these samples, the presence of metallic Cu and Cuprite can also be seen, while the absence of CuO could be due to its low quantity.

Regarding the sample “CuSn(II)5”, the Auger parameter indicates that the CuO is the only oxidation state composing the surface and validates the results of XRD, where a large amount of CuO has been observed.

Tab.3.2 Auger Parameters and oxidation states for the samples fabricated using CuSO₄.

Sample	Auger Parameter	Cu oxidation state
Cu	1848.9	(I)=(0)+(II)
CuSn(II)5	1851.1	(II)
CuSn(IV)5	1849.0	(I)=(0)+(II)
CuSn(IV)10	1848.8	(I)=(0)+(II)

3.1.3.2 CU(ACE)-BASED SAMPLES

Tab.3.3 shows that the main present elements are C, O and Cu and only traces of Sn can be found.

Tab.3.3 Relative atomic concentration and relative concentration of Cu and Sn.

Sample	Relative atomic concentration (atomic %) from HR				
	C	O	Cu	Sn	Cu/Sn
Cu(Ace)	75	-*	25	-	-
Cu(Ace)Sn(II)5	39.3	-*	60.7	<0.1	-
Cu(Ace)Sn(IV)5	73.6	-*	26.2	0.2	99.3/0.7
Cu(Ace)Sn(IV)10	34.1	42.1	232.6	0.2	99.1/0.9

*O1s signal has not been acquired in the HR mode.

Fig.3.13 and 3.14 represent the XPS results in the Cu2p and Auger CuLMM regions for samples fabricated with copper acetate. The necessity of investigating the CuLMM region is due to the overlapping of satellites in the Cu2p region that makes difficult to deconvolute the peak.

As shown in Fig.3.13, the surface of “Cu(Ace)”, “Cu(Ace)Sn(IV)5” and “Cu(Ace)Sn(IV)10” has mixed oxidation states of Cu: Cu(I) and Cu(II) with possible Cu(0), even though only Cu(I) is observed on all these samples from XRD analysis. The sample “Cu(Ace)Sn(II)5” presents the typical spectrum related to Cu(II) only [36].

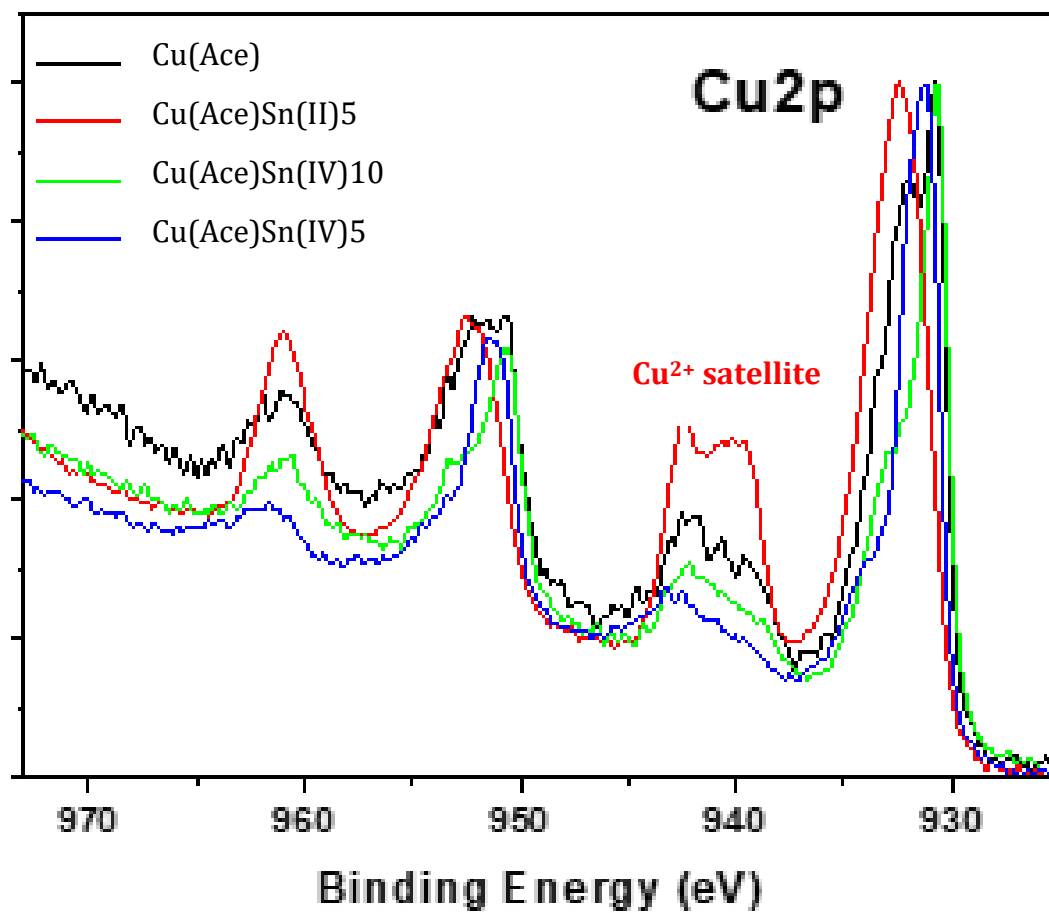


Fig.3.13 XPS results for Cu_{2p_{3/2}} of samples fabricated with copper acetate as precursor.

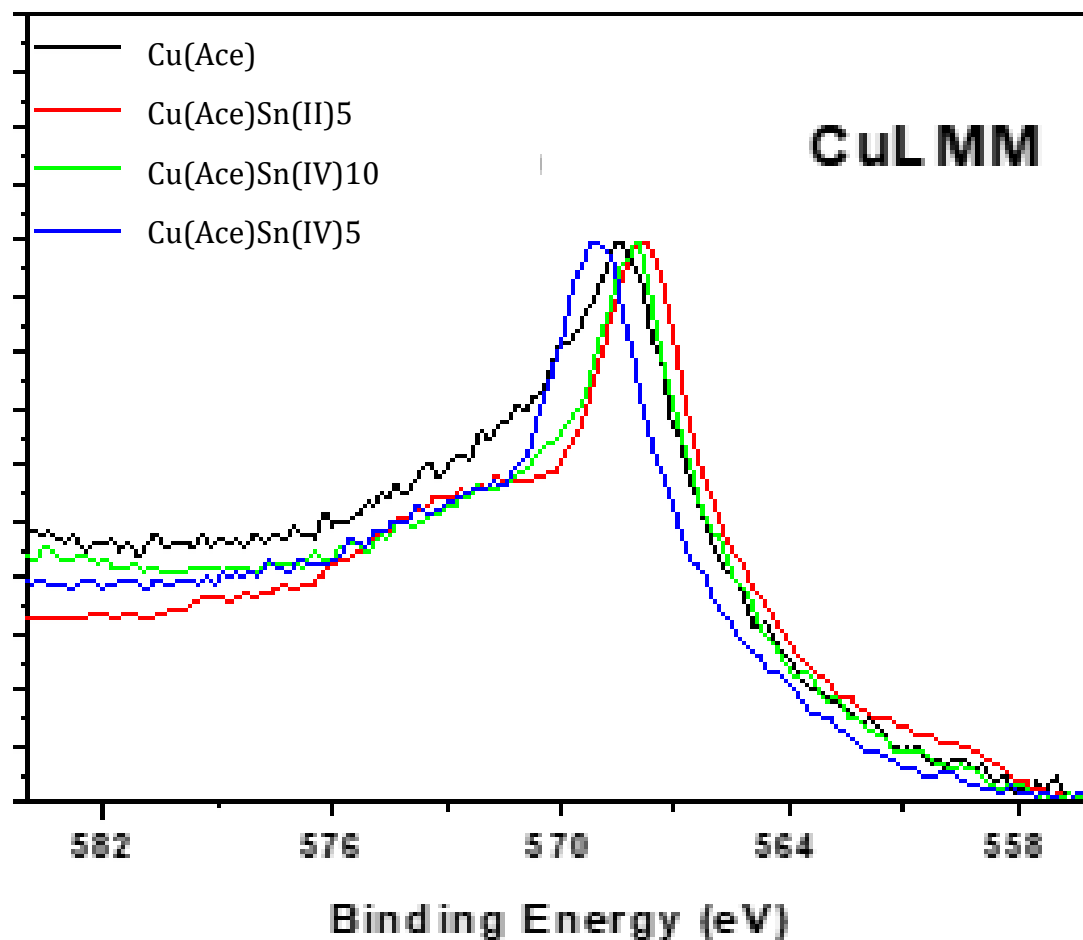


Fig.3.14 XPS results for CuLMM of samples fabricated with copper acetate as precursor.

The calculated Auger parameters (Tab.3.4) indicates that the surface of “Cu(Ace)”, “Cu(Ace)Sn(IV)5” and “Cu(Ace)Sn(IV)10” are formed by mixed oxidation states, while the surface of “Cu(Ace)Sn(II)” is composed by Cu(II) only.

Tab.3.4 Auger Parameters and oxidation states for the samples fabricated using Cu(CH₃COO)₂.

Sample	Auger Parameter	Cu oxidation state
Cu(Ace)	1848.9	(I)=(0)+(II)
Cu(Ace)Sn(II)5	1451.3	(II)
Cu(Ace)Sn(IV)5	1848.7	(I)=(0)+(II)
Cu(Ace)Sn(IV)10	1849.3	(I)=(0)+(II)

3.2 ELECTROCHEMICAL AND PRODUCTS ANALYSES

3.2.1 CA AND GC

Since CA and GC were run concomitantly, results are presented in the same paragraph.

Faradaic Efficiency (FE) was calculated by dividing the amount of electrons involved in the formation of the considered product (Eq.3.2) for the global amount of electrons (Eq.3.3), as described in Eq.3.4. Faradaic efficiencies were calculated at a representative time (40 min since the beginning of the tests), when the current was considered stable.

$$e_x^- = \frac{C_x \times 10^{-6} \times \dot{V}_x}{V_m} \times n \times t \quad \text{Eq.3.2}$$

$$Q = I \times t \quad \text{Eq.3.3}$$

$$FE_x = \frac{e_x^-}{Q} \quad \text{Eq.3.4}$$

where n is the number of electrons involved in the reduction reaction (2 both for CO and H₂); C_x is the concentration of the formed species in ppm (parts per million, 10⁻⁶); V_m is the molar volume, whose value is 22.4 ml mmol⁻¹; \dot{V}_x is the flux of the gas through the cell in mL min⁻¹; I is the measured current intensity in mA; t is the period considered.

Values of FE for the product HCOOH are not reported, since formic acid is not a focus in this work. However, it has to be highlighted that these values remained below 10% for all the samples at different potentials.

The ratios H₂/CO were calculated by dividing the H₂ concentration by the CO concentration at the representative time (40 minutes).

3.2.1.1 Cu

Sample “Cu” was investigated at two potentials (-0.6V and -0.7V vs RHE).

As shown in the graph (Fig.3.15), at -0.6V the current stabilizes after ca. 10minutes. The concentration of H₂, during the test, keep growing, slowing down after ca. 30 minutes; the concentration of CO is stable in a range of 400 ppm after ca. 15 minutes.

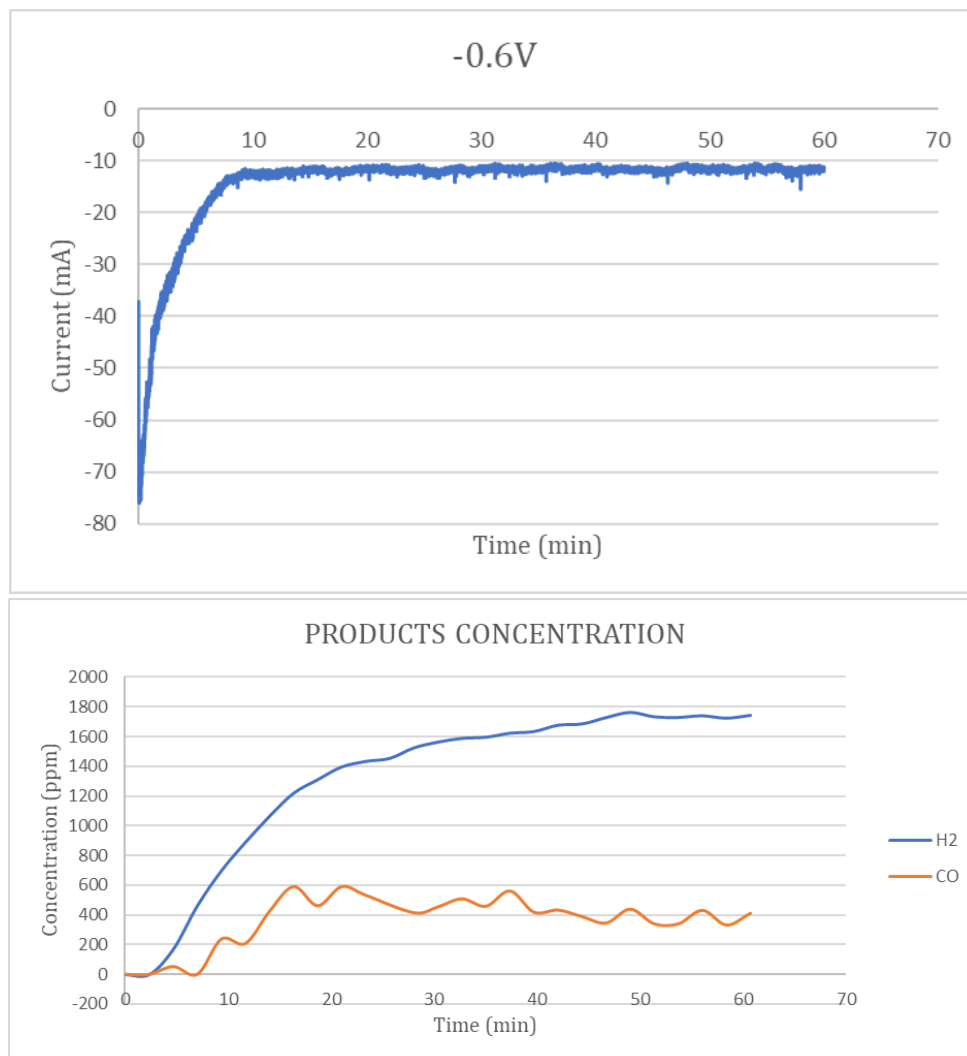


Fig.3.15 CA and products concentration of the sample Cu at -0.6 V vs RHE.

3. Results and discussion

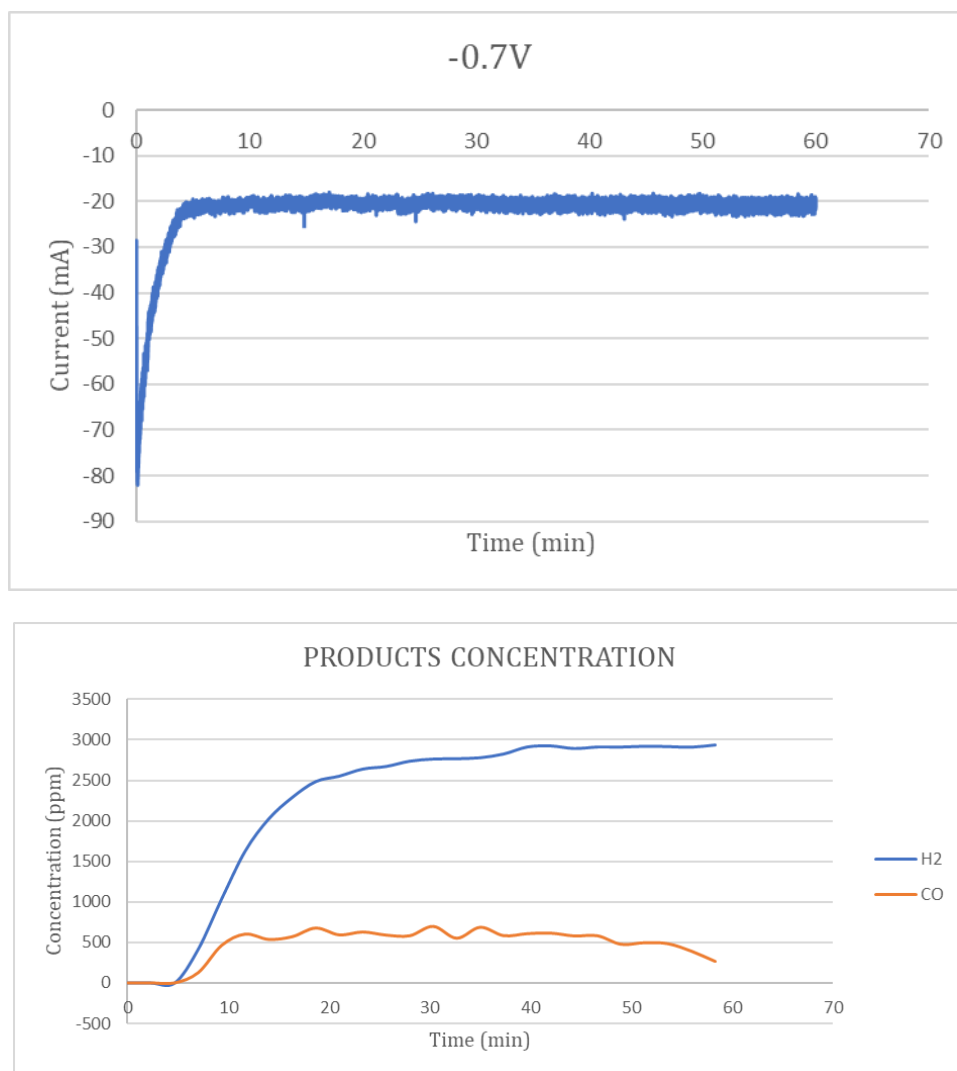


Fig.3.16 CA and products concentration of the sample Cu at -0.7 V vs RHE.

As shown in Fig.3.16, the trends of the production of H₂ and CO are similar to those at -0.6V, but the production of H₂ is almost doubled. The current shows a similar trend as well, but the value is almost increased by one-fold.

Tab. reports the current intensity values and the calculated FE and ratio between carbon monoxide and hydrogen for easier comparison of the catalysts' performances at different potentials. Fig.3.17 shows the great difference between the FE of H₂ and FE of CO.

Tab.3.5 Sum up of the main parameters: current values, FE and H₂/CO ratio at the tested potential (V vs RHE) for the sample Cu.

		-0.6V	-0.7V	-0.8V
Current (mA)		-11.7	-20.6	-
FE (%)	H₂	79.5	78.5	-
	CO	20.5	16.4	-
H₂/CO		3.9	4.8	-

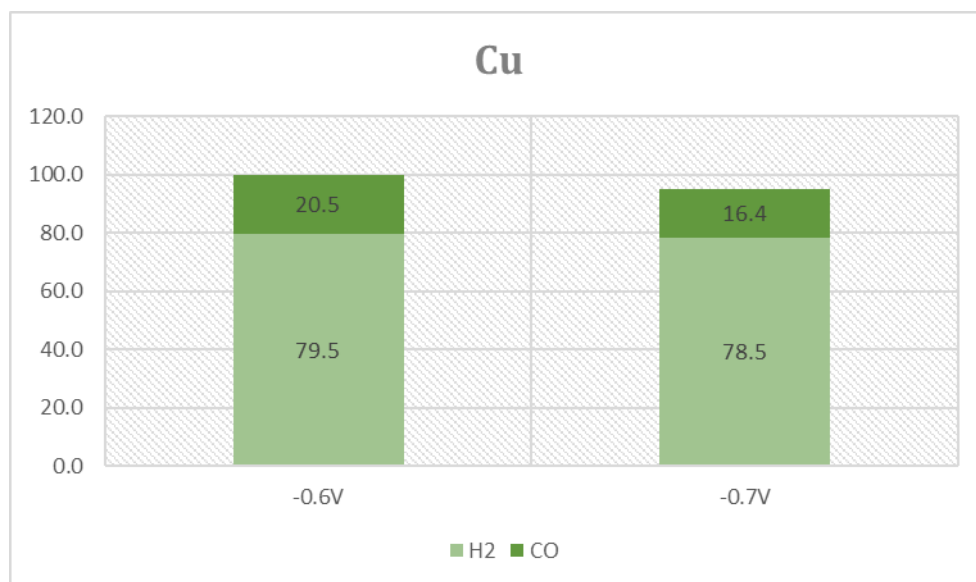


Fig.3.17 Faradaic efficiencies for hydrogen and carbon monoxide at the two different potentials for the sample Cu.

3. Results and discussion

3.2.1.2 *Cu(Ace)*

The sample “Cu(Ace)” was investigated at three potentials (-0.6V, -0.7V and -0.8V vs RHE).

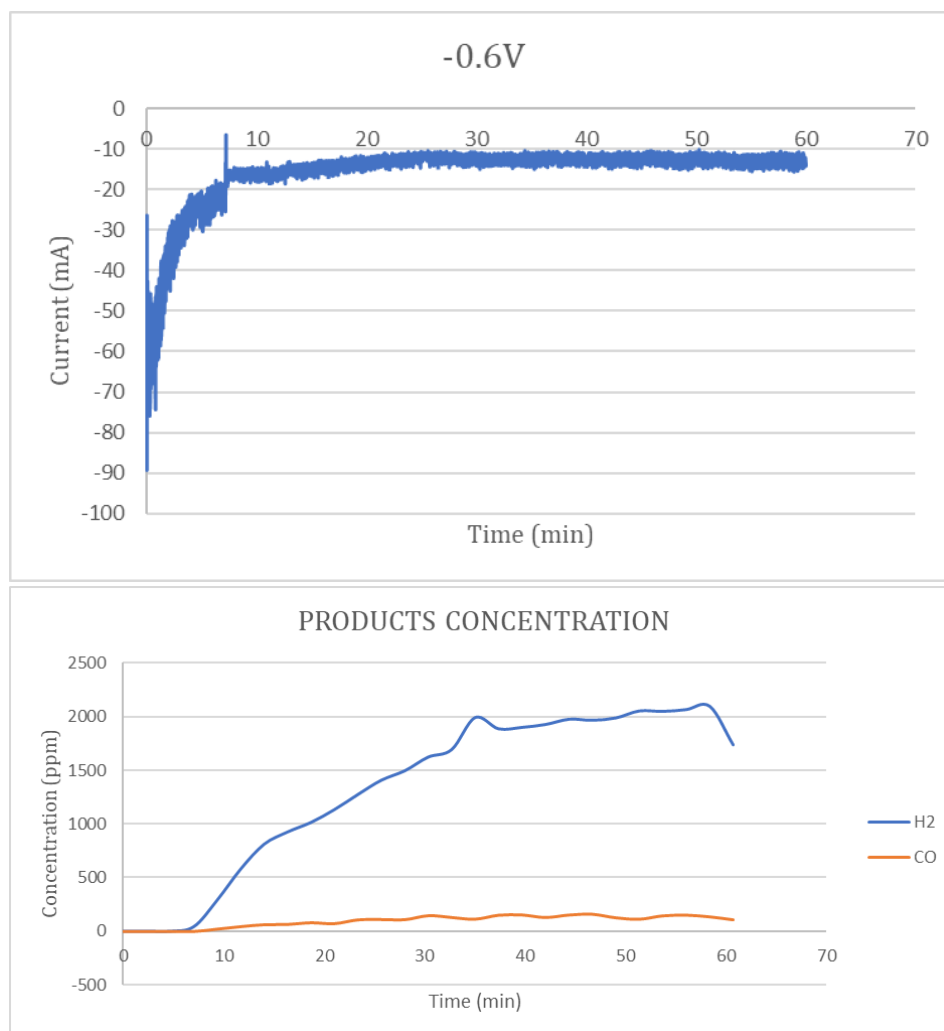


Fig.3.18 CA and products concentration of Cu(Ace) at -0.6 V vs RHE.

In Fig.3.18, it is possible to see the current stabilization at a value of ca. -10 mA in less than 10 minutes. The concentration of H₂ grows in time and stabilizes in about 35 minutes. CO concentration in time is stable from the beginning at low values.

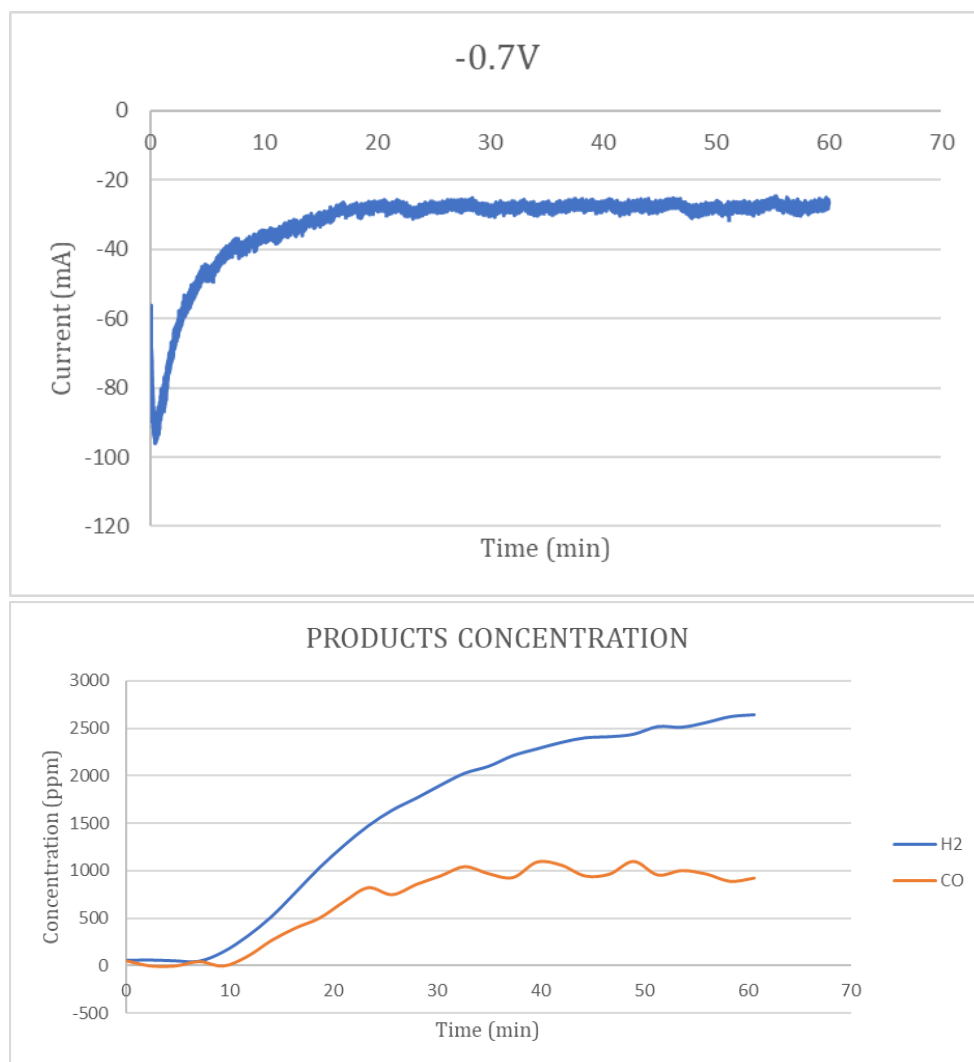


Fig.3.19 CA and products concentration of Cu(Ace) at -0.7 V vs RHE.

At -0.7V vs RHE, the production of CO is improved and the current value is more than doubled (Fig.3.19).

3. Results and discussion

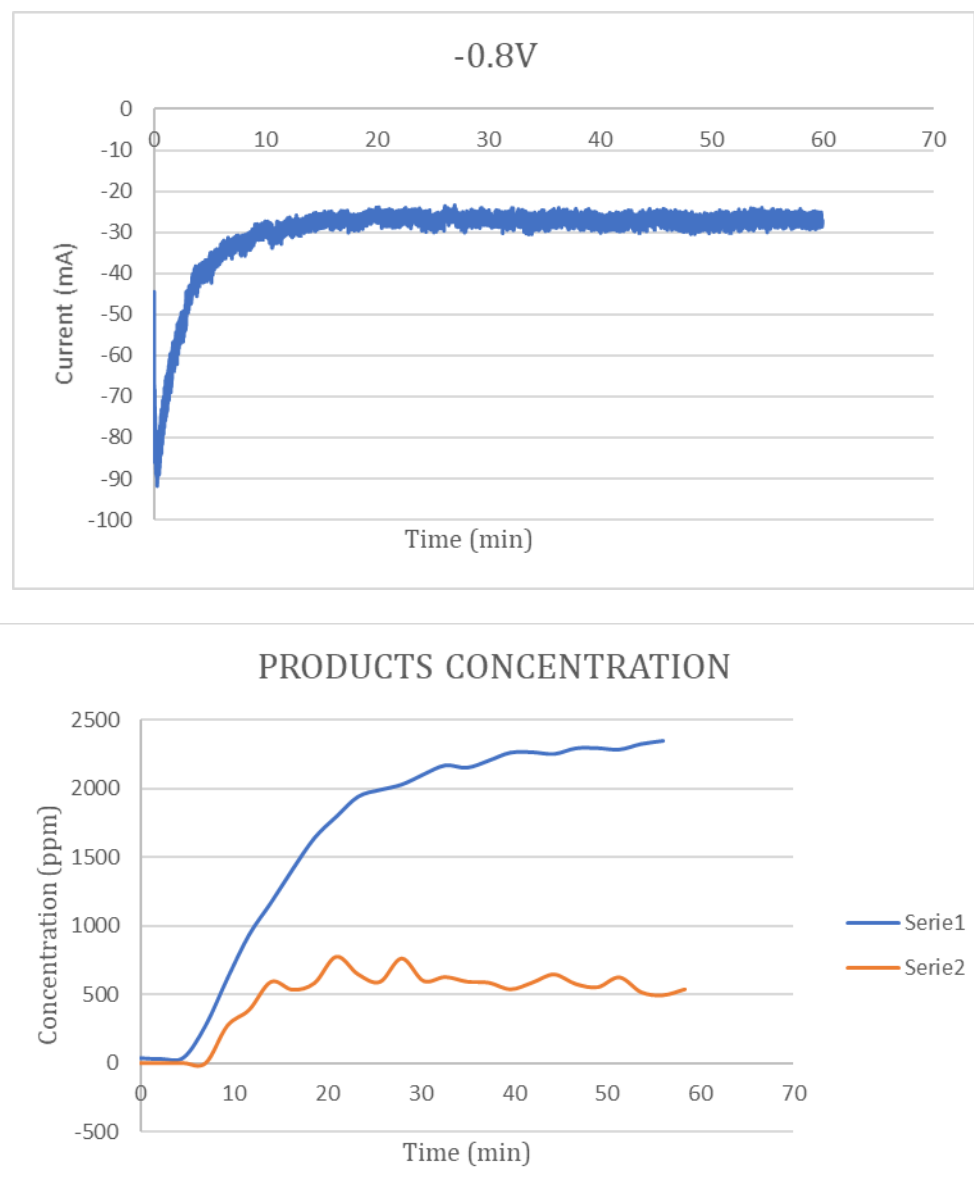


Fig.3.20 CA and products concentration for the sample Cu(Ace) at -0.8 V vs RHE.

The charts (Fig.3.20) show a similar trend with the one at -0.7V. Nevertheless, the production of CO is worse: the FE of CO decreased of 10% (Tab.3.6)

Tab.3.6 Sum up of the main parameters of Cu(Ace): current values, FE and H₂/CO ratio at the tested potential (V vs RHE).

		-0.6V	-0.7V	-0.8V
	Current (mA)	-12.5	-27.6	-27.2
FE (%)	H₂	79.8	64.2	75.1
	CO	20.2	28.9	18.9
	H₂/CO	3.9	2.2	4.0

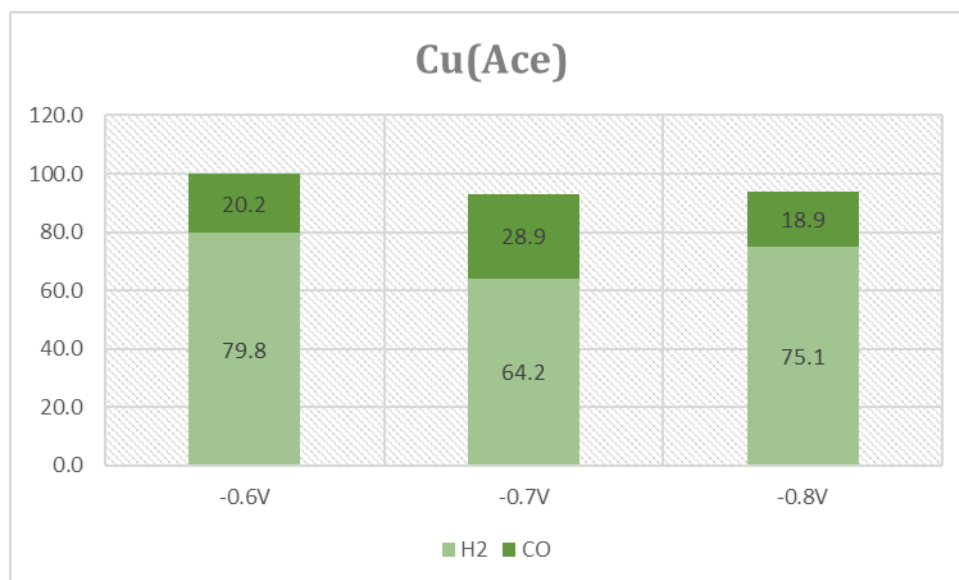


Fig.3.21 Faradaic efficiencies for hydrogen and carbon monoxide of Cu(Ace) at the three different potentials.

As it can be seen in Fig.3.21, this sample is not suitable for the reduction of CO₂, since the production of H₂ is much greater than the production of CO and does not produce a mixture H₂ – CO that can be further process as Syngas to obtain valuable products, as will be discussed in Section 3.4.

3. Results and discussion

3.2.1.3 CuSn(II)5

The sample "CuSn(II)5" was analysed at three potentials (-0.6V, -0.7V and -0.8V vs RHE).

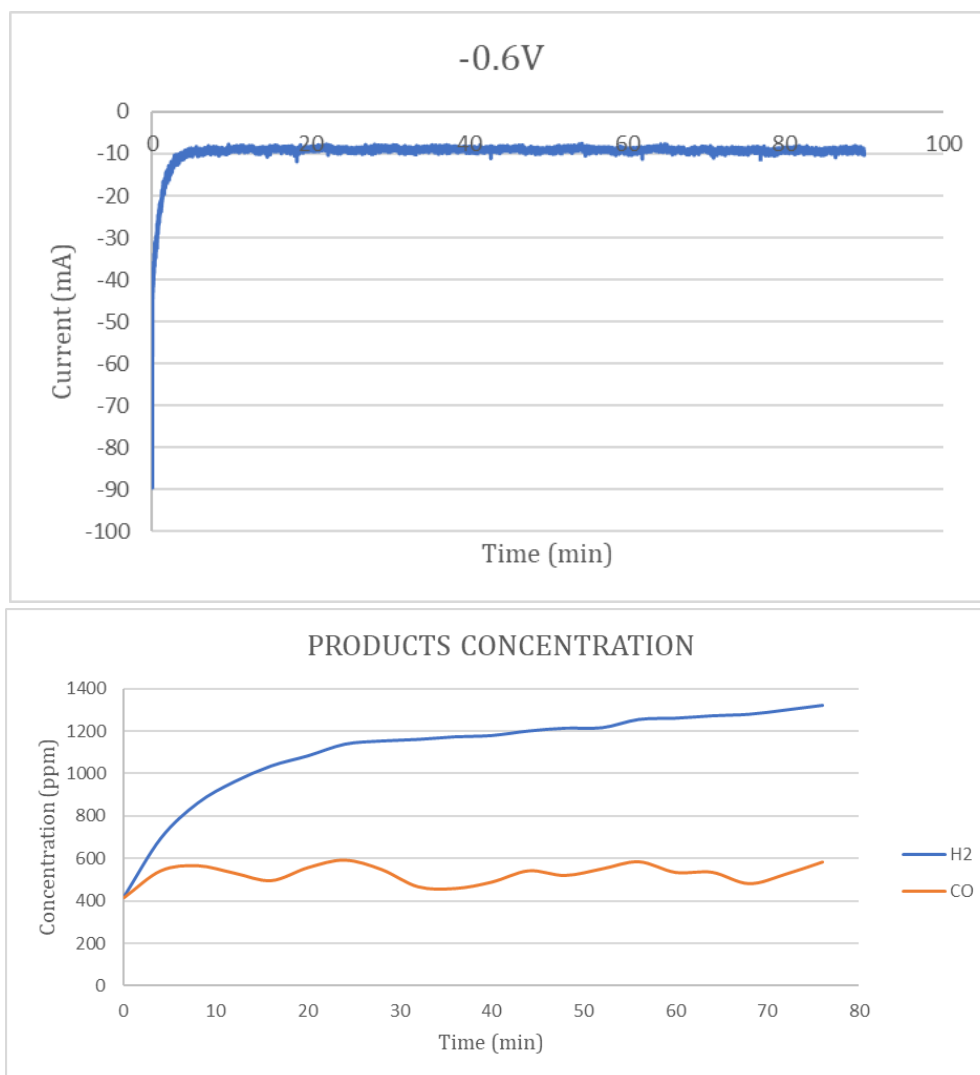


Fig.3.22 CA and products concentration of CuSn(II)5 at -0.6 V vs RHE.

Fig.3.22 shows stable current values and production of both hydrogen and carbon monoxide. H₂ concentration is greater than CO one.

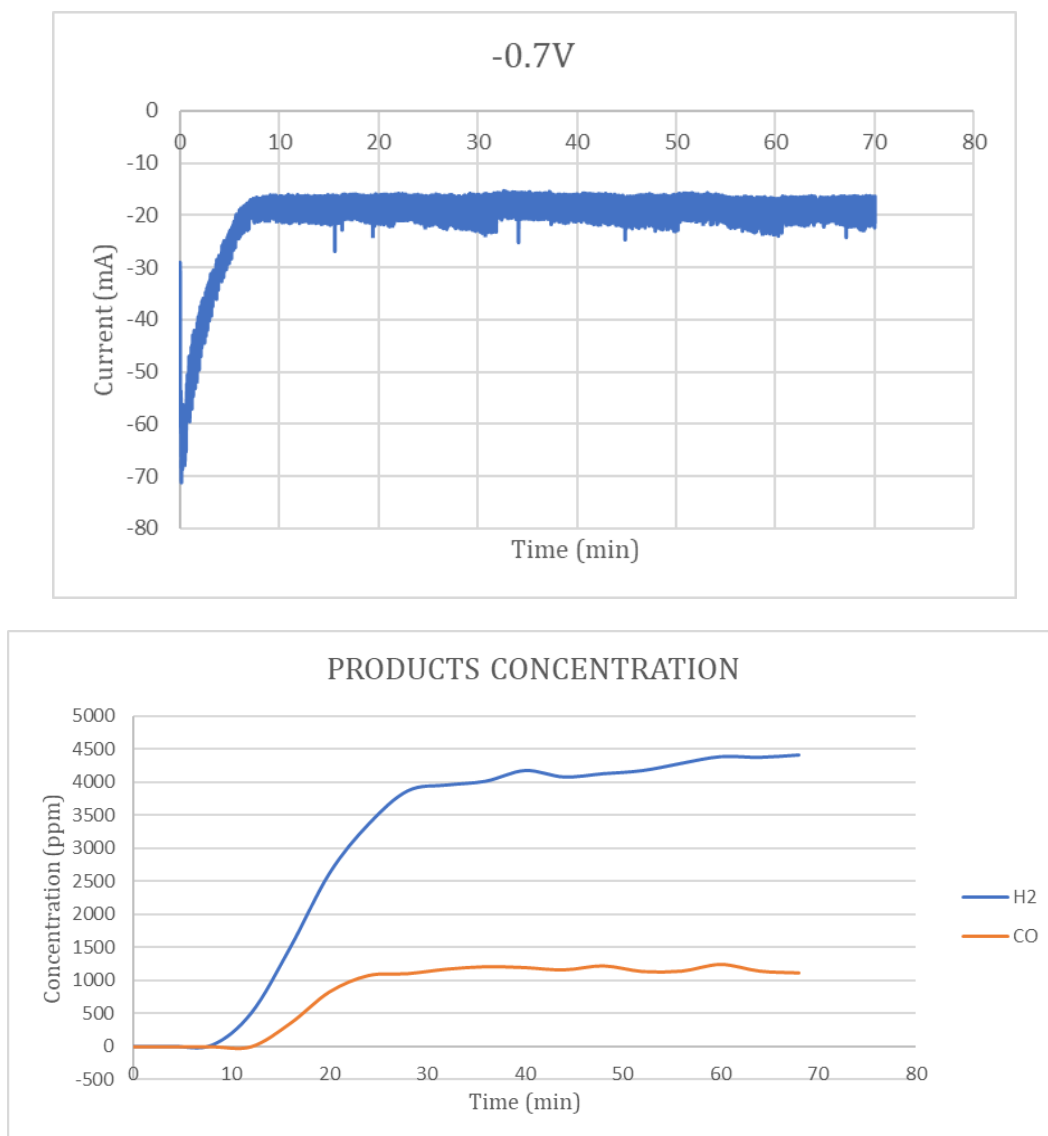


Fig.3.23 CA and products concentration for the sample CuSn(II)5 at -0.7 V vs RHE.

As it can be seen in Fig.3.23, the current graph presents some noise, but values are stabilized at ca. -20 mA. The concentration of H₂ has a great growth in the first 20 minutes and then stabilizes. CO concentration stabilizes after ca. 20 minutes as well.

3. Results and discussion

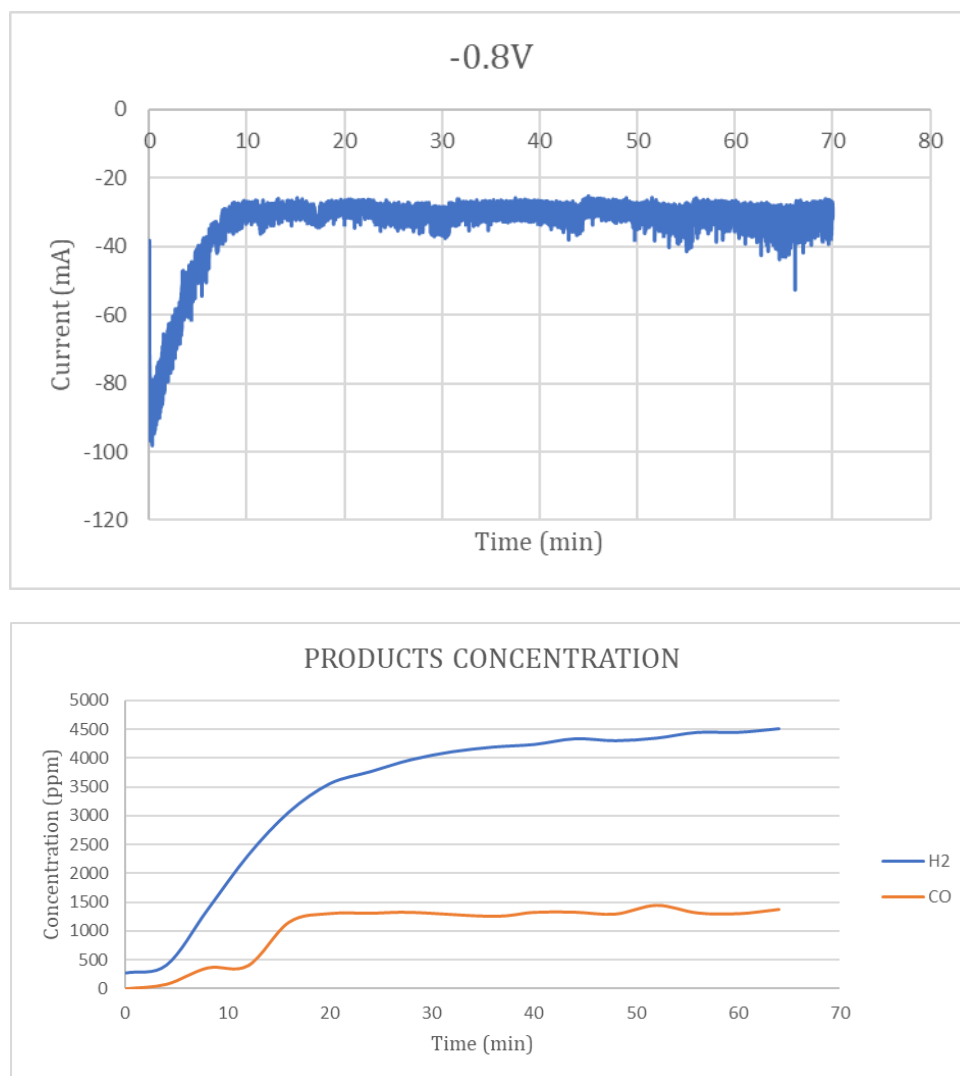


Fig.3.24 CA and products concentration of CuSn(II)5 at -0.8 V vs RHE.

It can be seen in Fig.3.24 that the values of current are increased if compared with the values at -0.6V and -0.7V, and so the production of CO, while the production of H₂ results similar.

From Tab.3.7 and Fig.3.25 it is discerned that the material does not show excellent ability in reducing CO₂, but the HER is the favoured reaction. Hence, the material is not suitable as catalyst for Syngas production, as will be discussed in Section 3.4.

Tab.3.7 Sum up of the main parameters of the sample CuSn(II)5: current values, FE and H₂/CO ratio at the tested potential (V vs RHE).

		-0.6V	-0.7V	-0.8V
FE (%)	H₂	79.8	73.2	73.3
	CO	20.2	20.8	22.8
H₂/CO		2.4	3.5	3.2



Fig.3.25 Faradaic efficiencies of CuSn(II)₅ for hydrogen and carbon monoxide at the three different potentials.

3. Results and discussion

3.2.1.4 $Cu(Ace)Sn(II)5$

Sample “Cu(Ace)Sn(II)5” was tested at two different overpotentials (-0.6V and -0.7V vs RHE).

Both currents values (Fig.3.26 and Fig.3.27) are stabilized in less than 10 minutes. Concentration of both CO and H₂ are similar in values and trends at different potentials (ca. 1500 ppm of H₂ and ca. 500 ppm of CO as average values).

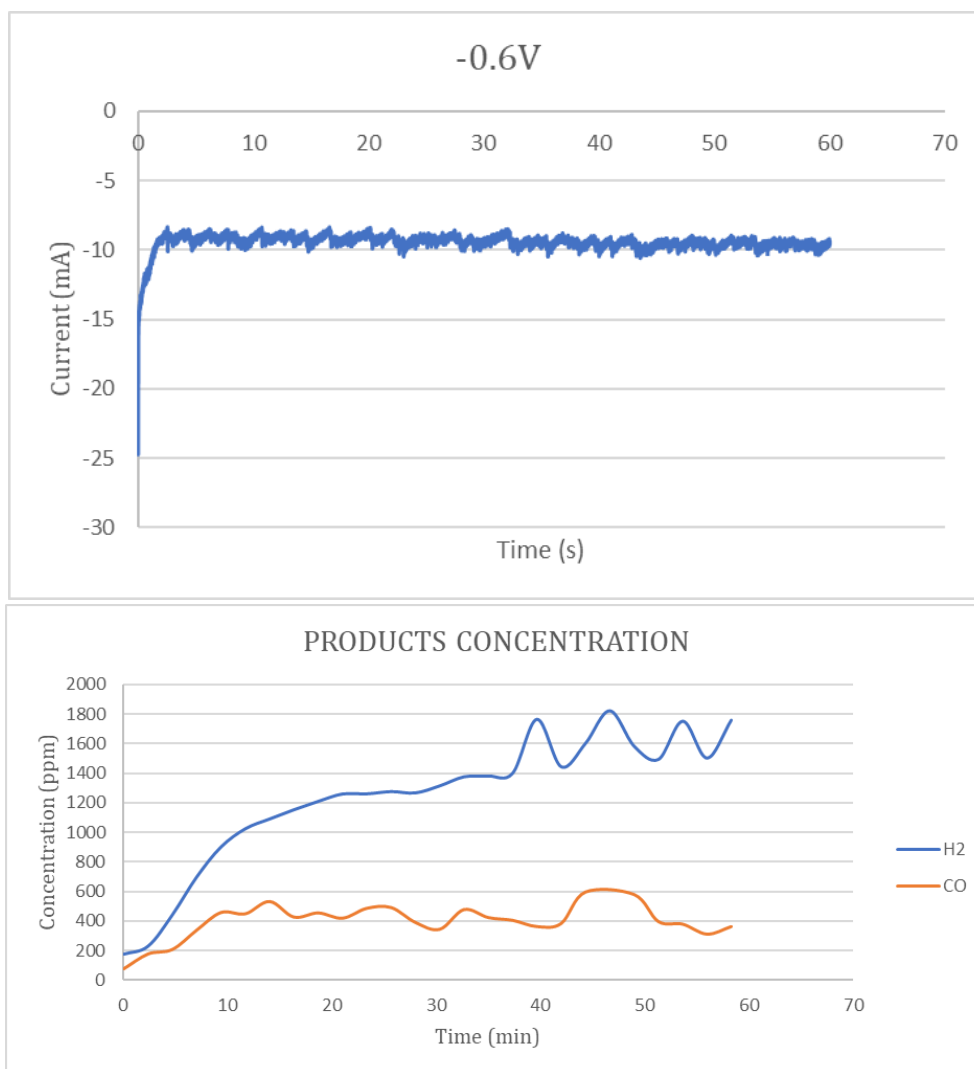


Fig.3.26 CA and products concentration at -0.6 V vs RHE for the sample Cu(Ace)Sn(II)5.

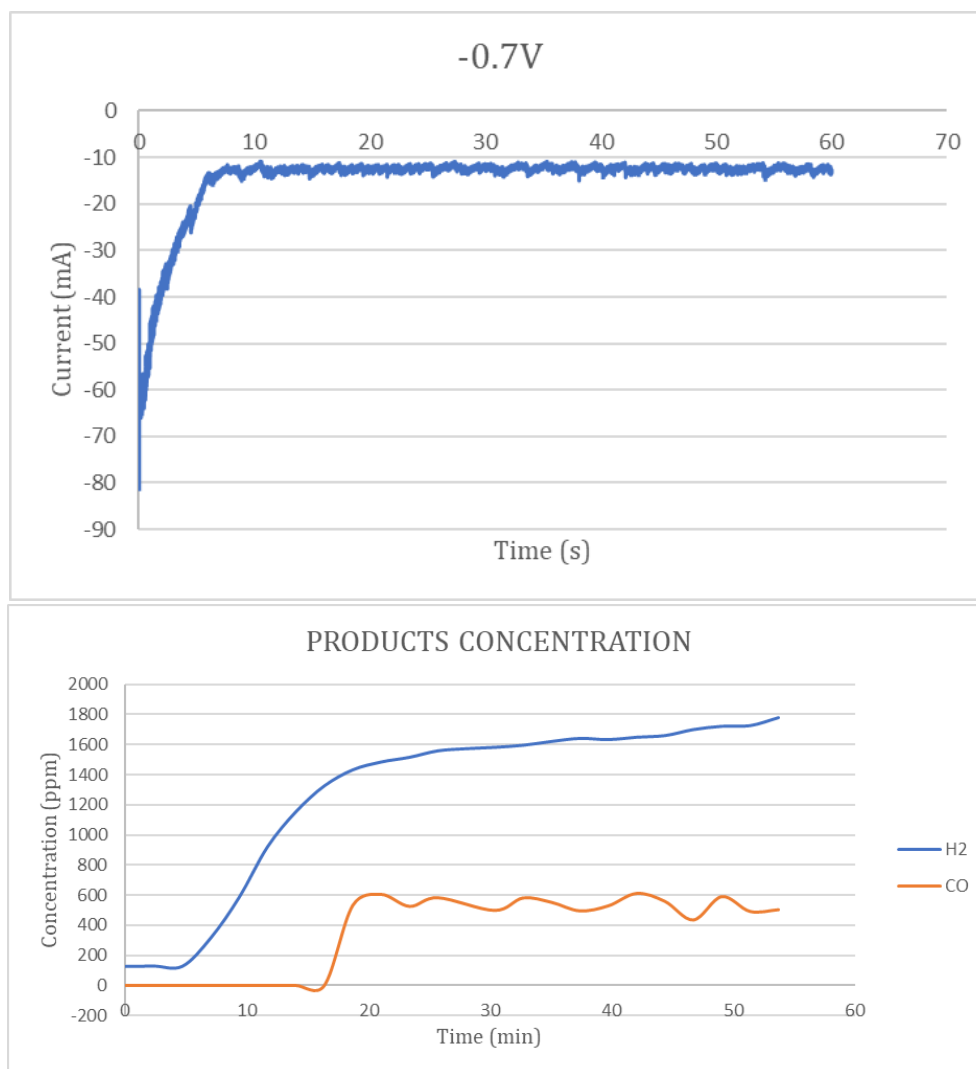


Fig.3.27 CA and products concentration of Cu(Ace)Sn(II)5 at -0.7 V vs RHE.

As shown in Tab.3.8 and Fig.3.28, adding tin salts did not improve the selectivity of the catalyst towards the CO₂RR and the HER remains the favoured one.

Tab.3.8 Sum up of the main parameters for Cu(Ace)Sn(II)5: current values, FE and H₂/CO ratio at the tested potential (V vs RHE).

		-0.6V	-0.7V	-0.8V
	Current (mA)	-9.7	-12.6	-
FE (%)	H₂	81.3	66.2	-
	CO	21.7	24.5	-
	H₂/CO	3.8	2.7	-

3. Results and discussion

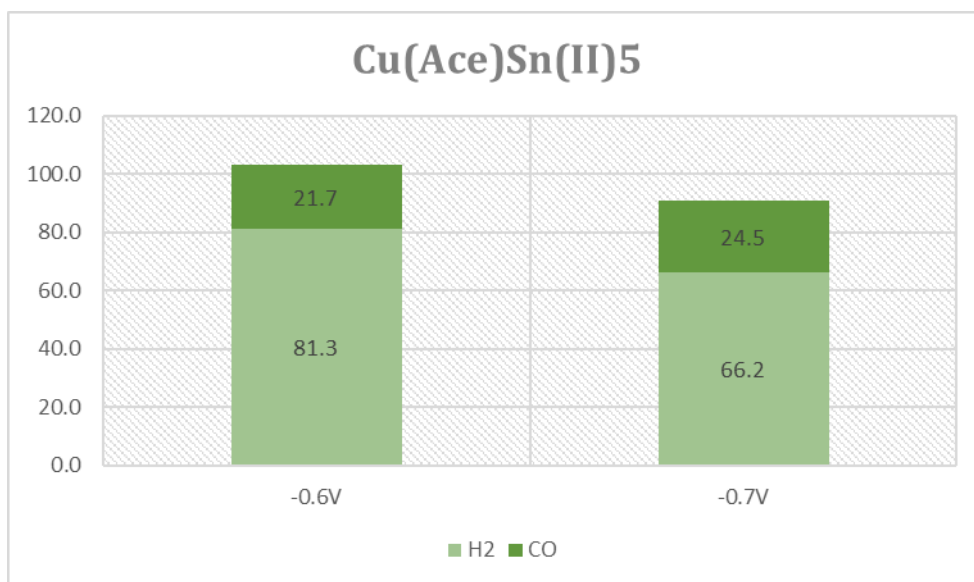


Fig.3.28 Faradaic efficiencies for hydrogen and carbon monoxide at the two different potentials calculated for Cu(Ace)Sn(II)5.

3.2.1.5 CuSn(IV)5

The sample “CuSn(IV)5” was tested at three potentials (-0.6V, -0.7V and -0.8V vs RHE).

Fig.3.29, Fig.3.30 and Fig.3.31 show that the current stabilizes in less than 10 minutes for each potential and its values increase with the increment of the potential.

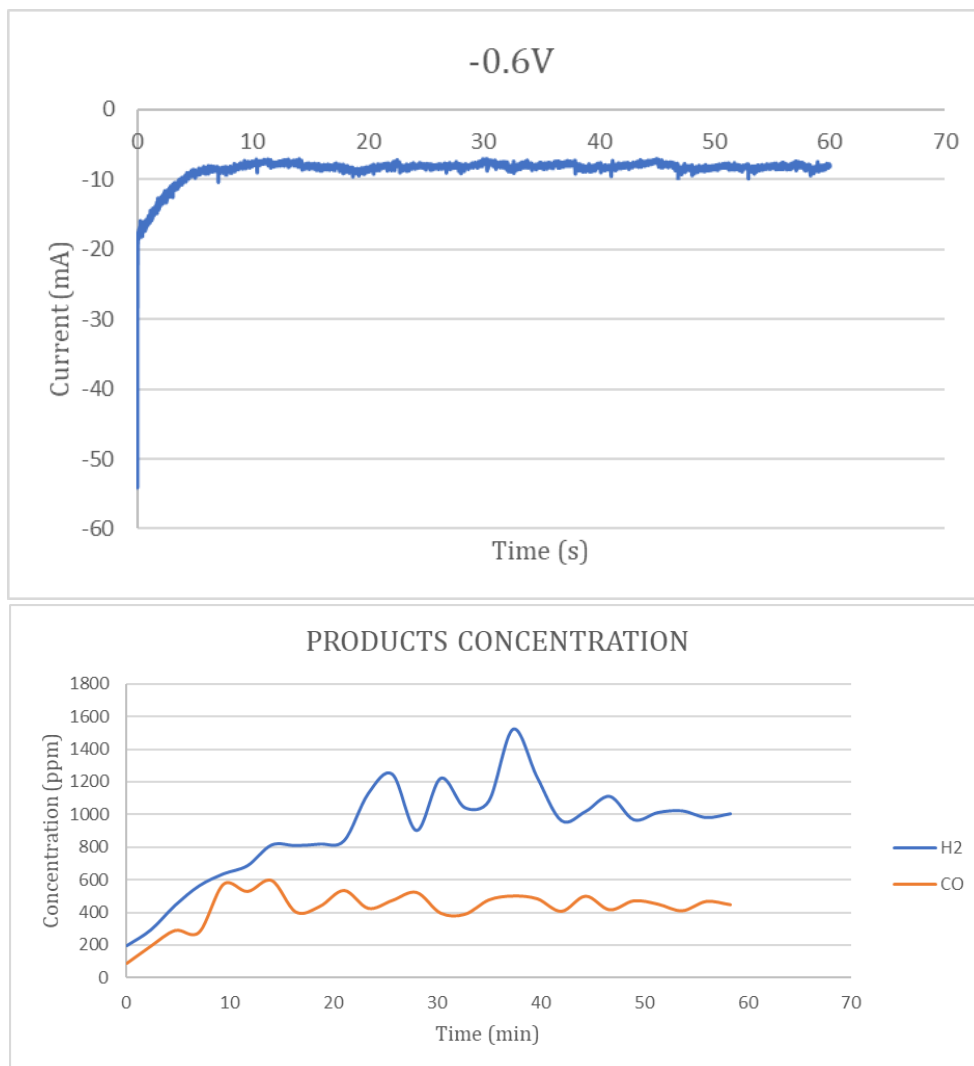


Fig.3.29 CA and products concentration for CuSn(IV)5 at -0.6 V vs RHE.

3. Results and discussion

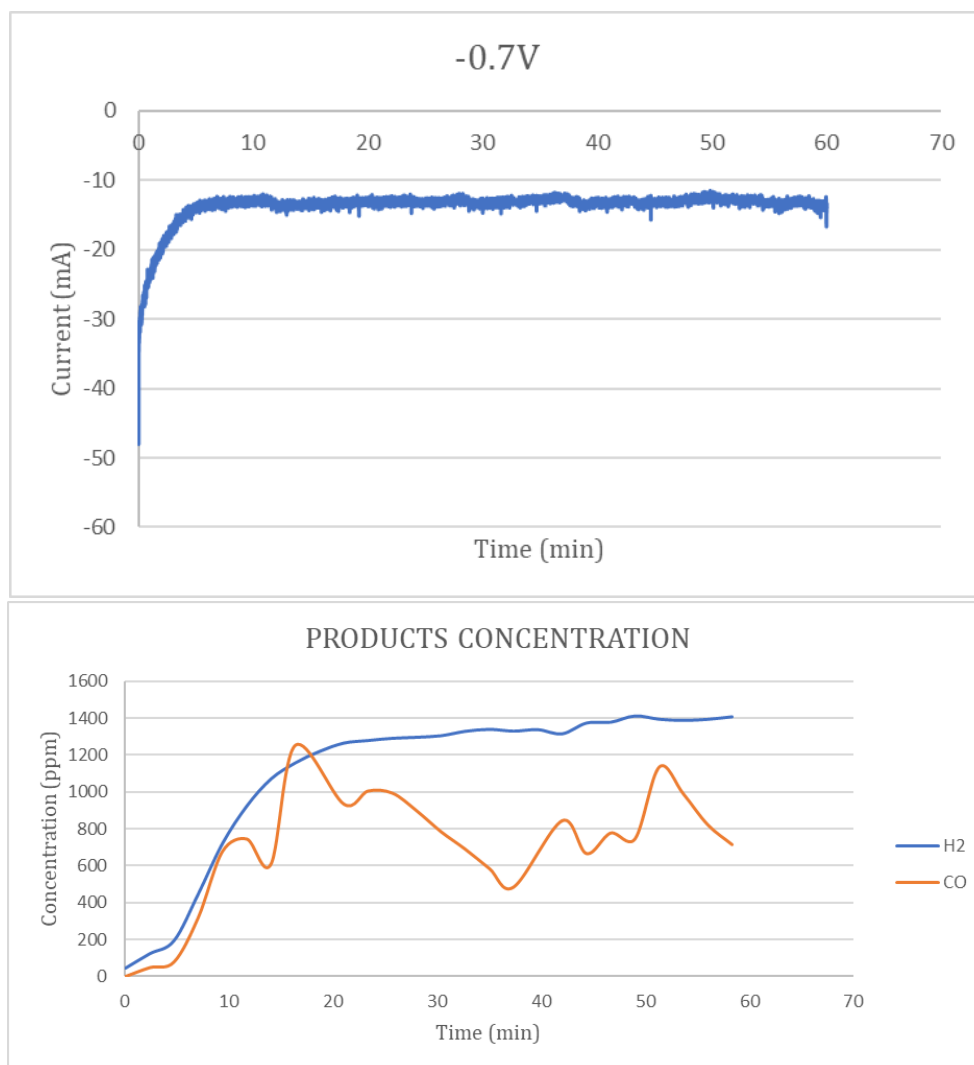


Fig.3.30 CA and products concentration at -0.7 V vs RHE of the sample CuSn(IV)5.

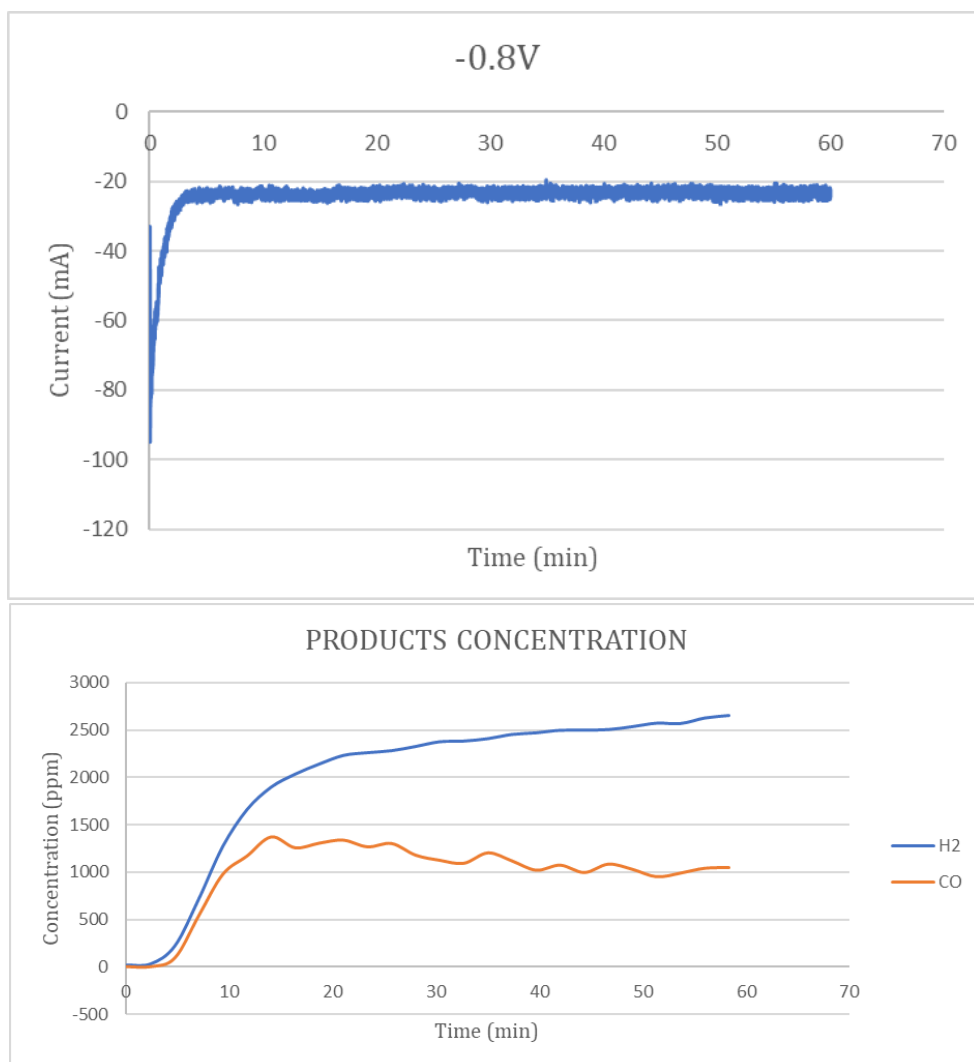


Fig.3.31 CA and products concentration at -0.8 V vs RHE for CuSn(IV)5 sample.

Tab.3.9 and Fig.3.32 show an increment in the CO production, with especially promising results at -0.7 V vs RHE.

Tab.3.9 Sum up of the main parameters presented by CuSn(IV)5: current values, FE and H₂/CO ratio at the tested potential (V vs RHE).

		-0.6V	-0.7V	-0.8V
	Current (mA)	-7.8	-13.2	-23.2
FE (%)	H₂	70.2	54.8	59.3
	CO	29.8	35.2	25.5
	H₂/CO	2.4	1.6	2.3

3. Results and discussion



Fig.3.32 Faradaic efficiencies of CuSn(IV)5 for hydrogen and carbon monoxide at the three different potentials.

3.2.1.6 Cu(Ace)Sn(IV)5

The sample “Cu(Ace)Sn(IV)5” was tested at -0.6V, -0.7V and -0.8V vs RHE. Due to a malfunctioning of the computer used to record GC and CA data, results for -0.7V were obtained at 40 minutes only and current vs time and products vs time plots are not available.

As it can be seen from Fig.3.33, at -0.6V the production of H₂ is greater than the production of CO. Similar trend but with different values can be appreciated at -0.8V (Fig.3.34).

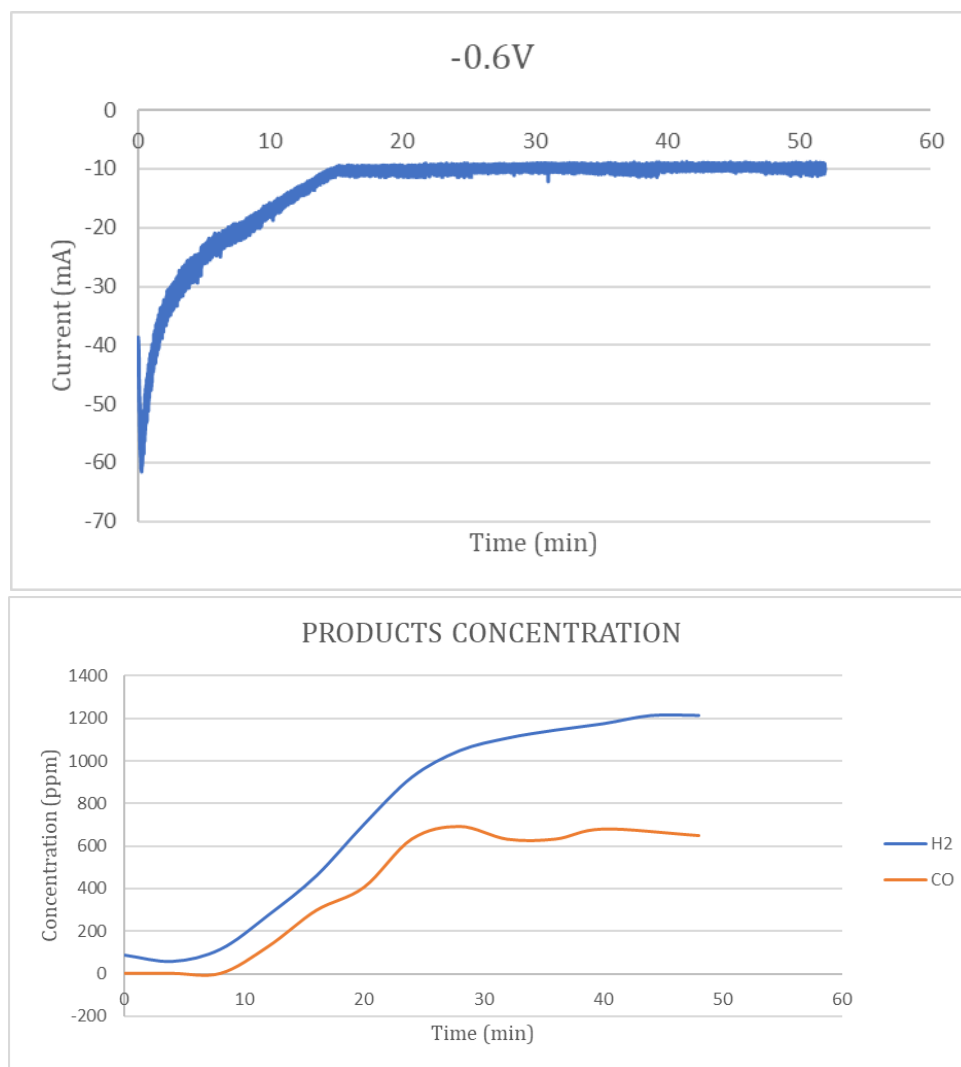


Fig.3.33 CA and products concentration at -0.6 V vs RHE for the sample Cu(Ace)Sn(IV)5.

The concentration of the products and current values evaluated at 40 minutes for -0.7V vs RHE are reported in Tab.3.10

Tab.3.10 Concentration of CO and H₂ and current at 40 minutes at -0.7V vs RHE for the sample Cu(Ace)Sn(IV)5.

	CO	H ₂
Concentration (ppm)	1040	1907
Current (mA)	-17.4	

3. Results and discussion

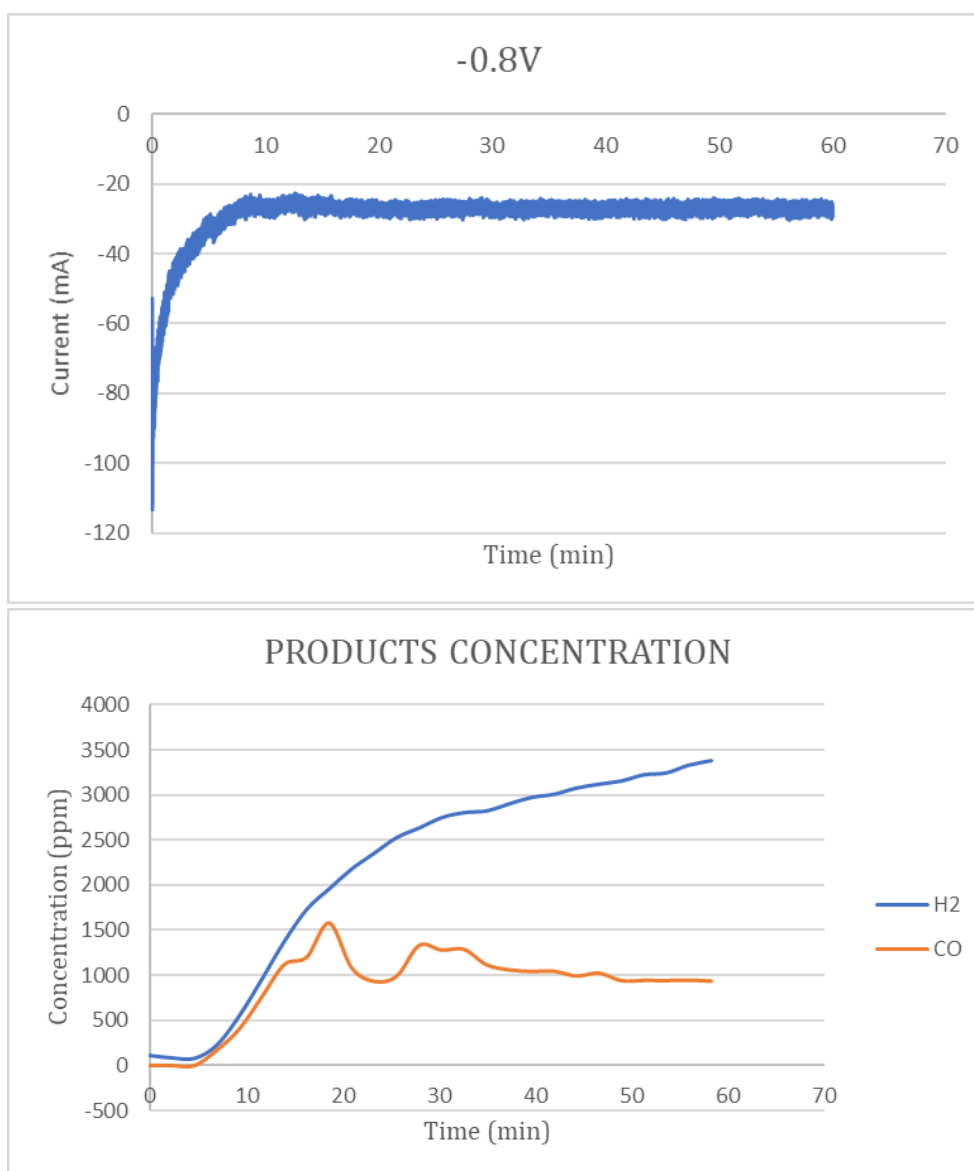


Fig.3.34 CA and products concentration at -0.8 V vs RHE for the sample Cu(Ace)Sn(IV)5.

The best results, regarding H₂/CO ratio and FEs, with this material were achieved at -0.6V vs RHE, as show in Tab.3.11 and Fig.3.35

Tab.3.11 Sum up of the main parameters of Cu(Ace)Sn(IV)5: current values, FE and H₂/CO ratio at the tested potential (V vs RHE).

		-0.6V	-0.7V	-0.8V
FE (%)	Current (mA)	-9.8	-17.4	-27.0
	H₂	63.4	59.0	62.7
	CO	36.6	32.2	21.9
H₂/CO		1.7	1.8	2.9

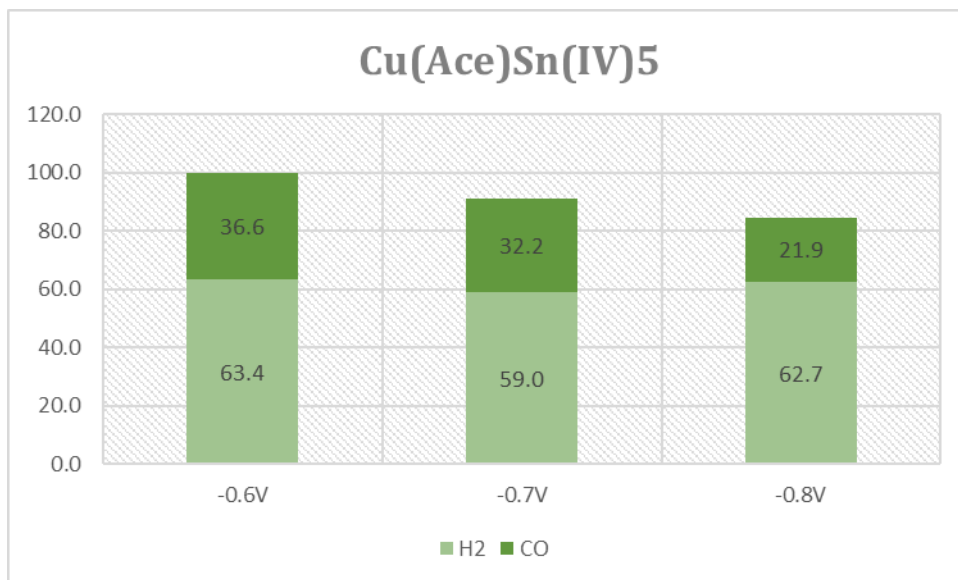


Fig.3.35 Faradaic efficiencies showed by Cu(Ace)Sn(IV)5 for hydrogen and carbon monoxide at the three different potentials.

3.2.1.7 *CuSn(IV)10*

The sample “CuSn(IV)10” was analysed at -0.6V, -0.7V and -0.8V vs RHE. Due to a malfunctioning of the computer used to record GC and CA data, results for -0.7V were obtained at 40 minutes only and current vs time and products vs time plots are not available.

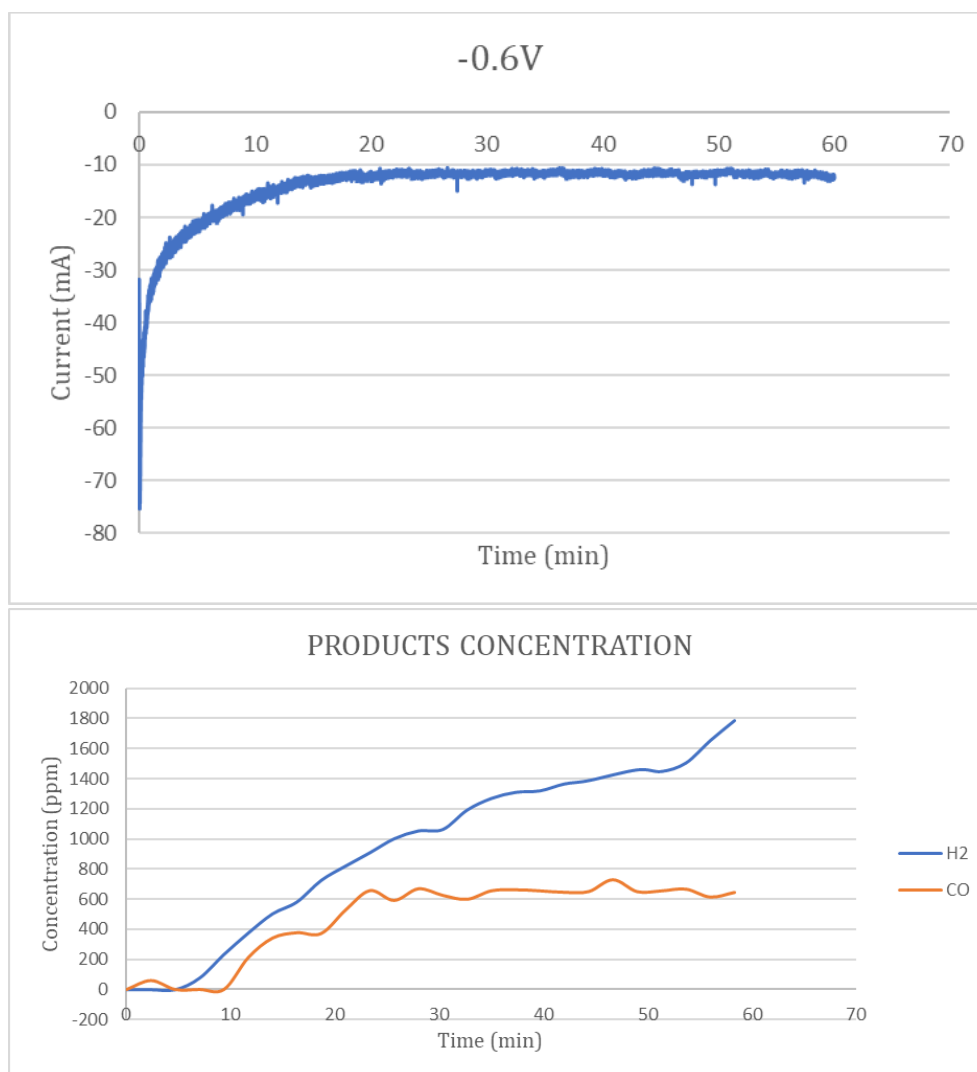


Fig.3.36 CA and products concentration at -0.6 V vs RHE for the sample CuSn(IV)10.

The concentration of the products and current values evaluated at 40 minutes for -0.7V vs RHE are reported in Tab.3.12

Tab.3.12 Concentration of CO and H₂ and current at 40 minutes at -0.7V vs RHE for CuSn(IV)10.

	CO	H ₂
Concentration (ppm)	1120	1286
Current (mA)		-15.0

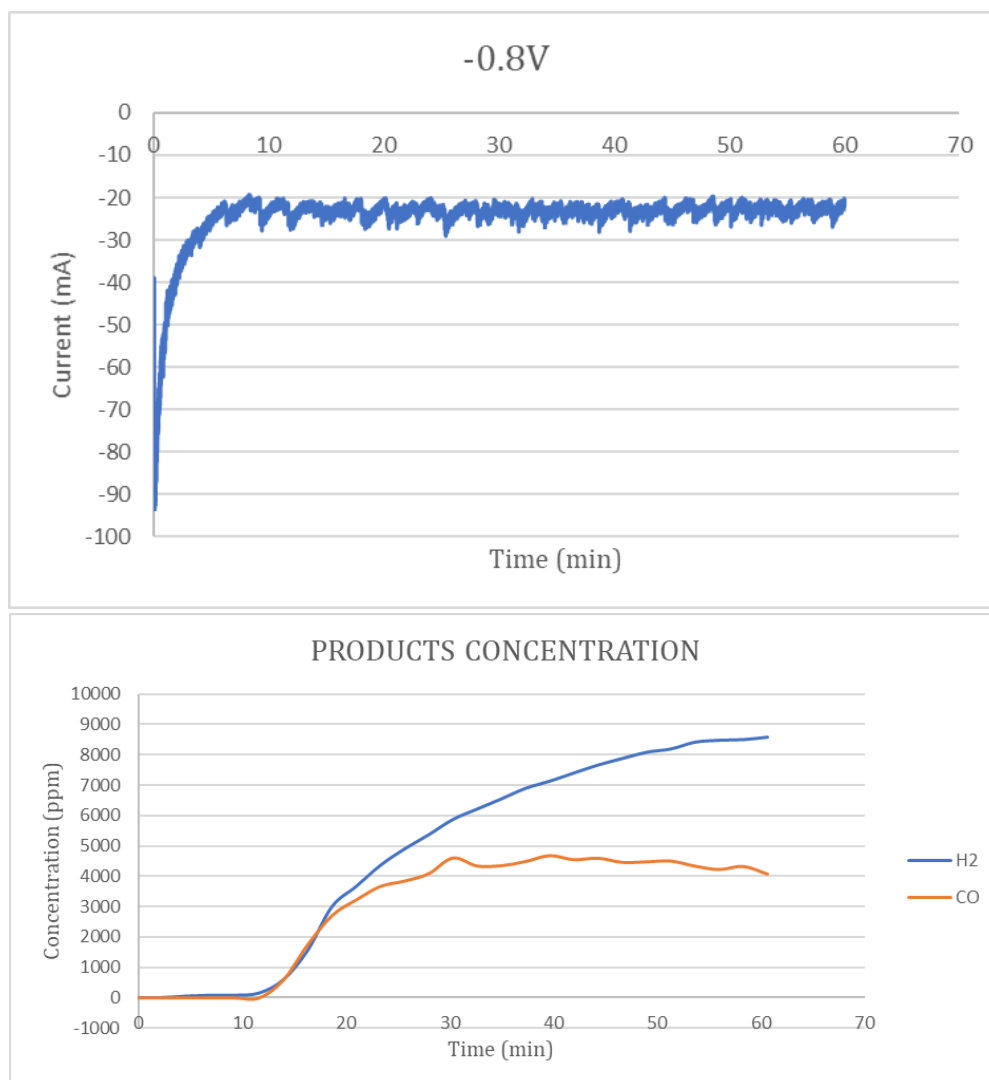


Fig.3.37 CA and products concentration of CuSn(IV)10 at -0.8 V vs RHE.

Fig.3.36, Fig.3.37 and Tab.3.12 show that the concentration of H₂ doubles the concentration of CO at 40 minutes, except at -0.7V, where the amount of CO is comparable with the amount of H₂.

As shown in Tab.3.13 and Fig.3.38, the best results regarding the ratio H₂/CO are achieved at -0.7V vs RHE. However, the sum of Faradic Efficiencies is 87%, meaning that HCOOH was produced in an appreciable way.

Tab.3.13 Sum up of the main parameters of the sample CuSn(IV)10: current values, FE and H₂/CO ratio at the tested potential (V vs RHE).

		-0.6V	-0.7V	-0.8V
FE (%)	H ₂	67.9	46.5	58.4
	CO	32.1	40.5	36.0
H ₂ /CO		2.1	1.1	1.6

3. Results and discussion

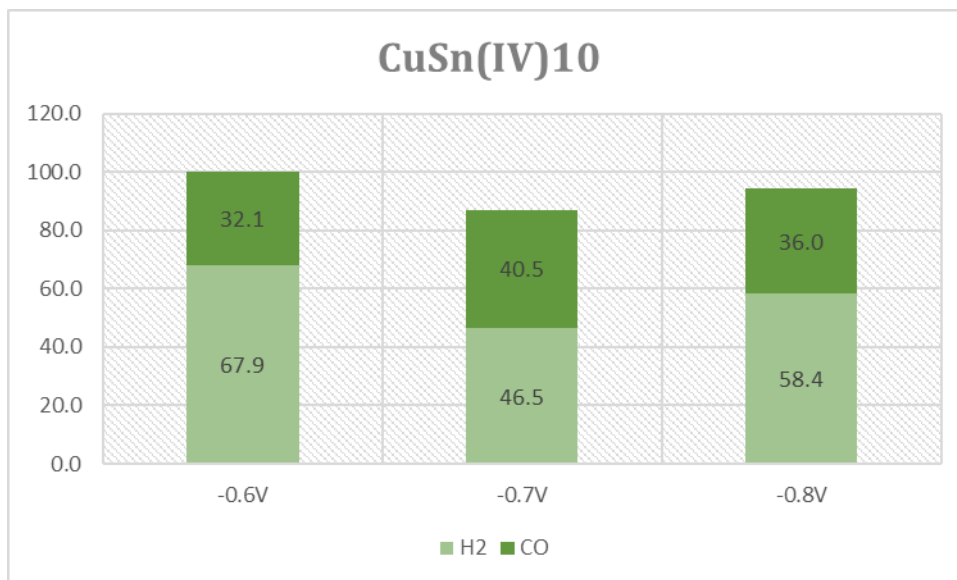


Fig.3.38 Faradaic efficiencies for hydrogen and carbon monoxide at the three different potentials displayed by CuSn(IV)10.

3.2.1.8 Cu(Ace)Sn(IV)10

The sample “Cu(Ace)Sn(IV)10” was tested at three different potentials (-0.6, -0.7V and -0.8V vs RHE).

In Fig.3.39, Fig.3.40 and Fig.3.41 the trends of CO and H₂ concentration and current vs time are shown.

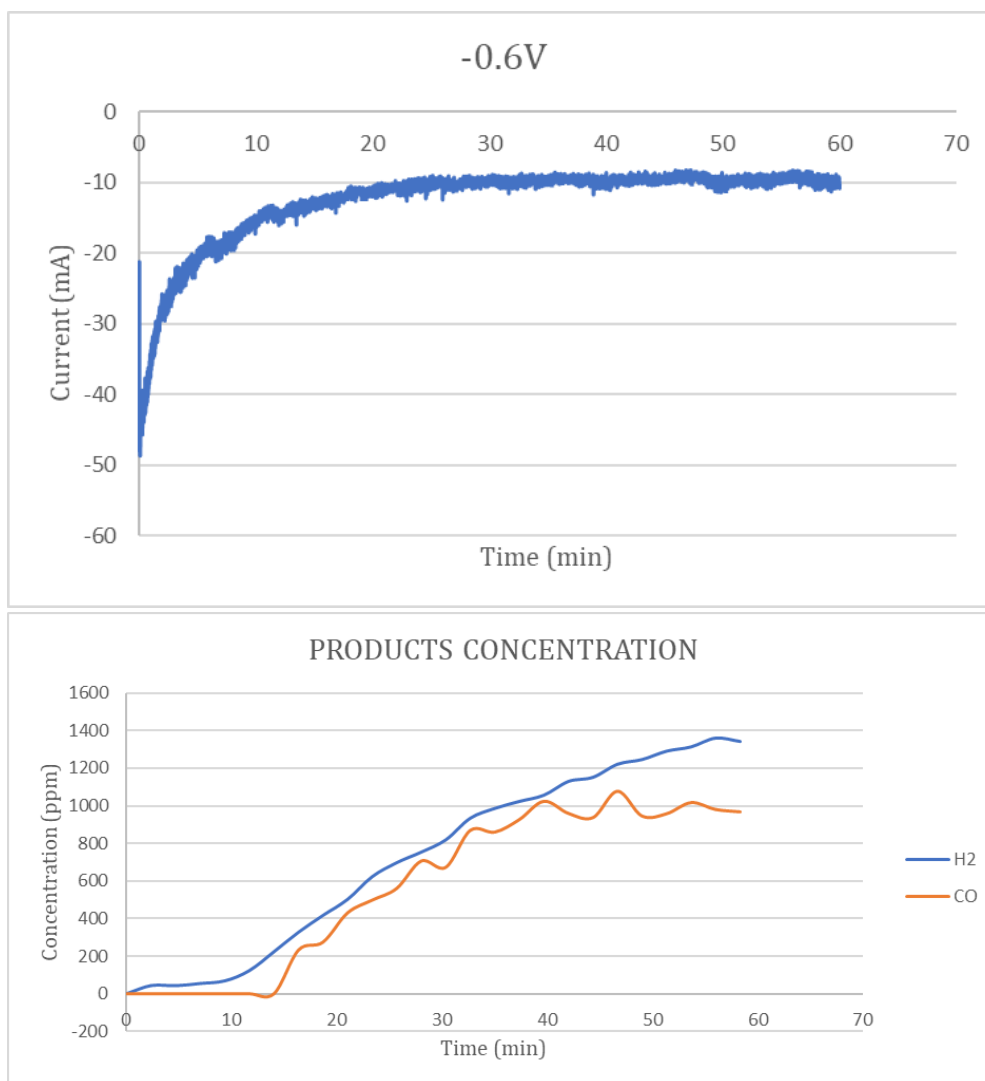


Fig.3.39 CA and products concentration for the sample Cu(Ace)Sn(IV)10 at -0.6 V vs RHE.

3. Results and discussion

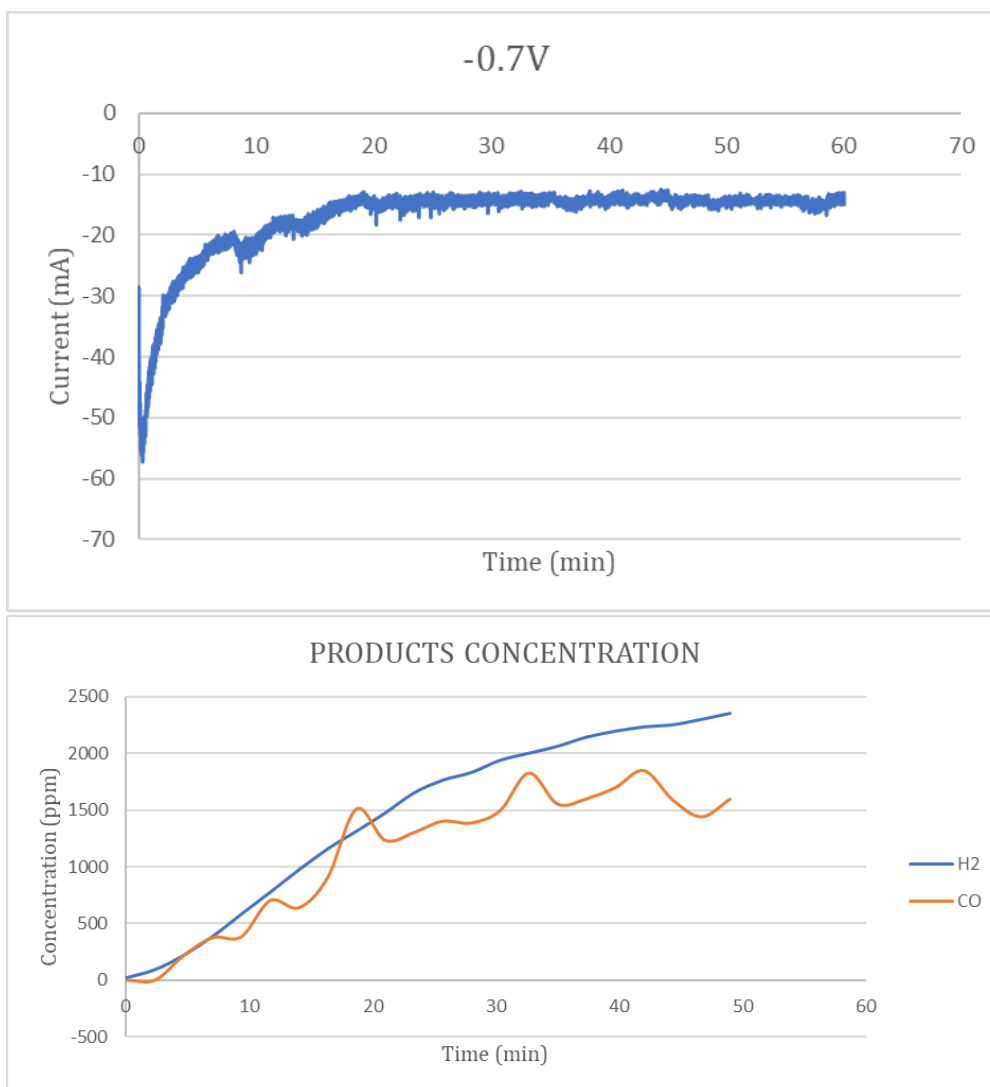


Fig.3.40 CA and products concentration recorded when testing Cu(Ace)Sn(IV)10 at -0.7 V vs RHE.

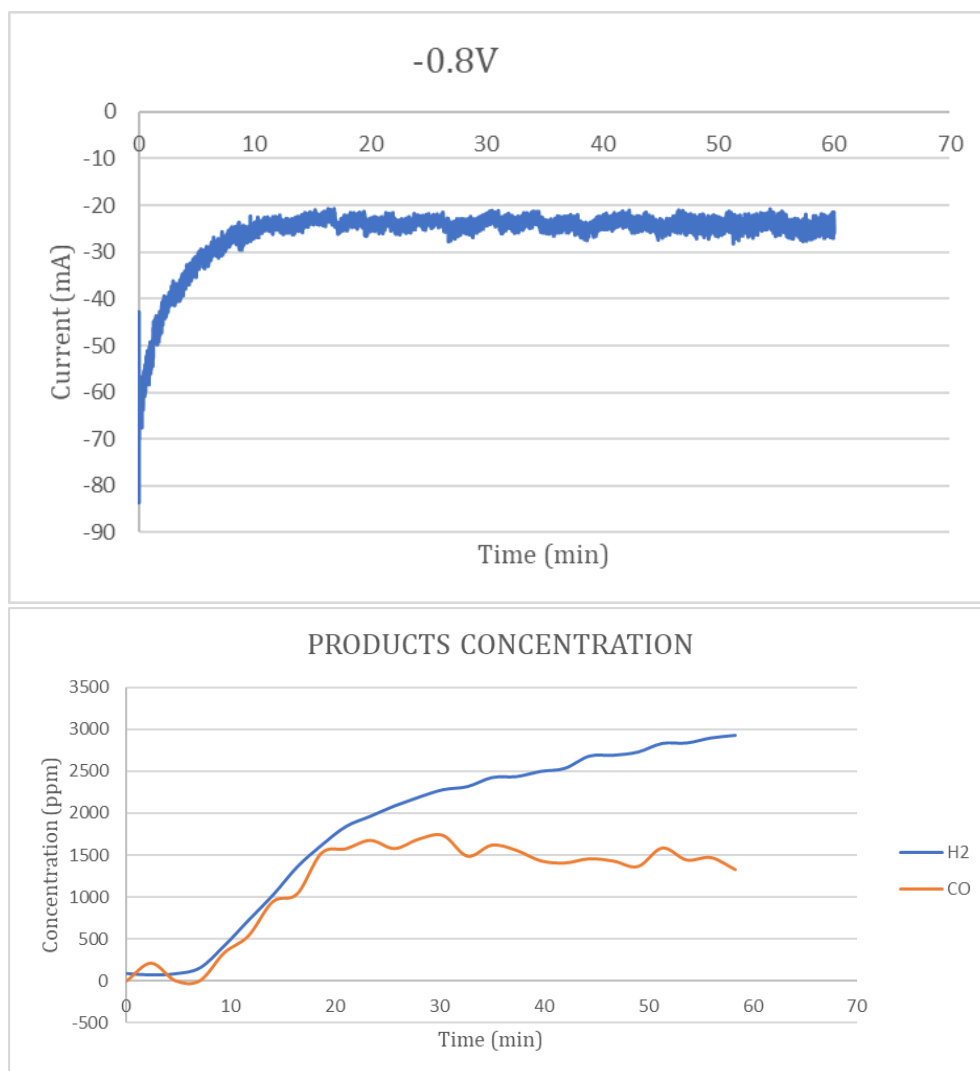


Fig.3.41 CA and products concentration at -0.8 V vs RHE for Cu(Ace)Sn(IV)10.

From Tab.3.14 and Fig.3.42, it is clear that the best overpotential for producing Syngas is -0.6V vs RHE: in fact, both the H₂/CO ratio value and the FEs values (whose sum is 100%) are very promising.

Tab.3.14 Sum up of the main parameters for the sample Cu(Ace)Sn(IV)10: current values, FE and H₂/CO ratio at the tested potential (V vs RHE).

		-0.6V	-0.7V	-0.8V
	Current (mA)	-9.5	-13.9	-23.8
FE (%)	H₂	54.0	50.0	54.1
	CO	46.0	41.4	30.0
	H₂/CO	1.2	1.2	1.8

3. Results and discussion

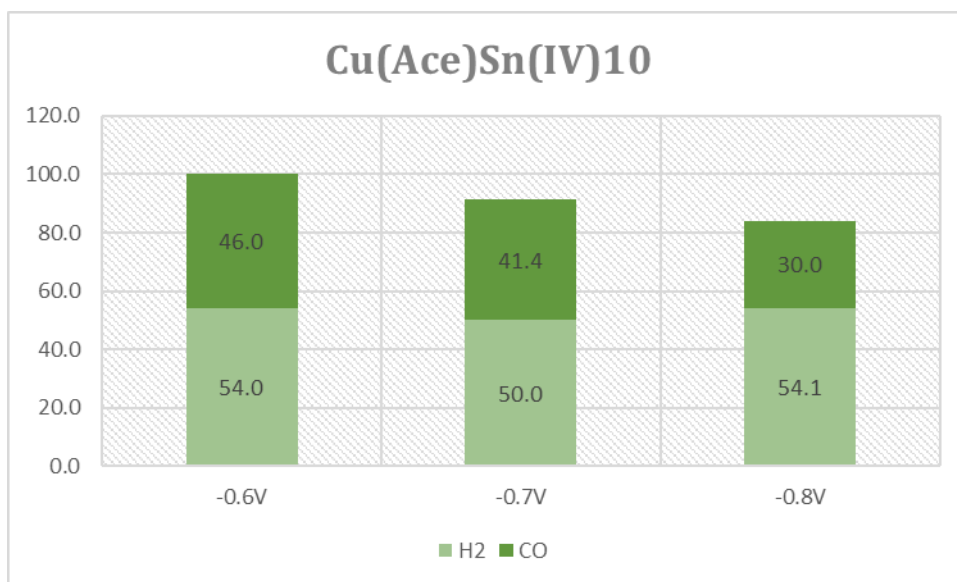


Fig.3.42 Faradaic efficiencies for hydrogen and carbon monoxide at the three different potentials for the sample Cu(Ace)Sn(IV)10.

3.3 COMPARISON OF RESULTS

Fig.3.43 shows the samples synthesized with CuSO₄ as the copper precursor. It is possible to appreciate how different tin salts and their concentration affected the morphology of the samples synthesized using copper salt CuSO₄: by using Sn(II), no morphological change occurred; by using Sn(IV), cubic particles were formed, with a rate depending on the concentration of the Sn precursor.

The difference may be explained by considering Sn(II) as inhibitor of agglomeration: in fact, it is possible to see that the first step of the formation of cubes is the agglomeration of particles.

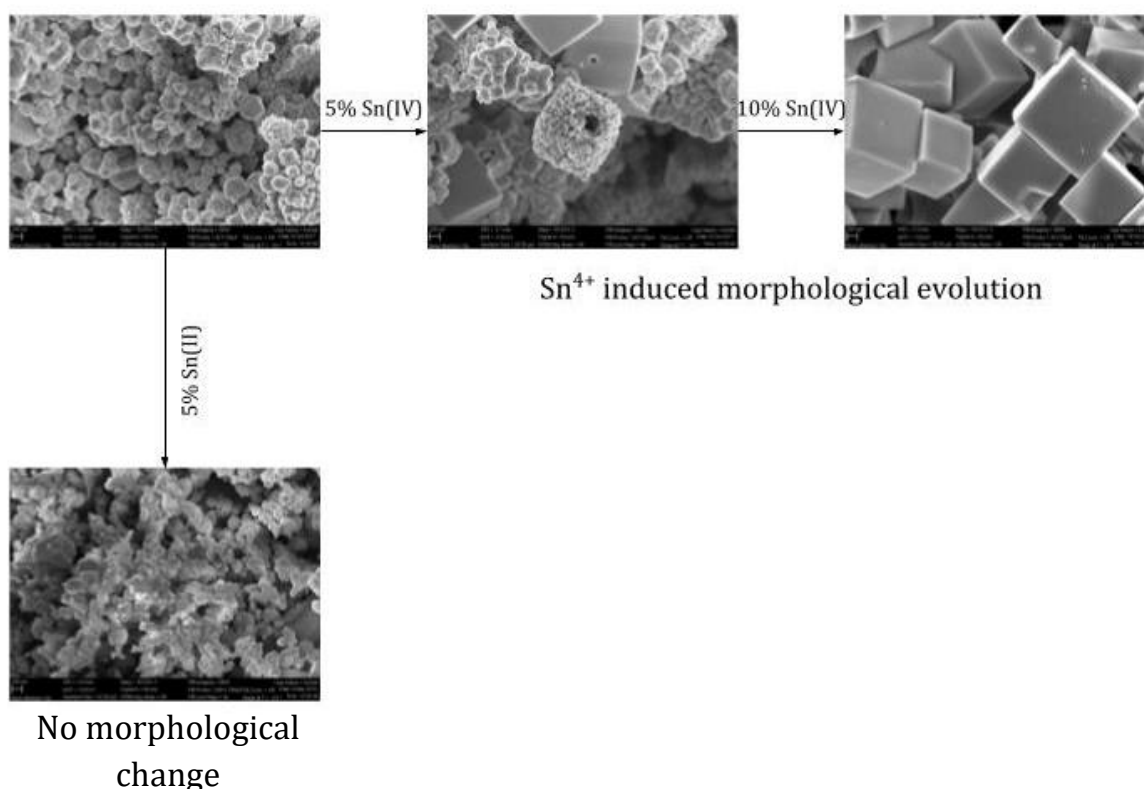


Fig.3.43 Effects of tin salts and their concentration on morphology of samples prepared with CuSO₄.

From XRD and XPS analysis, the Sn(IV) affected not only the morphology, but also the composition. The sample from CuSO₄ is composed mainly of metallic Cu and with mixed copper oxides on the surface, while those from CuSO₄ and Sn(IV) have a significant amount of Cu₂O and have also mixed surface oxides. In the synthesis, when adding alkaline solution 2 to solution 1, the blue Cu(OH)₂ precipitate is firstly formed. With increasing the pH, a clear and dark solution is obtained. The Cu(II) could exist as [Cu(OH)₄]²⁻ or [Cu(C₂H₄O₂)₂]²⁻ complexes in the alkaline EG/H₂O mixture [37, 38.]. The reduction of the Cu(II) complexes initially form Cu(I) and then it gets further reduced to metallic Cu at high reaction temperature. The high temperature (peak 180 °C) and high pH value (>12.5) are essential for yielding metallic Cu particles in EG, which is consistent with other reported works [39, 40]. When the temperature decreases to ambient condition, the surface of Cu particles can be easily oxidized into Cu₂O or CuO under air [41]. Hence, the sample from CuSO₄ is found to be composed of mainly metallic Cu and mixed copper oxides. With adding Sn(IV) in the precursor, the percentage of Cu(I) increases with respect to Cu(0) in the samples. The oxidation grade increases with increasing the quantity of Sn(IV) in the

3. Results and discussion

precursor. When the $\text{SnCl}_4:\text{CuSO}_4$ weight ratio increases to 1:10, the CuSn(IV)10 has mainly crystalline Cu_2O . It is likely that the introduction of Sn(IV) can inhibit further reduction of Cu(I) . According to Zheng et al.[42], the Sn(IV) could adhere on the surface of Cu(OH) , acting as a barrier between Cu(OH) and EG. Hence, the Cu(OH) can be stabilized instead of being further reduced by EG. The Cu(OH) then turns to Cu_2O . The initial size of the particles is smaller with the presence of Sn(IV) (in CuSn(IV)5), in agreement with the literature [42, 43]. The small particles then agglomerate and ultimately grow into Cu_2O cubes (in CuSn(IV)10).

Sn(II) appeared not to change the morphology, but it has significantly affected the surface composition of the sample when compared to “Cu”. Addition of Sn(II) can lead to the reduction of particle size. The nanosized particles are easier to be oxidized and thus display a large amount of CuO on the surface, as confirmed by XPS, while a large amount of Cu and Cu_2O were present in the inner layers as detected by XRD.

Fig.3.44 shows the samples synthesized with $\text{Cu(CH}_3\text{COO)}_2$ as the copper precursor. Compared to the samples from CuSO_4 precursor, the Cu(Ace) has distinct composition and morphology. It is mainly composed of Cu_2O and has cubic morphology. It is likely the presence of CH_3COO^- can weaken the reducing ability of EG. Sn(IV) produced a change in size: by increasing its concentration the size of the particles decreased.

Sn(II) acts both as a size reducing agent and as a dispersant, inhibiting the agglomeration of particles. Furthermore, Sn(II) changed the morphology of Cu(Ace) .

In all samples from both CuSO_4 and $\text{Cu(CH}_3\text{COO)}_2$ precursors, Sn element can be stabilized as HSnO_2^- and as SnO_3^{2-} ($\text{HSnO}_2^-/\text{Sn}$, -0.79 V; $\text{SnO}_3^{2-}/\text{HSnO}_2^-$, -0.69 V vs SHE) at 25 °C due to high pH (> 11.5) of the final solution [43]. These anions are soluble in H_2O or $\text{H}_2\text{O/EG}$, which can explain why no Sn can be detected in the final powder samples.

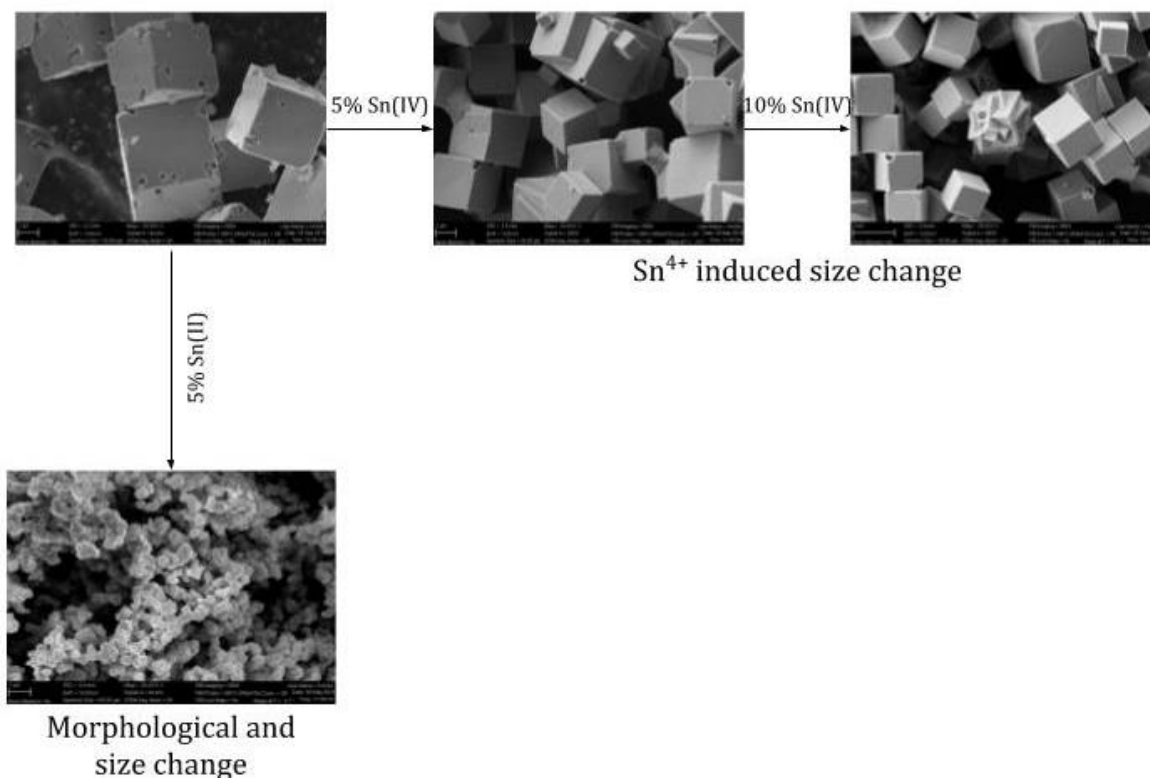


Fig.3.44 Effects of tin salts and their concentration on morphology of samples prepared with Cu(Ace).

From CA tests and on-line μ GC analysis, the Faradaic Efficiency largely depends on the applied potentials, but it is also possible to see from Fig.3.45, Fig.3.46 and Fig.3.47 that the the catalytic particles have great importance. In fact, the best results concerning FE for CO formation are generally given by samples “CuSn(IV)10” and “Cu(Ace)Sn(IV)10”.

This may be explained by the similarities in size and shape of the particles (Fig.3.48) and in the composition as well.

One exception is the sample “Cu(Ace)Sn(IV)5”, since at -0.6V vs RHE it shows a better performance than “CuSn(IV)10”, but also in this case the good Faradaic Efficiency for CO can be explained by the importance of the morphology on the catalytic activity, since it displays similar morphology as Cu(Ace)Sn(IV)10.

3. Results and discussion

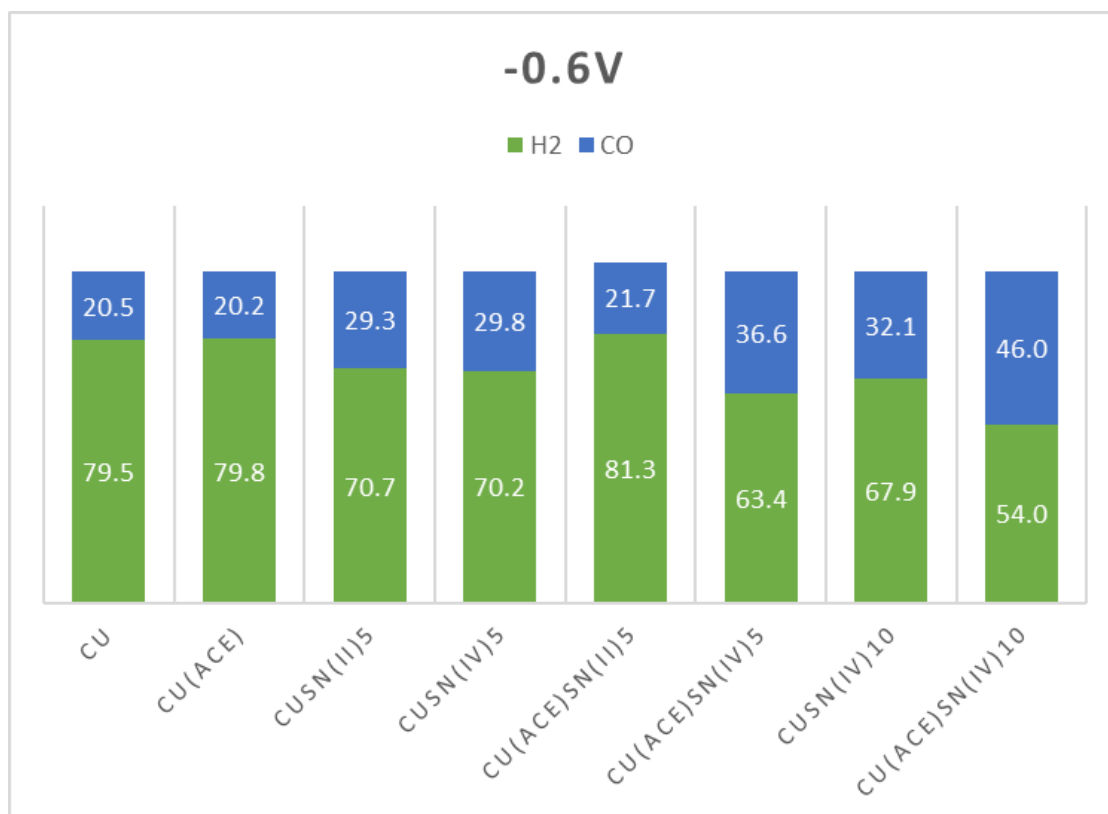


Fig.3.45 Faradaic Efficiencies for the different samples at -0.6V vs RHE.

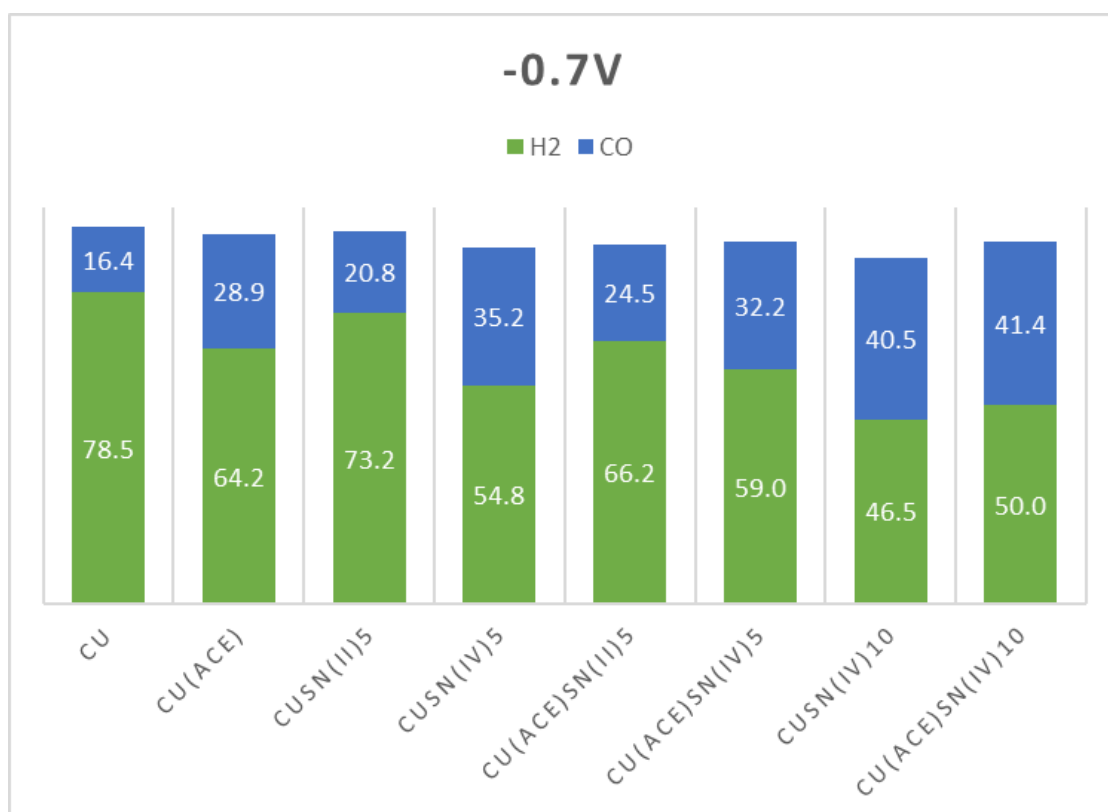


Fig.3.46 Faradaic Efficiencies for the different samples at -0.7V vs RHE.

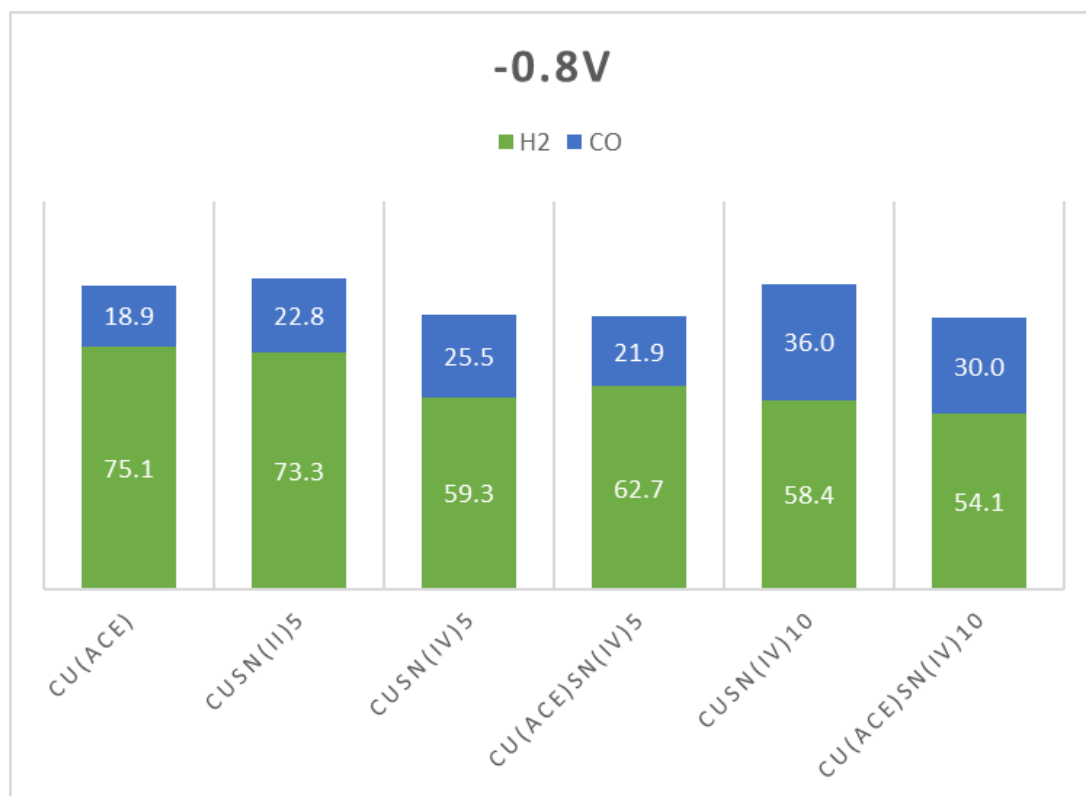


Fig.3.47 Faradaic Efficiencies for the different samples at -0.8V vs RHE.

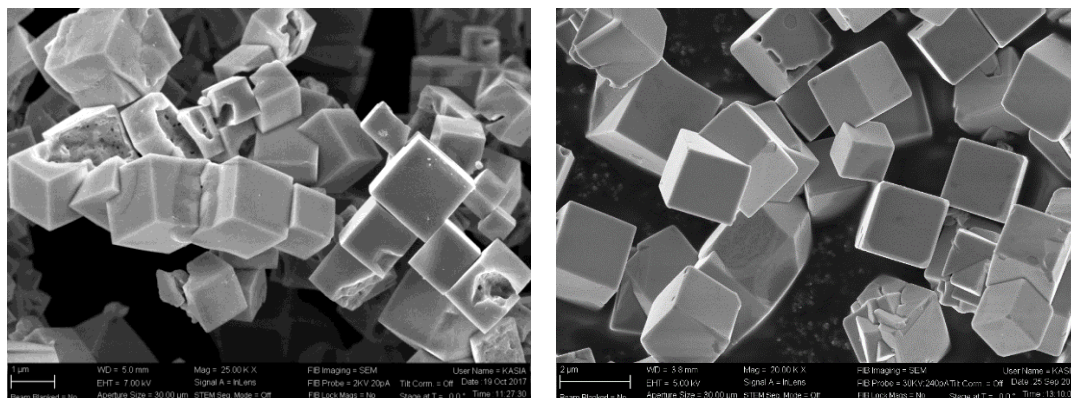


Fig.3.48 FESEM images of CuSn(IV)10 and Cu(Ace)Sn(IV)10 (from left to right). Size and morphology are very similar.

3.4 ABOUT SYNGAS

The materials were investigated with the main aim of reducing CO₂ with good efficiency and selectivity and of producing Syngas presenting H₂/CO ratio suitable for the production of valuable compounds.

From Tab.3.15, it is possible to understand that some materials produced a mixture of hydrogen and carbon monoxide proper for further processing.

3. Results and discussion

Tab.3.15 H₂/CO ratio for the different samples at the tested overpotentials.

	Cu	Cu(Ace)	CuSn(II)5	CuSn(IV)5	Cu(Ace)Sn(II)5	Cu(Ace)Sn(IV)5	CuSn(IV)10	Cu(Ace)Sn(IV)10
-0.6V	3.9	3.9	2.4	2.4	3.8	1.7	2.1	1.2
-0.7V	4.8	2.2	3.5	1.6	2.7	1.8	1.1	1.2
-0.8V	-	4.0	3.2	2.3	-	2.9	1.6	1.8

In particular, Cu(Ace)Sn(IV)5 and CuSn(IV)10 produced a mixture that can be used in the Fischer-Tropsch process or in the production of methanol, since presenting a H₂/CO ratio of approximately 2.

CuSn(IV)10 and Cu(Ace)Sn(IV)10 generated a mixture suitable for the production of Ethanol, since the H₂/CO ratio is very close to 1.

4. CONCLUSION AND FUTURE DEVELOPMENTS

The aim of this work was to synthesize and investigate materials for the electroreduction of CO₂.

The different catalytic powders were produced via microwave assisted thermal synthesis from two different copper salts and two different tin salts. The samples were characterized by FESEM, XPS and XRD analysis. The products were examined via GC while performing CA.

The choice of the microwave-assisted method for the synthesis of the samples was dictated by the advantages that this technology presents, especially regarding the smaller energy consumption.

The work showed the effects of the two different tin salts on the morphology and the composition, and, hence, on the catalytic activity. It is, in fact, interesting to notice that, since its presence in the sample was negligible, Sn does not have effect on the catalytic activity per se, but it is indirectly of great importance because of its effects on morphology and composition.

Samples synthesized using Sn(IV) chloride showed better results regarding both the FEs for the production of CO and the ratio H₂/CO for the production of Syngas. This can be explained by the similarities (in morphology and composition) that the materials fabricated by using Sn(IV) present.

Further electrochemical analyses must be performed in order to have a complete picture of the most promising materials. The abovementioned analyses are Electrochemical Impedance Spectroscopy (EIS) and Cyclic Voltammetry (CV).

With EIS analysis, the material is subjected to an AC potential and module and phase of the resulting AC current are analysed. The measurements are carried out in a wide frequency range. By analysing the results, it is possible to distinguish the contributions to the tendency of the material to oppose to current flow given by the following three phenomena: transport of charges in the material; transfer of charges at the interface with the electrolyte; transport of charges in the solution [29, 30].

CV is an analytic method which allows to find the relation between current and potential in a system and with which is possible to investigate the redox potential and reaction rate. Furthermore, by observing the hysteresis of the produced curves, it is possible to examine the ability of the material to maintain its characteristic after several cycles [31].

During a cyclic voltammetry the potential is cyclically varied, and the corresponding current is measured [32], as shown in Fig.4.1: positive peaks represent oxidations, negative peaks represent reductions.

4. Conclusion and future developments

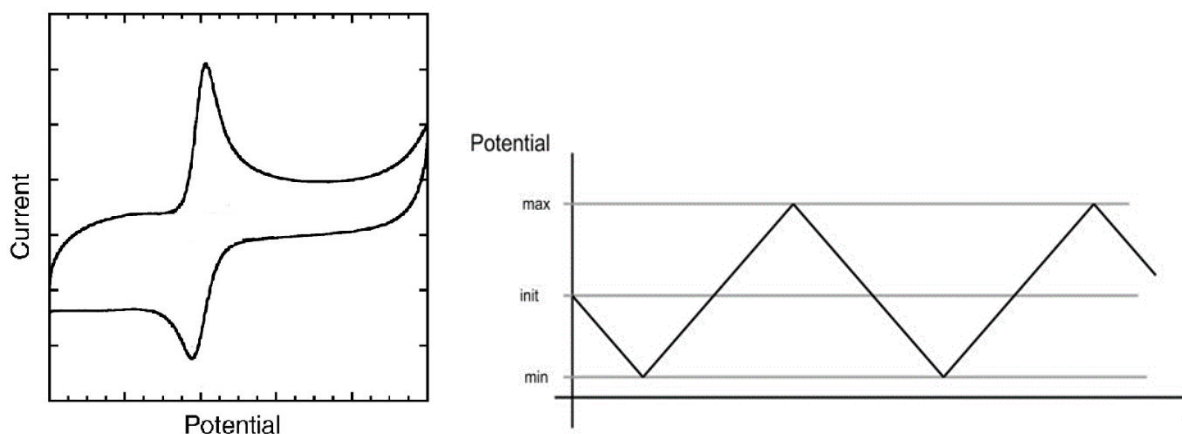


Fig.4.1 From left to right: trend of the applied potential; generic cyclic voltammogram

Further tests must be run to examine the durability of the catalyst.

Finally, a model describing the kinetic of the CO₂ electroreduction reaction must be design and evaluated.

In conclusion, this study showed that the microwave-assisted technology is able to carry out synthesis comparable to classic solvothermal methods, but with the use of less energy and time, in addition to a better process parameters control.

The materials synthesised via microwave present different characteristics depending on the precursors and their concentration. Most of the fabricated catalysts are suitable for the production of Syngas.

The achievements obtained in this study will be further investigated, since the promising results are consistent with the goals of solving the problem of the global warming and of leading the use of greener fuels.

REFERENCES

- [1] www.nasa.gov/topics/earth/features/climate_by_any_other_name.html, last visited 5-5-2019
- [2] IPCC, 2018: Summary for Policymakers. In: Global Warming of 1.5°C. An IPCC Special Report on the impacts of global warming of 1.5°C above pre-industrial levels and related global greenhouse gas emission pathways, in the context of strengthening the global response to the threat of climate change, sustainable development, and efforts to eradicate poverty [Masson-Delmotte, V., P. Zhai, H.-O. Pörtner, D. Roberts, J. Skea, P.R. Shukla, A. Pirani, W. Moufouma-Okia, C. Péan, R. Pidcock, S. Connors, J.B.R. Matthews, Y. Chen, X. Zhou, M.I. Gomis, E. Lonnoy, Maycock, M. Tignor, and T. Waterfield (eds.)]. World Meteorological Organization, Geneva, Switzerland, 32 pp.
- [3] Simelys Hernández, M. Amin Farkhondehfal Sastre, Michiel Makkee, Guido Saracco, Nunzio Russo, *Syngas production from electrochemical reduction of CO₂: current status and prospective implementation*, *Green Chem.*, 2017, **19**, 2326-2345.
- [4] IPCC, 2014: Climate Change 2014: Synthesis Report. *Contribution of Working Groups I, II and III to the Fifth Assessment Report of the Intergovernmental Panel on Climate Change* [Core Writing Team, R.K. Pachauri and L.A. Meyer (eds.)]. IPCC, Geneva, Switzerland, 151 pp.
- [5] Allen, M.R., O.P. Dube, W. Solecki, F. Aragón-Durand, W. Cramer, S. Humphreys, M. Kainuma, J. Kala, N. Mahowald, Y. Mulugetta, R. Perez, M. Wairiu, and K. Zickfeld, 2018: Framing and Context. In: *Global Warming of 1.5°C. An IPCC Special Report on the impacts of global warming of 1.5°C above pre-industrial levels and related global greenhouse gas emission pathways, in the context of strengthening the global response to the threat of climate change, sustainable development, and efforts to eradicate poverty* [Masson-Delmotte, V., P. Zhai, H.-O. Pörtner, D. Roberts, J. Skea, P.R. Shukla, A. Pirani, W. Moufouma-Okia, C. Péan, R. Pidcock, S. Connors, J.B.R. Matthews, Y. Chen, X. Zhou, M.I. Gomis, E. Lonnoy, T. Maycock, M. Tignor, and T. Waterfield (eds.)]. In Press.
- [6] M. R. Islam, M. M. Khan, A. B. Chhetri, and M. R. Islam, *Green Petroleum: How Oil and Gas Can Be Environmentally Sustainable; A Companion to the Philosophy of Technology*, Hoboken, NJ, USA: John Wiley & Sons, Inc, 2012.
- [7] Walker Richard P., Swift, Andrew Hoboken, *Wind Energy Essentials*, Hoboken, NJ, John Wiley & Sons, Inc, 2015.
- [8] Huan Xiea, Tanyuan Wanga, Jiashun Lianga, Qing Li, Shouheng Sun, *Cu-based nanocatalysts for electrochemical reduction of CO₂*, *Nano Today*, 2018, **21**, 41-54.
- [9] Myhre, G., D. Shindell, F.-M. Bréon, W. Collins, J. Fuglestedt, J. Huang, D. Koch, J.-F. Lamarque, D. Lee, B. Mendoza, T. Nakajima, A. Robock, G. Stephens, T. Takemura and H. Zhang, 2013: Anthropogenic and Natural Radiative Forcing. In: *Climate Change 2013: The Physical Science Basis. Contribution of Working Group I to the Fifth Assessment Report of the Intergovernmental Panel on Climate Change* [Stocker, T.F., D. Qin, G.-K. Plattner, M. Tignor, S.K. Allen, J. Boschung, A. Nauels, Y. Xia, V. Bex and P.M. Midgley (eds.)]. Cambridge University Press, Cambridge, United Kingdom and New York, NY, USA.

References

- [10] J. Grace, *Carbon Cycle*, in *Encyclopedia of Biodiversity*, 2nd Edition, Volume 1, Edinburgh, Elsevier, 2013, pp.674-684.
- [11] FAO. 2018. *The State of the World's Forests 2018 - Forest pathways to sustainable development*. Rome.
- [12] Bijandra Kumar, Joseph P. Brian, Veerendra Atla, Sudesh Kumari, Kari A. Bertam, Robert T. White, Joshua M. Spurgeon, *New trends in the development of heterogeneous catalysts for electrochemical CO₂ reduction*, *Catalysis Today*, 2016, **270**, 19-30.
- [13] Huan Xie, Tanyuan Wang, Jiashun Liang, Qing Li, Shouheng Sun, *Cu-based nanocatalysts for electrochemical reduction of CO₂*, *Nano Today*, 2018, **21**, 41-54.
- [14] Siglinda Perathoner and Gabriele Centi, *CO₂ Recycling: A Key Strategy to Introduce Green Energy in the Chemical Production Chain*, *ChemSusChem*, 2014, **7**, 1274-1282.
- [15] R. Reske, H. Mistry, F. Behafarid, B. Roldan Cuenya, P. Strasser, *Particle size effects in the catalytic electroreduction of CO₂ on Cu nanoparticles*, *J. Am. Chem. Soc.* **136**, 2014, 6978–6986.
- [16] Juqin Zeng, Katarzyna Bejtka, Wenbo Jub, Micaela Castellino, Angelica Chiodoni, Adriano Sacco, M. Amin Farkhondehfal, Simelys Hernández, Daniel Rentsch, Corsin Battaglia, Candido F. Pirri, *Advanced Cu-Sn foam for selectively converting CO₂ to CO in aqueous solution*, *Applied Catalysis B: Environmental*, **236**, 2018, 475-482.
- [17] Tiago Pardal, Sofia Messias, Margarida Sousa, Ana S. Reis Machado, Carmen M. Rangel, Daniela Nunes, Joana V. Pinto, Rodrigo Martins, Manuel Nunes da Ponte, *Syngas production by electrochemical CO₂ reduction in an ionic liquid based-electrolyte*, *Journal of CO₂ Utilization*, **18**, 2017, 62–72.
- [18] Jon-Sverre Schanche, *Microwave synthesis solutions from personal chemistry*, *Molecular Diversity*, vol.7, 291-298.
- [19] Dandan Sun, Yi Du, Xiuying Tian, Zhongfu Li, Zhongtao Chen, Chaofeng Zhu, *Microwave-assisted synthesis and optical properties of cuprous oxide micro/nanocrystals*, *Materials Research Bulletin*, **60**, 2014, 704–708.
- [20] Satoshi Horikoshi, Nick Serpone, *Microwaves in Nanoparticle Synthesis: Fundamentals and Applications*, Hoboken, NJ, John Wiley & Sons, Inc, 2013.
- [21] Tsuji Masaharu, Hashimoto Masayuki, Nishizawa Yuk, Kubokawa Masatoshi, Tsuji Takeshi, *Microwave-assisted synthesis of metallic nanostructures in solution*, *Chemistry – A European Journal*, 07 January 2005, Vol.11(2), pp.440-452
- [22] John-Paul Jones, G. K. Surya Prakash, George A. Olah, *Electrochemical CO₂ Reduction: Recent Advances and Current Trends*, *Isr. J. Chem.*, **54**, 2014, 1451-1466.
- [23] Shigeyuki Somiya, *Handbook of Advanced Ceramics : Materials, Applications, Processing, and Properties*, 2nd Edition, Elsevier Science & Technology, 2013.
- [24] Ruren Xu, Wenqin Pang, Qisheng Huo, *Modern Inorganic Synthetic Chemistry*, Elsevier, 2010.

- [25] Ahmed Waqar, Jackson Mark J., *Emerging Nanotechnologies for Manufacturing*, Elsevier, 2009.
- [26] Léonard François, *Physics of Carbon Nanotube Devices*, William Andrew Publishing, 2009.
- [27] Graciela Wild Padua, Qin Wang, *Nanotechnology Research Methods for Food and Bioproducts*, John Wiley & Sons, Inc, 2013.
- [28] Yang Leng, *Materials Characterization: Introduction to Microscopic and Spectroscopic Methods*, John Wiley & Sons, Incorporated, 2013.
- [29] Vadim F. Lvovich, *Impedance Spectroscopy: Applications to Electrochemical and Dielectric Phenomena*, John Wiley & Sons, Incorporated, 2012.
- [30] Alberto Escarpa, María Cristina González, Miguel Ángel López, *Agricultural and Food Electroanalysis*, John Wiley & Sons, Incorporated, 2015.
- [31] Derek Pletcher, Zhong-Qun Tian, David Williams, *Developments in Electrochemistry: Science Inspired by Martin Fleischmann*, John Wiley & Sons, Incorporated, 2012.
- [32] Noemie Elgrishi, Kelley J. Rountree, Brian D. McCarthy, Eric S. Rountree, Thomas T. Eisenhart, Jillian L. Dempsey, *A Practical Beginner's Guide to Cyclic Voltammetry*, J. Chem. Educ. 2018, **95**, 197–206
- [33] Cynthia G. Zoski, *Handbook of Electrochemistry*, Elsevier Science & Technology, 2006.
- [34] Cordero C.; Liberto E.; Sgorbini B.; Rubiolo P.; Bicchi C., *Chemical Analysis of Food: Techniques and Applications*, Elsevier, 2012.
- [35] Jinli Qiao, Yuyu Liu, Feng Hong, Jiujun Zhang, *A review of catalysts for the electroreduction of carbon dioxide to produce low-carbon fuels*, Chem. Soc. Rev., 2014, **43**, 631-675.
- [36] Mark C. Biesinger, Leo W.M. Lau, Andrea R. Gerson, Roger St.C. Smart, *Resolving surface chemical states in XPS analysis of first row transition metals, oxides and hydroxides: Sc, Ti, V, Cu and Zn*, Applied Surface Science, Volume 257, **3**, 2010, 887-898.
- [37] Yen-Yau H. Chao David R. Kearns, *Electron spin resonance investigation of the soluble blue copper(II) hydroxide complex*, J. Phys. Chem., 1977, **81**, 666–668.
- [38] H. Rivers, K. J. Carroll, R. A. Jones and E. E. Carpenter, *A copper–polyol complex: [Na₂(C₂H₆O₂)₆][Cu(C₂H₄O₂)₂]*, Acta Crystallogr., Sect. C: Cryst. Struct. Commun., 2010, **66**, m83–m85.
- [39] Hideya Kawasaki, Yuka Kosaka, Yuki Myoujin, Takashi Narushima, Tetsu Yonezawa and Ryuichi Arakawaa, *Microwave-assisted polyol synthesis of copper nanocrystals without using additional protective agents*, Chem Commun, 2011, **47**, 7740-7742.
- [40] M. Ibrahim Dar, S. Sampath, S. A. Shivashankar, *Microwave-assisted, surfactant-free synthesis of air-stable copper nanostructures and their SERS study*, J. Mater. Chem., 2012, **22**, 22418-22423

References

- [41] Johannes Teichert, Thomas Doert, Michael Ruck, *Mechanisms of the polyol reduction of copper(II) salts depending on the anion type and diol chain length*, Dalton Trans., 2018, **47**, 14085-14093
- [42] Rui Chen, Juan Lu, Zuoshan Wang, Qingqing Zhou, Min Zheng, *Microwave Synthesis of Cu/Cu₂O/SnO₂ Composite with Improved Photocatalytic Ability Using SnCl₄ as a Protector*, 2018, J. Mat. Sc., vol.53, **13**, 9557-9566.
- [43] Yongling Du, Nuo Zhang, Chunming Wang, *Photo-catalytic degradation of trifluralin by SnO₂-doped Cu₂O crystals*, Catalysis Communications, 2010, vol. 11, **7**, 670-674.
- [43] Tianzu Yang, Pengchun Zhu, Weifeng Liu, Lin Chen, Duchao Zhang, *Recovery of tin from metal powders of waste printed circuit boards*, Waste Management, 2017, **68**, 449-457.

ACKNOWLEDGEMENT

First of all, I would like to thank Juqin and Adriano for their support during all this work and for making me learn and enjoy new things: to Juqin, xièxiè; to Adriano, di cori t'arringrazio.

I would like to thank my advisor, Prof. Pirri.

I would like to acknowledge Micaela Castellino and Katarzyna Bejtka for their help.

Thanks to my parents, for their support, love and precious teachings.

Thanks to Ignazio, for supporting and caring for me and, most of all, for introducing me to Adriano and Juqin: without this event, I wouldn't have become able to appreciate catalysts.

Thanks to Giuseppe, just for being my brother.

Thanks to my friends: most of them shared the joys and sorrows of being enrolled in Poli with me, and, even if they didn't, thanks for their support and company.

Thanks to the people from IIT, they made my time in the laboratory a really good time.

Thanks to Daniele, for being on my side, even when far away.